NUWC-NPT Technical Report 10,685
11 August 1994



# Observations of ELF Propagation at High Latitudes During the Sporadic-E Conditions of November 1986

J. R. Katan
D. J. Saleem
Submarine Electromagnetic Systems Department

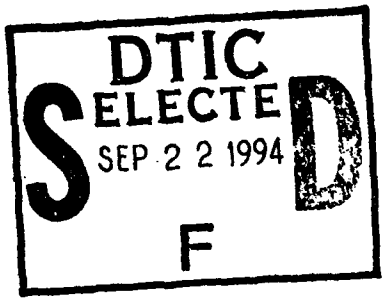


"Original contains color plates: All DTIC reproductions will be in black and white"


Naval Undersea Warfare Center Division
Newport, Rhode Island







## PREFACE

This research was conducted under an independent study and was partially funded under job order M51007.

The Technical Reviewer for this report was R. J. Pellowski (Code 3422).

**Reviewed and Approved:** 11 August 1994

**D. M. Viccione**
**Head, Submarine Electromagnetic Systems Department**

# DISCLAIMER NOTICE

THIS DOCUMENT IS BEST QUALITY AVAILABLE. THE COPY FURNISHED TO DTIC CONTAINED A SIGNIFICANT NUMBER OF COLOR PAGES WHICH DO NOT REPRODUCE LEGIBLY ON BLACK AND WHITE MICROFICHE.

# REPORT DOCUMENTATION PAGE

*Form Approved*
*OMB No. 0704-0188*



| 1. AGENCY USE ONLY (Leave Blank) | 2. REPORT DATE | 3. REPORT TYPE AND DATES COVERED |
|---|---|---|
| | 11 August 1994 | Final |

**4. TITLE AND SUBTITLE**

Observations of ELF Propagation at High Latitudes During the Sporadic-E Conditions of November 1986

**5. FUNDING NUMBERS**

PR M51007

**6. AUTHOR(S)**

J. R. Katan and D. J. Saleem

**7. PERFORMING ORGANIZATION NAME(S) AND ADDRESS(ES)**

Naval Undersea Warfare Center Detachment
39 Smith Street
New London, Connecticut 06320-5594

**8. PERFORMING ORGANIZATION REPORT NUMBER**

TR 10,687

**9. SPONSORING/MONITORING AGENCY NAME(S) AND ADDRESS(ES)**

Naval Undersea Warfare Center
1176 Howell Street
Newport, Rhode Island 02841-1708

**10. SPONSORING/MONITORING AGENCY REPORT NUMBER**

**11. SUPPLEMENTARY NOTES**

**12a. DISTRIBUTION/AVAILABILITY STATEMENT**

Approved for public release; distribution is unlimited.

**12b. DISTRIBUTION CODE**

**13. ABSTRACT (Maximum 200 words)**

This report presents the results of an ELF propagation study at high latitudes during the sporadic-E conditions of November 1986.

**14. SUBJECT TERMS**

**15. NUMBER OF PAGES**
72

**16. PRICE CODE**

| 17. SECURITY CLASSIFICATION OF REPORT | 18. SECURITY CLASSIFICATION OF THIS PAGE | 19. SECURITY CLASSIFICATION OF ABSTRACT | 20. LIMITATION OF ABSTRACT |
|---|---|---|---|
| Unclassified | Unclassified | Unclassified | SAR |

## TABLE OF CONTENTS

## LIST OF ILLUSTRATIONS

## LIST OF ILLUSTRATIONS (CONT'D)

## LIST OF ILLUSTRATIONS (CONT'D)



## LIST OF TABLES

# OBSERVATIONS OF ELF PROPAGATION AT HIGH LATITUDES DURING THE SPORADIC-E CONDITIONS OF NOVEMBER 1986

## INTRODUCTION

Almost from its inception, researchers in extremely low frequency (ELF) radio propagation have speculated on the effects of disturbed ionospheric conditions. Over the years, it has been observed that, although the propagation of ELF signals is remarkable for its relative stability, these signals are nevertheless influenced by many of the same types of disturbances that afflict higher frequency bands. Indeed, some of the early measurements by Bannister [1975] and Davis [1976] revealed not only ELF's stable, predictive features (e.g., the smooth transitions through daytime and nighttime periods), but also its unexplainable, sudden decreases in nighttime signal strength.

One of the most dramatic natural events for the radio propagationist to study is the solar proton event (SPE). During polar-cap absorption (PCA) events, an earthly response to an SPE, energetic protons from the sun penetrate the polar ionosphere. In the process, interactions with a variety of atmospheric constituents result in an increase in the ionization density to altitudes of 30 km or less.

A few years ago, Fraser-Smith and Helliwell [1980] carried out a series of measurements of the properties of ELF spherics (at 75 Hz) at Byrd Station, Antarctica, during a moderately large SPE. Their measurements suggest that an SPE can significantly alter the characteristics of ELF signals as they propagate through the polar regions. Although there was a reduction in the mean amplitudes and rates of occurrence for these spherics, there was no polar "blackout."

In a paper by Katan and Bannister [1987], the first confirmed observations of cause and effect associations were reported that summarized the effects of an SPE on ELF wave propagation using a man-made source. During November and December 1982, ELF field-strength measurements were taken at one mid-latitude (Connecticut) and three high-latitude (within the polar-cap in Greenland and under the auroral oval in both Norway and the Gulf of Alaska) locations. Two small PCA events occurred on 22 and 24 November while a moderate-to-large event occurred on 8 December. ELF propagation effects were observed before, during, and after these events.

The most striking observation was the high value of inferred attenuation rate calculated during disturbed propagation conditions along the Wisconsin-to-Gulf of Alaska path (2.51 dB/Mm at night and 2.66 dB/Mm during the day). The attenuation rate was substantially higher, more than 1 dB larger, than that measured during ambient or quiet propagation conditions for this path. Less strident were the effects along the Wisconsin-to-Greenland and Connecticut-to-Norway paths.

These observations, however, only solved part of the puzzle. Few, if any, of the sudden signal decreases reported by Bannister [1982] occurred during periods of PCA events. Most of these fades were during nighttime conditions. Because of this, a moving nocturnal sporadic-E layer was suggested as a prime candidate for the cause of these nighttime abnormalities.

## THE IMPORTANCE OF THE IONOSPHERIC WAVEGUIDE BOUNDARY

In a series of papers, Greifinger and Greifinger [1978, 1979a, 1979b] derived simple-form approximate expressions for the transverse electromagnetic (TEM) eigenvalues (propagation constants) for ELF propagation in the earth-ionosphere waveguide. The eigenvalues obtained by their methods were in agreement with the classical full-wave numerically calculated eigenvalues. The results of these techniques can be applied for the rapid evaluation of the effects of a variety of ionospheric disturbances on ELF communication systems. They further showed that the propagation constant depends on four parameters (two altitudes and a scale height associated with each).

The lower altitude, $h_0$, is the height at which the conduction current parallel to the magnetic field becomes equal to the displacement current. The associated scale height, $¥_0$, is the local scale height of the parallel conductivity. Under daytime ionospheric conditions, the upper altitude, $h_1$, is the height at which the local wavenumber becomes equal to the reciprocal of the local scale height, $¥_1$ of the refractive index. Under the simplest nighttime conditions, the second set of parameters is replaced by the altitude of the E-region bottom, $h_E$, and the local wavenumber just inside the E-region is inversely proportional to the electron density. Within this formulation there are two principal attenuation mechanisms. In the vicinity of the lower altitude, there is Joule heating by the longitudinal currents while at the upper altitude there is leakage of the whistler component of the ELF wave (x wave).

The Greifingers' development and the extensions presented in Bannister [1985] and in Katan and Bannister [1985] provide a convenient method of depicting the interrelationship of both the D- and E-regions on ELF propagation. Some typical values are listed in table 1 for the Connecticut to Norway propagation path.

As can be seen from table 1, the inferred ionospheric reflection height at ELF is approximately 50 km during the day and 75 km during the night. During the initial phases of a PCA, the nighttime ionosphere is further depressed and takes on characteristics of a daylight ionosphere. However, this effect seems to last only for a few hours, the reasons for which remain unknown.

***Table 1. Connecticut/Norway Path Interpretation at 76 Hz***

| Path Condition | Year | $\alpha$ (dB/Mm) | $h_0$ (km) | $¥_0$ (km) | $h_E$ (km) |
|---|---|---|---|---|---|
| Quiet Day | 1982 | 1.20 | 56.7 | 3.07 | |
| Quiet Night | 1982 | 1.12 | 71.6 | 2.66 | 92.0 |
| Disturbed Night | 1982 | 1.68 | 60.1 | 3.67 | |
| Disturbed Sunrise | 1984 | 1.77 | 65.1 | 4.19 | |

## SUMMARY OF THE PROPERTIES OF THE D- AND E-REGIONS

Within the atmosphere, the reflection region at ELF is referred to as the mesosphere and includes the lower ionosphere. Much of the lower ionosphere, the upper D- and E-regions, is under solar control. (See table 2 for types of sporadic E [Wakai et al. 1984].) The first of these regions, the D-region, is generally shielded from most of the solar short-wave radiation that is responsible for ionizing the air molecules in the upper layers. However, in the 1020 to 1220 Å band, there are certain windows above the D-region in which no absorption occurs. One source, a hydrogen line called Lyman-$\alpha$ (1215 Å), is thus able to penetrate into the D-region through the upper atmosphere. Within this altitude regime, the solar dependence (proportional to the solar-zenith angle) exists to about 70 km. Below this altitude, this dominance is foreshadowed by galactic cosmic rays that quickly become the dominant source of ionization by 65 km.

*Table 2. Types of Sporadic-E [Wakai, 1985]*

| Type | Description |
|---|---|
| f<br>Flat | The virtual height of this type does not change as the frequency increases. |
| l<br>Low | This is a flat Es trace appearing at a height equal to or less than the minimum virtual height of the normal E-layer. |
| c<br>Cusp | This is an Es trace that shows a comparatively symmetrical cusp at a frequency at or below $f_0E$. |
| h<br>High | This is a trace that shows a discontinuity in height with the normal E-layer trace. |
| q<br>Equatorial | This is a trace that is commonly found in the vicinity of the magnetic dip equator. |
| r<br>Retardation | This trace shows an increase similar in shape to the group retardation in virtual height near the top frequency. |
| a<br>Auroral | This is exclusively observed in high latitudes in association with auroral activity. |
| s<br>Slant | This is a diffuse trace where its virtual height steadily increases with frequency. |
| d<br>D-region | A weak diffuse trace that appears normally at heights below 95 km. |
| k | This indicates the presence of a particle-E layer. |

Remarkably, the normal behavior of the E-region is very close to that put forward by Chapman in the early days of radio. The E-region is strongly dependent on the sun for its formation. On average, the critical frequency of this region varies with the solar zenith angle ($\tau$) as $[\cos \tau]^{1/4}$ which implies that the peak electron density varies as $[\cos \tau]^{1/2}$. This dependence on the sun is further enhanced by a weaker dependence on the solar cycle. Soft x-rays can ionize various constituents in this region. The intensity of these incident x-rays varies considerably with the solar cycle and is empirically accounted for through R, the Zurich sunspot number.

Despite these solar dependencies, the E-region does not disappear entirely at night but remains weakly ionized, perhaps by meteors that burn up in the atmosphere [Hargreaves 1979].

Near or within the E-region, there often exists an irregular or enhanced ionization that results in an electron density inconsistent with the predictions based on the above solar dependencies. This may result in regions of thick or thin, highly ionized strata or groups of scattered patches of ionization. These departures from normal behavior are called sporadic-E, which is in general present to some degree at all latitudes. Both the equatorial and auroral zones show no seasonal dependence. However, the occurrence of sporadic-E in the equatorial zone peaks during the day while for the auroral zone, the peak is during the night. At mid-latitudes there is a seasonal dependence with peaking at noon in the summer.

Over the last decade, a significant theoretical foundation was formulated by Barr [1974], Pappert and Moler [1978] and others regarding the influence of a sporadic-E layer that encompasses the nighttime ELF propagation path. Additional studies by Pappert and Shockey [1978] and Pappert [1980] indicated that a sporadic-E patch roughly 1000 km by 500 km could account for many of the more commonly observed signal fades in the 3 to 4 dB range.

## DIAGNOSTIC INSTRUMENTATION FOR OBSERVING THE IONOSPHERE

The irregular structure of the lower ionosphere has been monitored through ionospheric soundings from the earliest days of radio. From its beginnings in 1925, such soundings provided the impetus for many technological changes that grew out of the understanding of radio propagation, which these measurements provided.

The ionosounder is a vertically incident, high frequency (HF) radar that provides information about the virtual height and critical frequency of the ionospheric reflections. An ionogram is a recording of the observed delay time of the emitted radio frequency (RF) pulses as a function of transmitted frequency, generally in the range of 1 MHz to 20 MHz. The virtual height is calculated from the delay time it takes the transmitted signal to return to the monitoring point from each reflection(s). Since radio waves travel slower than light, the recorded heights are somewhat higher than the true reflection heights. The critical frequency is the highest frequency that can be reflected from a specific ionospheric layer.

For this experiment, ionospheric soundings provided the primary means of detailing the structure of the lower ionosphere in the vicinity of the receiver. Additional geophysical data, detailing fluctuations in the earth's magnetic field (magnetometer) and the degree of ionospheric absorption (riometer), were made on a routine basis by personnel at the Andøya Rocket Range in northern Norway. Those data coincident with this experiment were requested for processing at the Naval Underwater Systems Center (NUSC) -- now the Naval Undersea Warfare Center Division. This information is also presented in this report and provides an overview of the structure and disturbed quality of the ionosphere. Details of the digital ionosonde, riometer and magnetometer are given in the Appendix.

## DATA COLLECTION

Ionospheric soundings were made with the digital ionosonde located at the Andøya Rocket Range (geographical coordinates: lat. 69.30° N; long. 16.00° E). The operational characteristics of the ionosonde employed for this experiment were

- a frequency range of 1.0 to 20.0 MHz,
- a height range of 400 km, and
- a height resolution of 2 km.

Ionograms and ELF recordings were made over the course of two weeks, from 3-7 November and 10-14 November in 1986.

One ionogram was made every 15 minutes for each hour of the ten day experiment. One set of ionograms was archived at the site and another copy was sent to NUSC for scaling. The virtual height and the critical frequencies for each reflected layer were scaled and entered into a database. If there were no reflections due to ionospheric absorption, this was so indicated. It should be noted that ionograms were not available on hardcopy for every hour of each day for a variety of reasons, most having to do with the unattended operation of the HP ThinkJET printer. However, approximately 80 percent of the potential time is represented. For the ELF data, nearly 90 percent of the available time is represented. Riometer and magnetometer data were available for the entire experiment.

The ELF signals were recorded on analog tape and sent back to NUSC for data reduction. All pertinent information, including timing pulses, synchronization, and calibration signals, were recorded on the tape at the site. Each tape contained approximately 12 hours of data. As the tapes must be played back in real-time, this is also the amount of time required to examine each tape. The tapes were processed through an ELF receiver at NUSC.

During data reduction, estimates of relative signal and effective-noise* levels, signal-to-noise ratios (SNR), and relative signal phase are acquired. By monitoring the level of a continuous calibration signal, also recorded on tape, absolute signal and effective-noise levels may also be obtained. Depending on the SNR, these estimates can be obtained as often as every 5 minutes. In general, the receiver manages the reception time to be the minimum required (in 5 minute increments) to achieve a specified SNR. The value of SNR is a function of the receiver operating specifications.

Riometer and magnetometer data for the entire period were sent to NUSC on a digital tape for analysis. The quiet day curve was subtracted from each day's riometer values. The resultant values are plotted for in figures 12 through 21. The three axial, magnetometer values appear in figures 22 through 31.

---

* The effective noise spectrum level (in dBA/m • √{1 Hz}) is defined as the spectrum level of ELF noise at the signal frequency divided by the improvement (in SNR), using nonlinear processing.

## OBSERVATIONS

The Space Environment Services Center (SESC) in Boulder, Colorado, reported [SESC 1986a, 1986b] the following highlights for the observation periods in question. For the week 3-7 November 1986, solar activity was very low. There were several radio sweeps, burst and noise storms, but no new regions on the sun were numbered. The various daily solar indices showed moderate activity during the first half of the week. The Ottawa 10.7 cm radio flux was higher during the first week of experimentation. The radio flux observed values were 82 to 84 during the first half of the week and dropping to 73 by weeks end. A similar pattern was observed for the sunspot number (SSN) with an SSN high of 50 being observed on 4 November 1986. By the end of the week, this index returned to the low values ($0 \leq SSN \leq 15$) normally associated with the current solar cycle minimum.

The geomagnetic field was unsettled to active on 3 November, the first day of the experiment. On 3 November, a sudden storm commencement (SSC) was observed at mid-latitude at Fredericksburg late (at 2354 UT*). The SSC was also observed at high latitude as the magneto-meter observations at Andøya clearly demonstrate (figures 22 and 23). This event was followed by minor to major storm conditions on 4 November (see table 3) decreasing from active to minor storm conditions on the following day. By 1500 UT on 5 November, the storm ended. The remainder of the period was generally quiet to unsettled.

***Table 3. Daily Solar and Geometric Indices [SESC, 1986a, 1986b]***

| | Fredericksburg | | Anchorage | | |
|---|---|---|---|---|---|
| | Middle Latitude | | High Latitude | | |
| Date | A | K-Indices | A | K-Indices | SSN |
| 03 November | 12 | 2-3-2-1-1-1-2-5 | 16 | 2-3-4-3-2-3-3-4 | 46 |
| 04 November | 42 | 6-5-4-5-5-4-4-4 | 91 | 5-7-6-7-6-6-7-4 | 50 |
| 05 November | 18 | 5-5-4-2-1-1-1-2 | 38 | 5-5-6-6-3-3-2-3 | 37 |
| 06 November | 9 | 2-2-3-1-2-1-3-3 | 14 | 3-2-3-2-3-3-4-3 | 32 |
| 07 November | 5 | 3-1-1-1-2-1-0-2 | 8 | 3-2-2-2-2-2-2-2 | 27 |
| 10 November | 4 | 1-2-0-0-1-1-2-2 | 8 | 2-2-2-2-2-1-3-3 | 11 |
| 11 November | 14 | 2-5-4-2-2-1-2-2 | 21 | 3-4-6-3-2-2-3-2 | 0 |
| 12 November | 7 | 4-2-2-1-1-1-0-1 | 10 | 4-3-3-2-2-0-2-1 | 0 |
| 13 November | 3 | 1-0-1-0-2-1-2-1 | 9 | 2-1-2-2-3-3-3-2 | 0 |
| 14 November | 5 | 2-2-1-2-1-1-1-1 | 7 | 2-1-1-3-3-1-2-2 | 12 |

*UT, universal time.

No significant proton enhancements were observed at satellite altitudes. A Forbush decrease* began early on 4 November and continued through 5 November. A brief polar cap absorption event associated with the geomagnetic storm was observed to last for one hour at the beginning of 4 November.

Solar and geomagnetic activity was much lower for the second week of the experiment. Solar activity was very low. The SSN values for the second week were well within the current solar minimum range. Again during this second period of measurements, there were no significant proton enhancements at satellite altitudes. There was a major to minor storm at high latitudes in the early hours on 11 November. The geomagnetic field gradually reverted to quiet to unsettled conditions by the end of the experiment.

Typically, the F2-layer is dominant during the daytime. This dominance is clearly illustrated for the hours 0500 to 1800 UT in figure 1. In this figure, the monthly median values of the critical frequency of the F2-region for the month of November is presented as a function of the hour of the day (UT). The critical frequency ($f_0F2$) starts to increase at sunrise, peaking about an hour after the sun reaches its zenith, then decreasing until midnight when it stabilizes. Conversely, the virtual height (h'F2) begins to decrease at sunrise, reaching a minimum about the same time the critical frequency has peaked and then increases until midnight. The inclusion of the F-region scaling serves as an additional diagnostic for gleaning the relative stability of the lower altitudes. This layer is normally present and is the first to reform after an absorption event.

Using the sunrise and sunset times in table 4, periods of ionospheric disturbances (PID) were derived from scaled ionograms. In general, these PIDs (figures 2 through 11) show the expected F2-region variation for the day. These figures illustrate both the critical frequency versus time (the "A" figures) and the virtual height as a function of time of day (the "B"figures). In all cases, the upper pane in the figures indicates the scaled values for all layers present. The color coded bar (which is defined on the bottom of each figure) indicates the specific region present. The lower pane indicates in the color ROSE those periods for which there was a sporadic-E condition. This catalogs all sporadic-E conditions observed, including type 'a' for which neither critical frequencies nor virtual heights are attributable. Periods in BLUE indicate absorption periods. Periods for which no data are available are indicated by the absence of data in both the upper and lower panes. A good example of the classic F2-region behavior occurs on 12 November (figures 9A and 9B). The F2-region decreases after sunset and seemingly disappears primarily because of the blanketing of the layer caused by the Es-region. Periods of absorption can be seen in the late evening hours on 3 November (figures 2A and 2B).

All the ELF reception data (as illustrated in figures 32 through 41) contain three pieces of information, i.e., (1) the relative signal level (RED), (2) the 90 percent confidence interval (SILVER), and (3) the number of message measured intervals (MMIs) required for the estimate (BLUE) or if this number is multiplied by 5, it is the actual time in minutes. Figure 42 is the hourly average ELF signal strength observed during the ten day campaign period.

---

* A Forbush decrease generally starts at or a few hours after the onset of a geomagnetic storm. The cosmic ray intensity may decrease rather sharply for a day to a minimum that can be as much as 10 percent below the original value. The intensity then increases rather slowly, generally taking several days to recover [Valley 1965].

*Table 4. Sunrise and Sunset Times (UT) Over the Andøya Rocket Range*

| | Altitude of 100 km | | Altitude of 300 km | |
|---|---|---|---|---|
| Date | Sunrise | Sunset | ≈ Sunrise | ≈ Sunset |
| 03 November | 05h 05m | 16h 13m | 03h 45m | 17h 50m |
| 04 November | 05h 08m | 16h 10m | 03h 49m | 17h 45m |
| 05 November | 05h 12m | 16h 06m | 03h 53m | 17h 41m |
| 06 November | 05h 15m | 16h 03m | 03h 57m | 17h 36m |
| 07 November | 05h 18m | 16h 00m | 04h 01m | 17h 32m |
| 10 November | 05h 28m | 15h 51m | 04h 13m | 17h 18m |
| 11 November | 05h 32m | 15h 48m | 04h 18m | 17h 13m |
| 12 November | 05h 35m | 15h 45m | 04h 22m | 17h 09m |
| 13 November | 05h 38m | 15h 42m | 04h 26m | 17h 04m |
| 14 November | 05h 41m | 15h 39m | 04h 30 m | 17h 00m |

The 90 percent confidence interval depicted for each estimate is based on the average SNR in effect during the estimation period. The value of SNR is such that each signal estimate has a rather large uncertainty (approximately ±3 dB) associated with it. Ideally, one would prefer a smaller confidence interval, i.e., one that is less than any changes one wishes to observe. Along with a smaller confidence range, a finer time resolution (ideally an estimate every MMI or 5 minutes) would also be desirable.

The first of these features (a smaller confidence range) is primarily a function of the receiver's software and is not easily changed. The second feature (finer time resolution) is a function of the SNR. At this point, because of the near optimum noise processing performed within the ELF receiver, one would essentially have to increase the transmitter power in order to increase the SNR.

As mentioned earlier, SESC reported that a brief PCA was observed on 4 November between 0015 and 0115 UT. Also reported was the major to minor geomagnetic storm conditions that lasted throughout 4 November and into 5 November and ended sometime around 1500 UT. Both the riometer and magnetometer data for these two days corroborate these conditions.

On 4 November, the riometer data (figure 13) shows two maximum absorption periods. The brief PCA event itself is vividly recorded both in the riometer data (figure 13) and the magnetometer data (figure 23), in particular the H-axis (DARK BLUE). The other major absorption period occurred between 0500 and 0645 UT. In both cases, one can see corresponding periods of absorption indicated on the PIDs (see the lower panes of figures 3A and 3B). Throughout the day, prolonged periods of sporadic-E conditions are also present. Despite this extensive activity,

period occurred between 0500 and 0645 UT. In both cases, one can see corresponding periods of absorption indicated on the PIDs (see the lower panes of figures 3A and 3B). Throughout the day, prolonged periods of sporadic-E conditions are also present. Despite this extensive activity, there are no indications that there was any abnormal behavior at ELF (figure 34). As noted earlier, the large confidence limits associated with each signal estimate may mask any effect.

The riometer and magnetometer data for 5 November exhibit the full duration of the storm activity. Unfortunately, because of a paucity of soundings on 5 November, one cannot monitor the ionospheric recovery from this particular storm.

The remainder of the experimental period is relatively quiet except for the occurrence of two minor storms. Both of these events are clearly recorded by the riometer and the magnetometer--the first on 11 November (figures 18 and 26), occurred between the hours of 0600 and 0900 UT (K=6 Observed) and the second, on 12 November (figures 19 and 27) between 0000 and 0300 UT (K=4 Observed). There is neither ionosonde nor ELF data for this time period.

## CONCLUSIONS AND RECOMMENDATIONS

The first ever co-locational, simultaneous measurements of the earth magnetic field, incoming cosmic energy, and the structure of the ionosphere and ELF signal variations (at a site 20 km distant) were made over a two week period during the first half of November 1986. During this time period, there were several minor geomagnetic storm periods, as well as a major storm event. Also occurring was a brief PCA event associated with the major storm.

Despite the presence of prolonged periods of ionospheric absorption interspersed with sporadic-E conditions, there is no clear indication of any effect at ELF.

A repeat of this experiment would be strongly recommended after the U.S. Navy's second ELF transmitter becomes operational. This should permit smaller observational times and, on occasion, smaller confidence limits because of the increased signal strength associated with the combined transmitting facility.

# Monthly Mean Values for November

## Critical Frequency vs. Time

Source: CCIR Report 340; Oslo, 1966

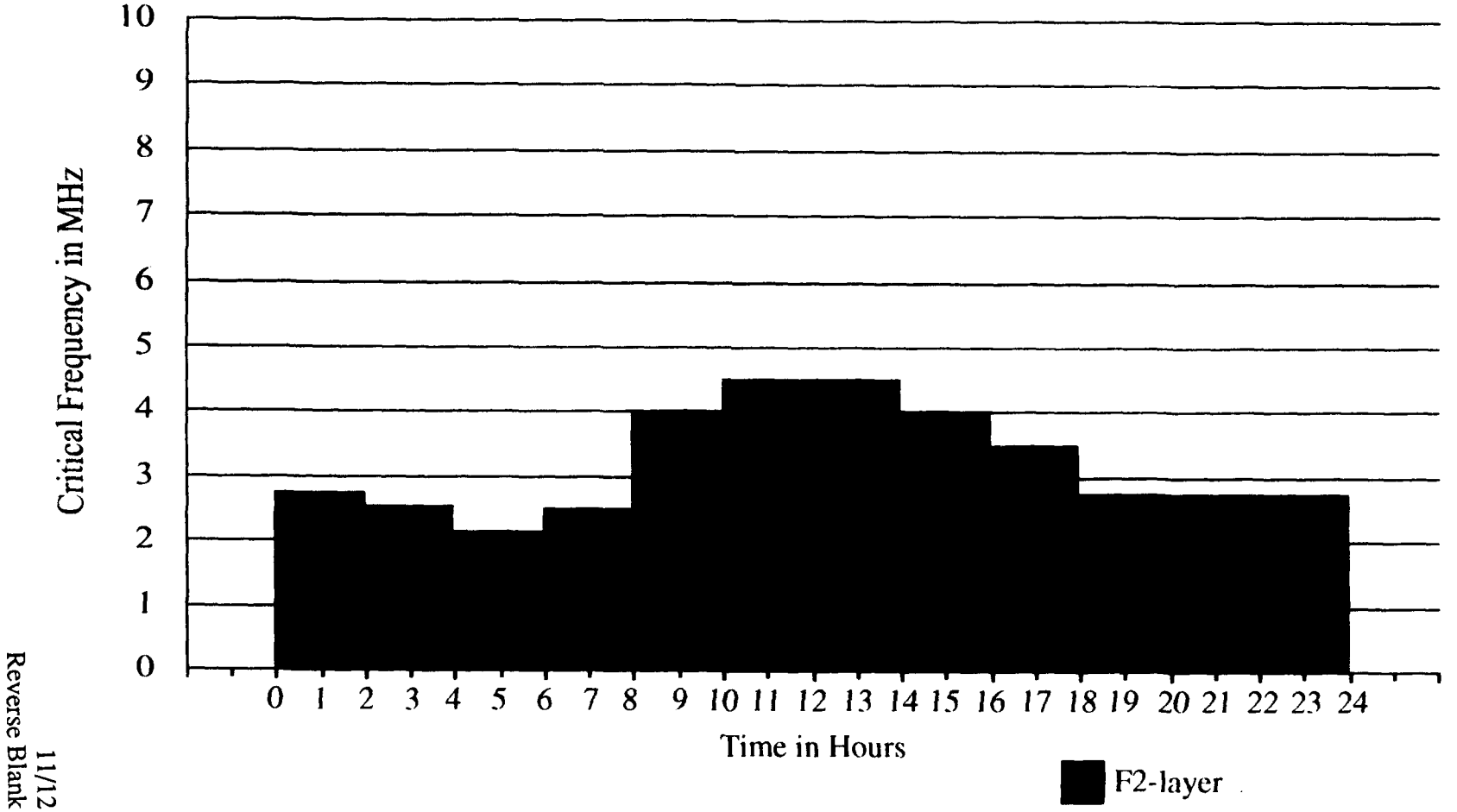


Figure 1. Monthly Mean Values for November

Reverse Blank 11/12

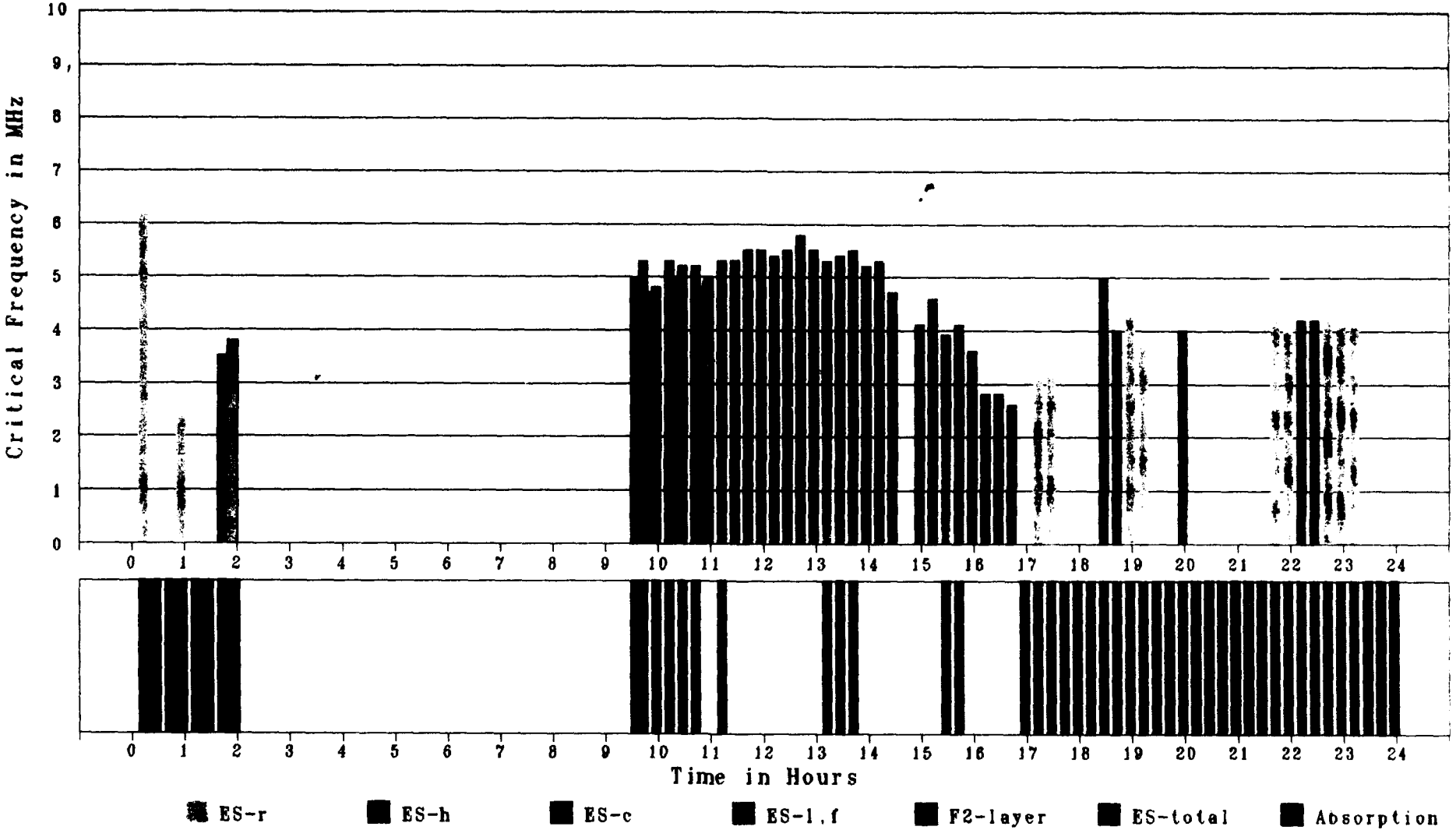


Figure 2A. Critical Frequency vs. Time

Figure 2. Periods of Ionospheric Disturbances, 3 November 1986

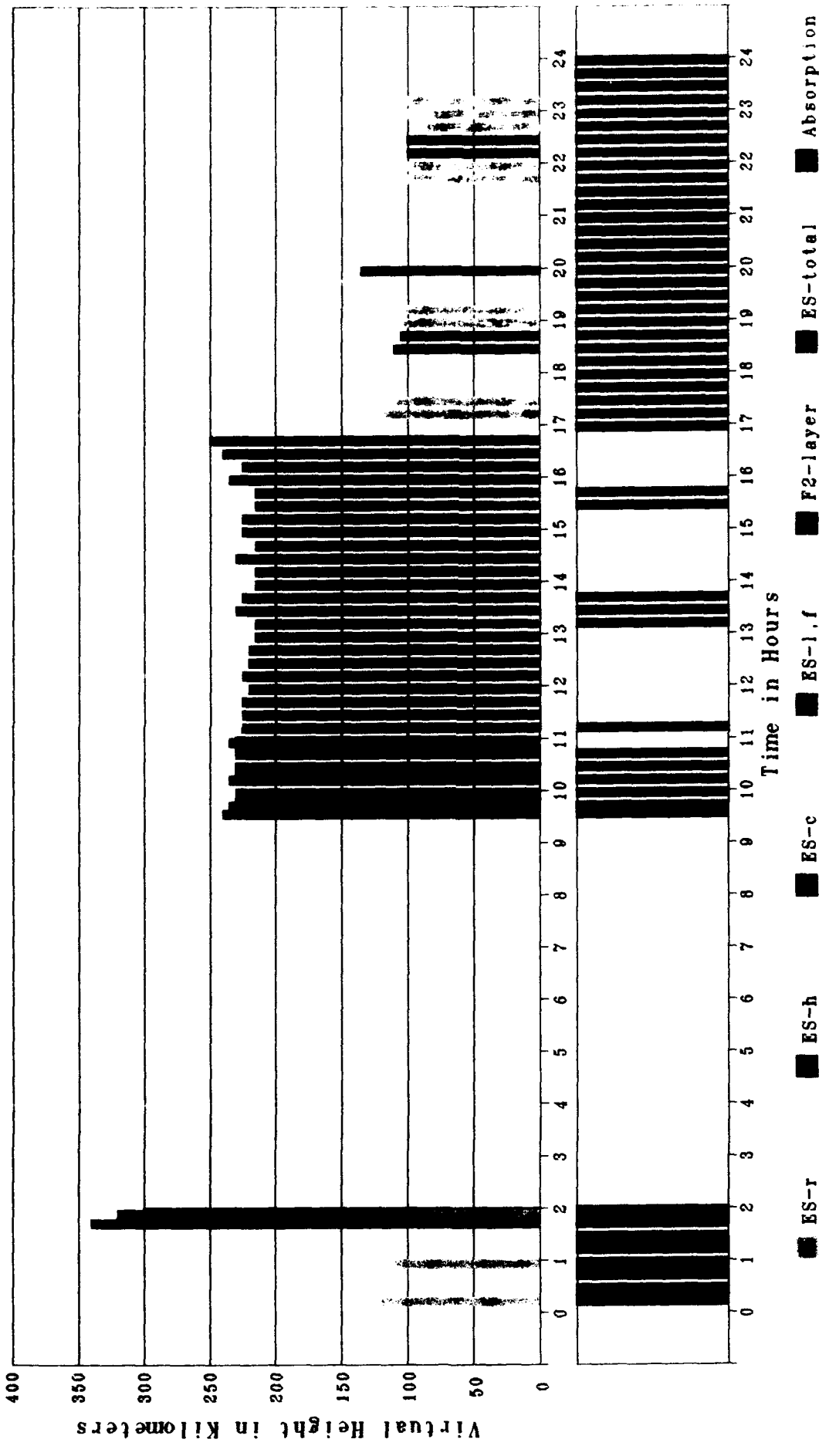


Figure 2B. Virtual Height vs. Time

Figure 2. Periods of Ionospheric Disturbances, 3 November 1986 (Cont'd)

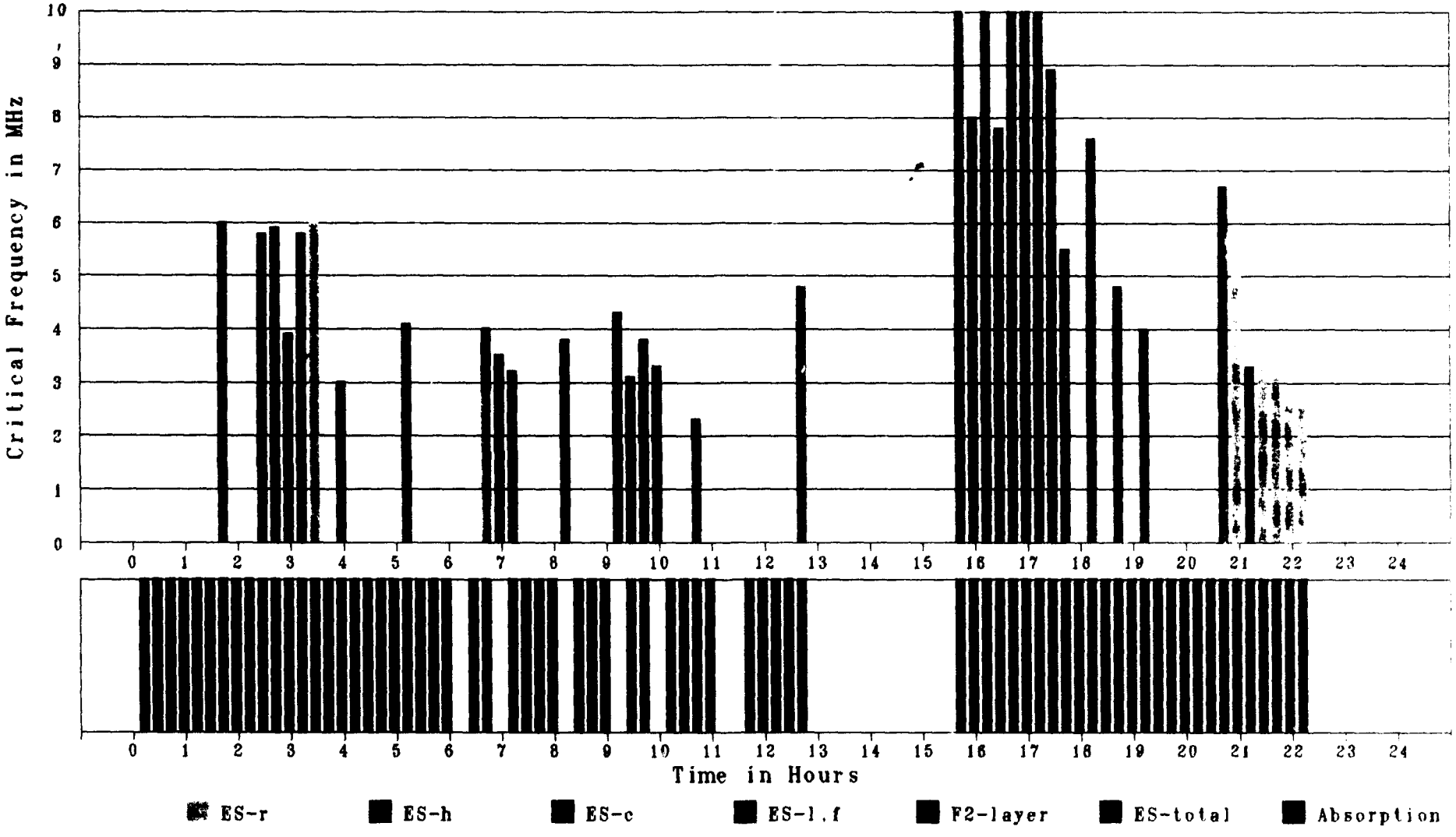


Figure 3A. Critical Frequency vs. Time

Figure 3. Periods of Ionospheric Disturbances, 4 November 1986



Reverse Blank

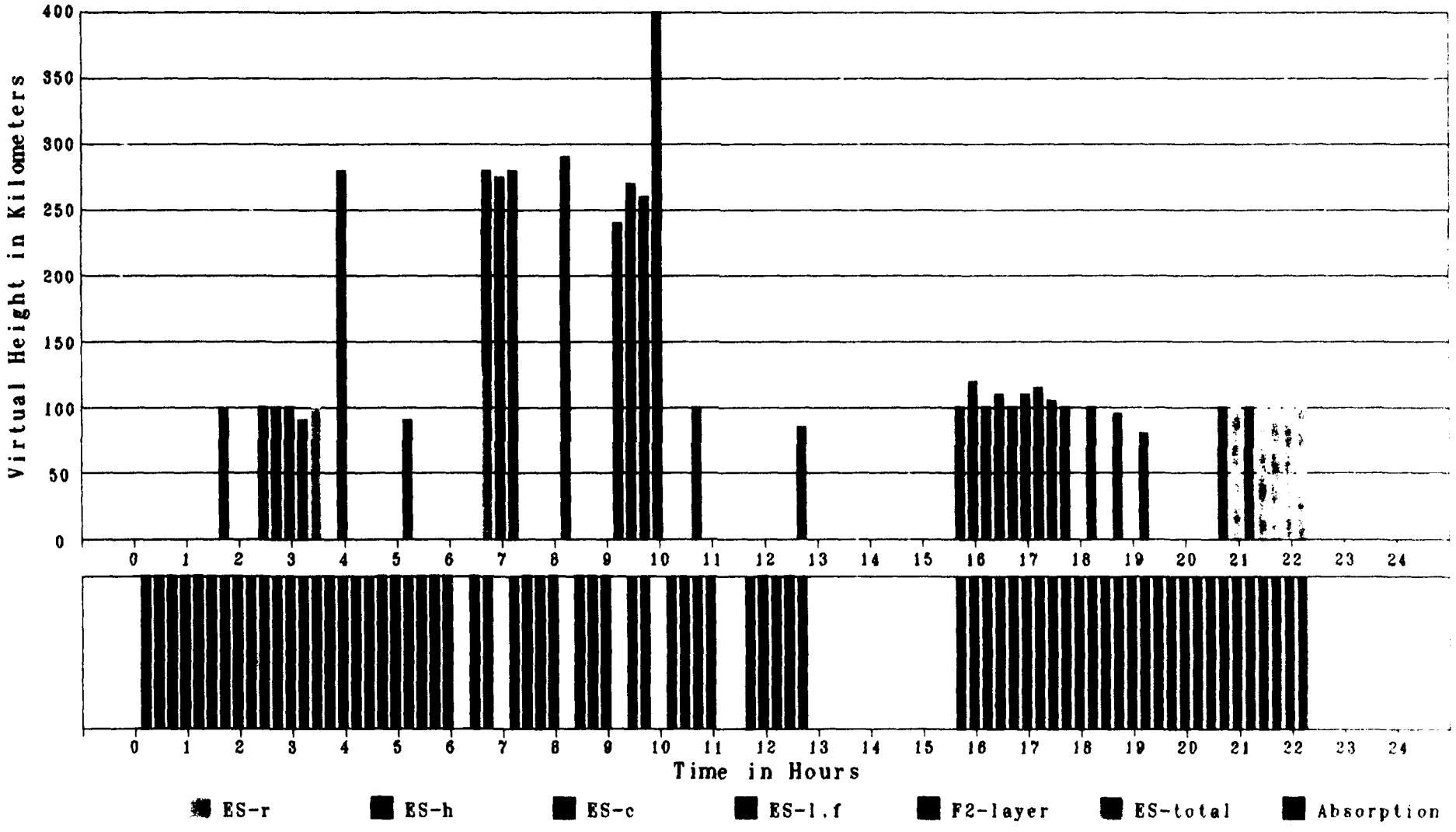


Figure 3B. Virtual Height vs. Time

Figure 3. Periods of Ionospheric Disturbances, 4 November 1986 (Cont'd)



Reverse Blank

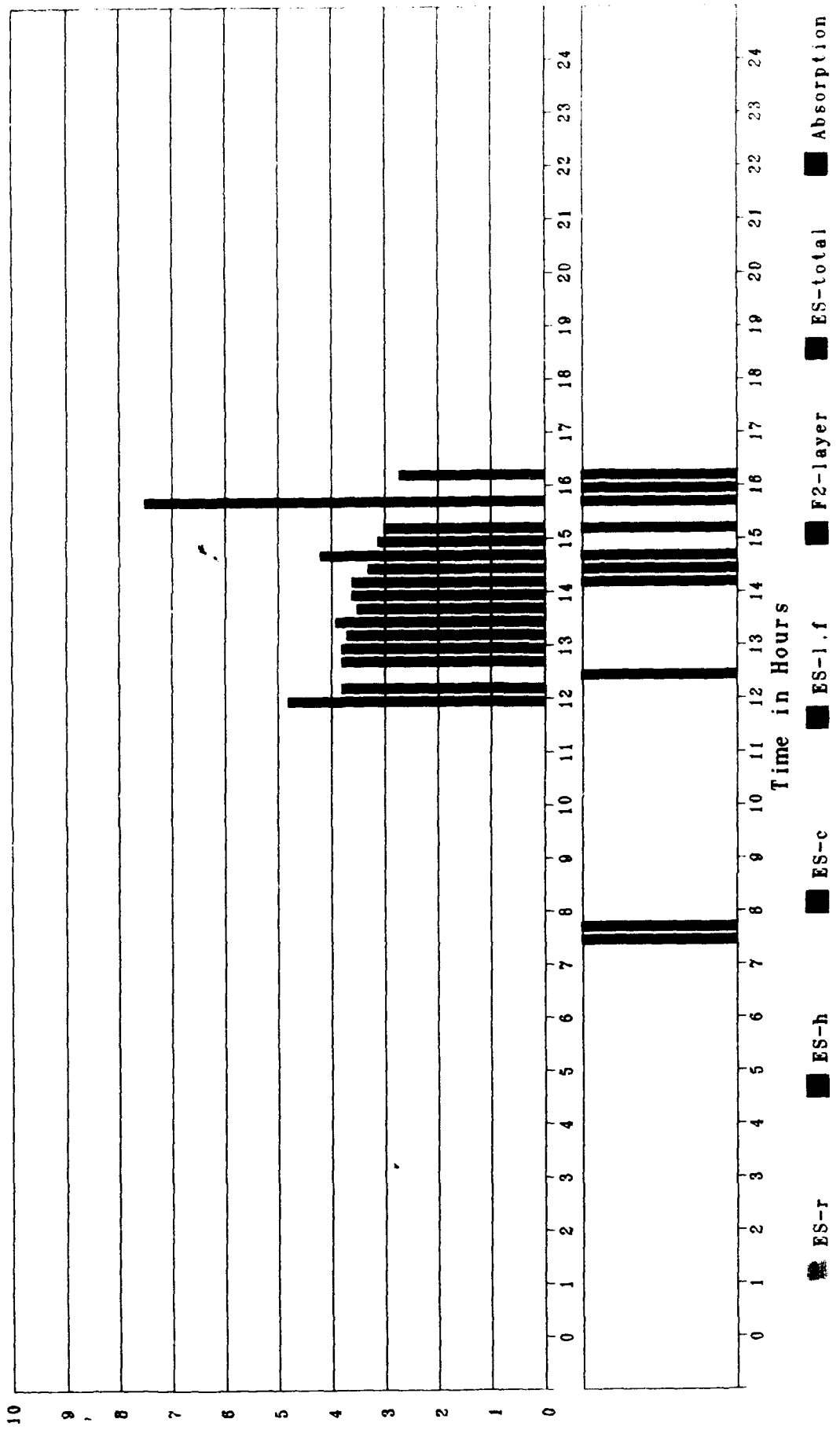


Figure 4A. Critical Frequency vs. Time

Figure 4. Periods of Ionospheric Disturbances, 5 November 1986

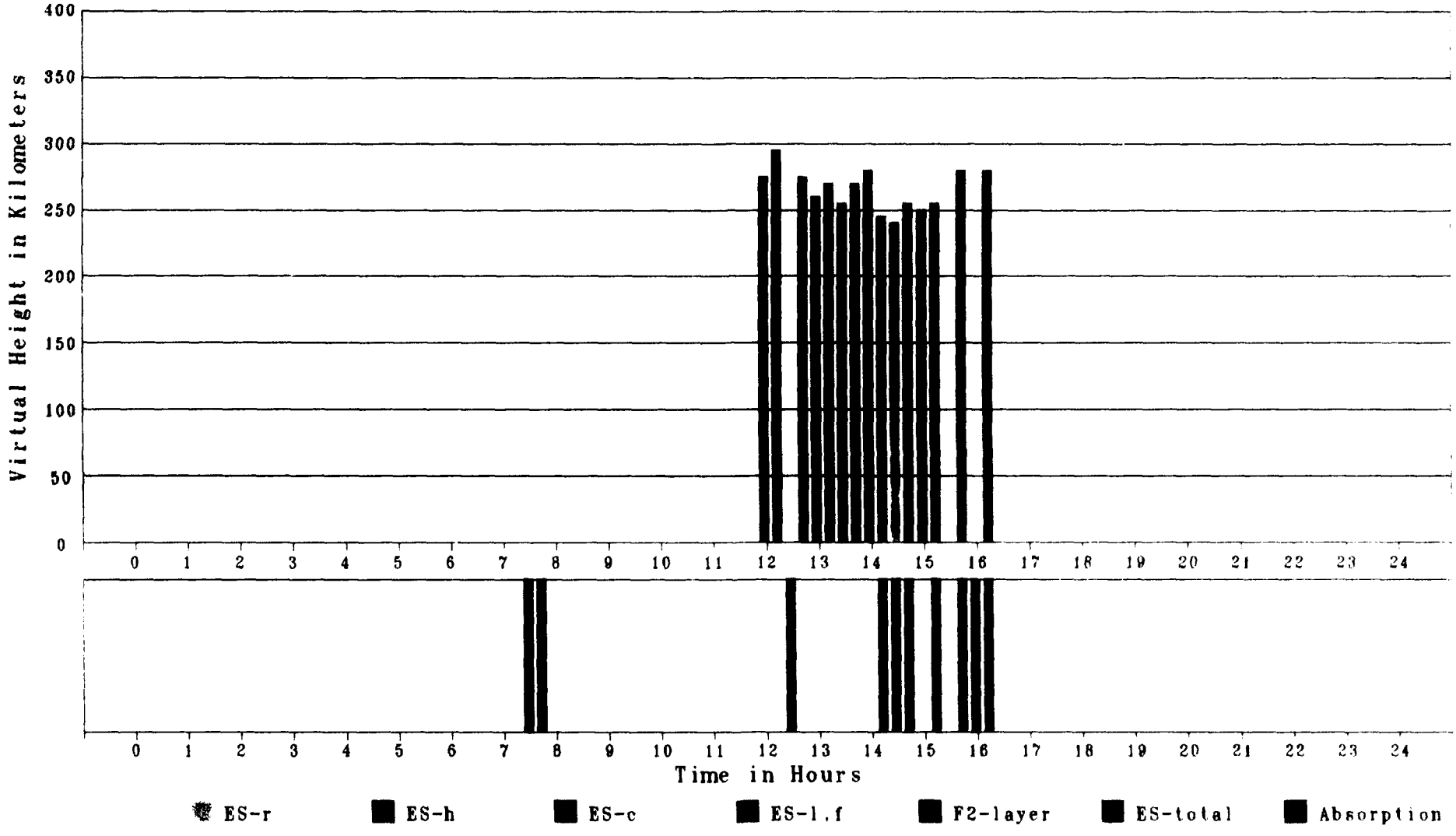


Figure 4B. Virtual Height vs. Time

Figure 4. Periods of Ionospheric Disturbances, 5 November 1986 (Cont'd)



Reverse Blank

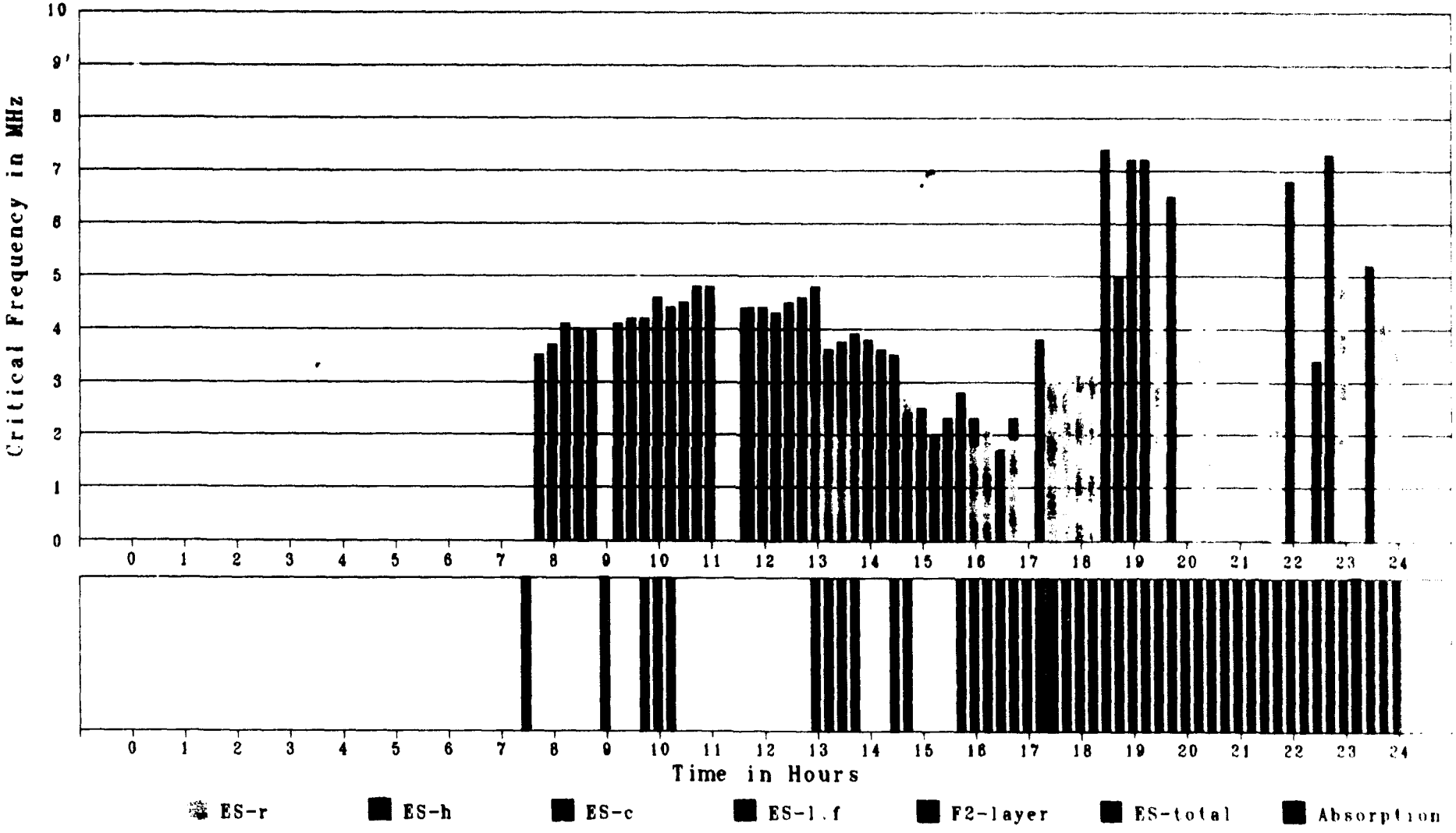


Figure 5A. Critical Frequency vs. Time

Figure 5. Periods of Ionospheric Disturbances, 6 November 1986

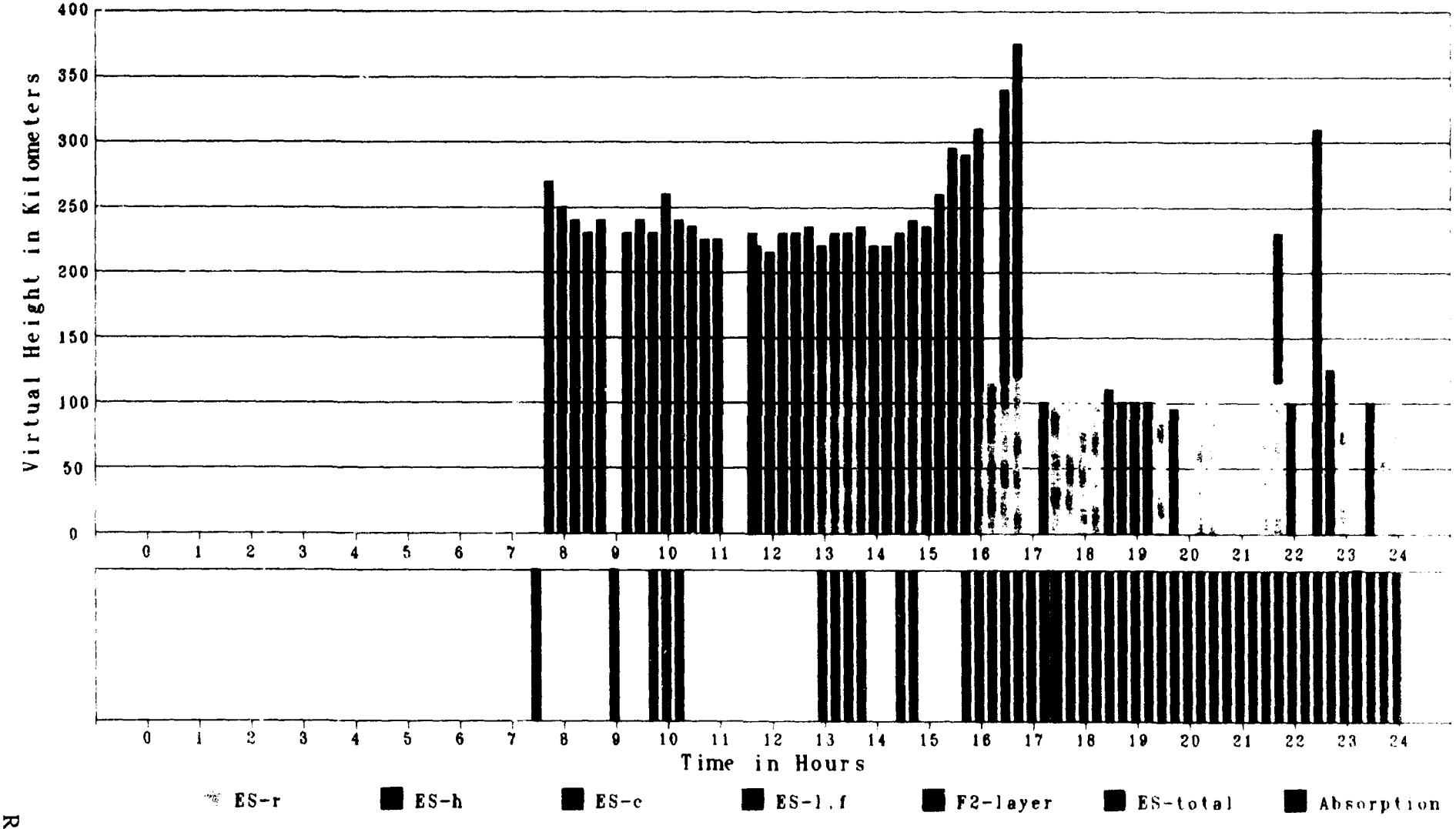


Figure 5B. Virtual Height vs. Time

Figure 5. Periods of Ionospheric Disturbances, 6 November 1986 (Cont'd)

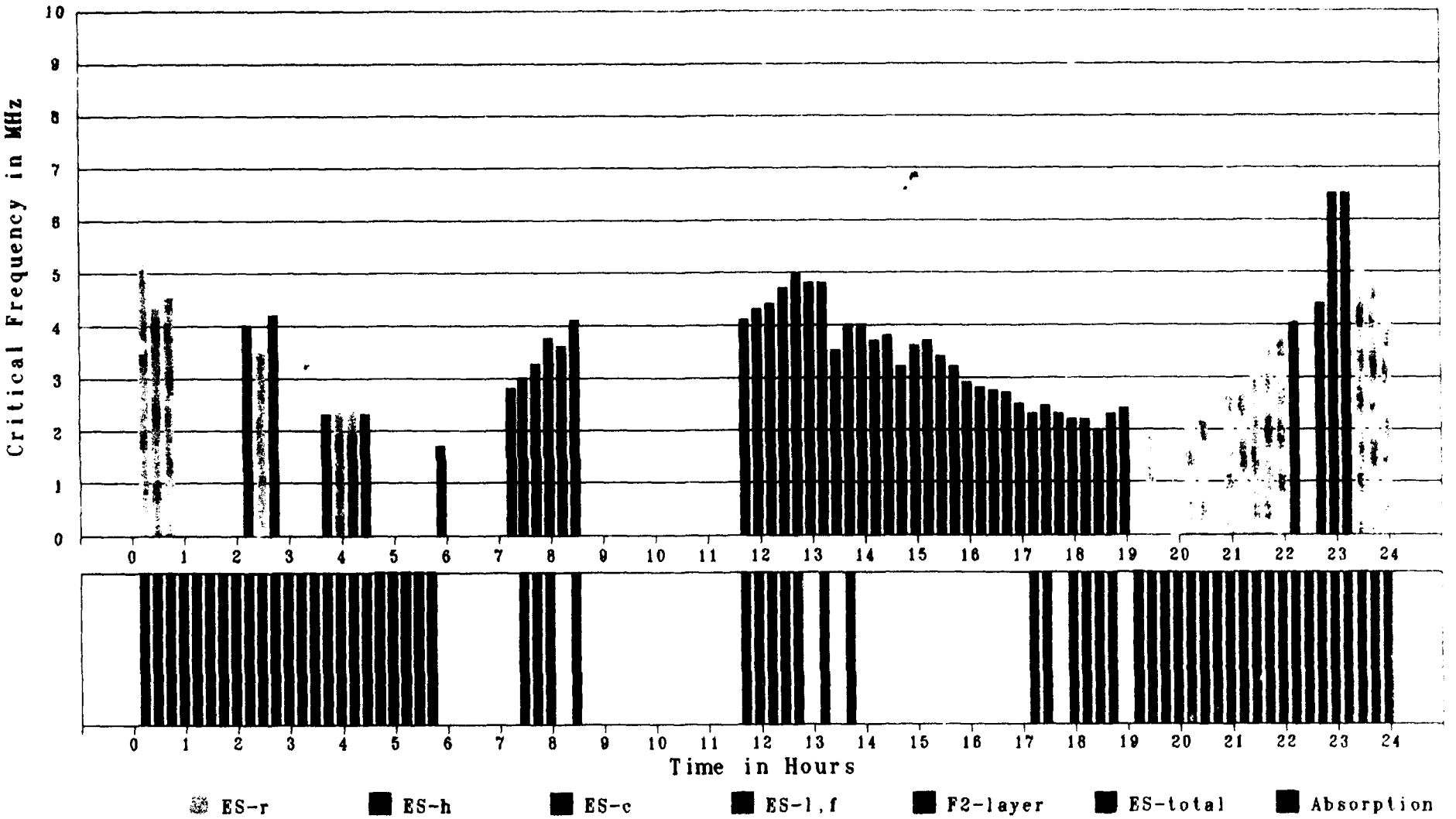


Figure 6A. Critical Frequency vs. Time

Figure 6. Periods of Ionospheric Disturbances, 7 November 1986



Reverse Blank

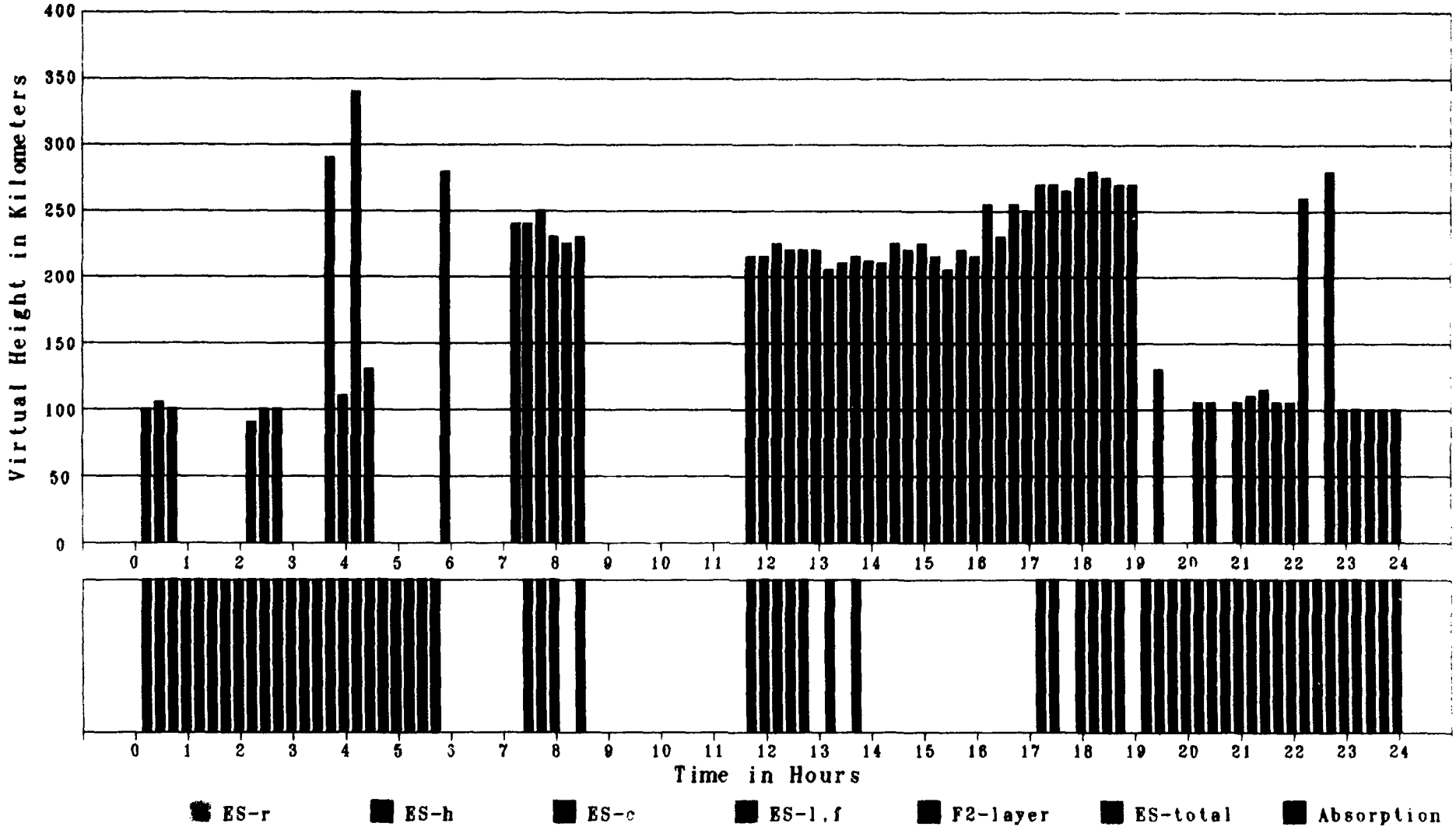


Figure 6B. Virtual Height vs. Time

Figure 6. Periods of Ionospheric Disturbances, 7 November 1986 (Cont'd)

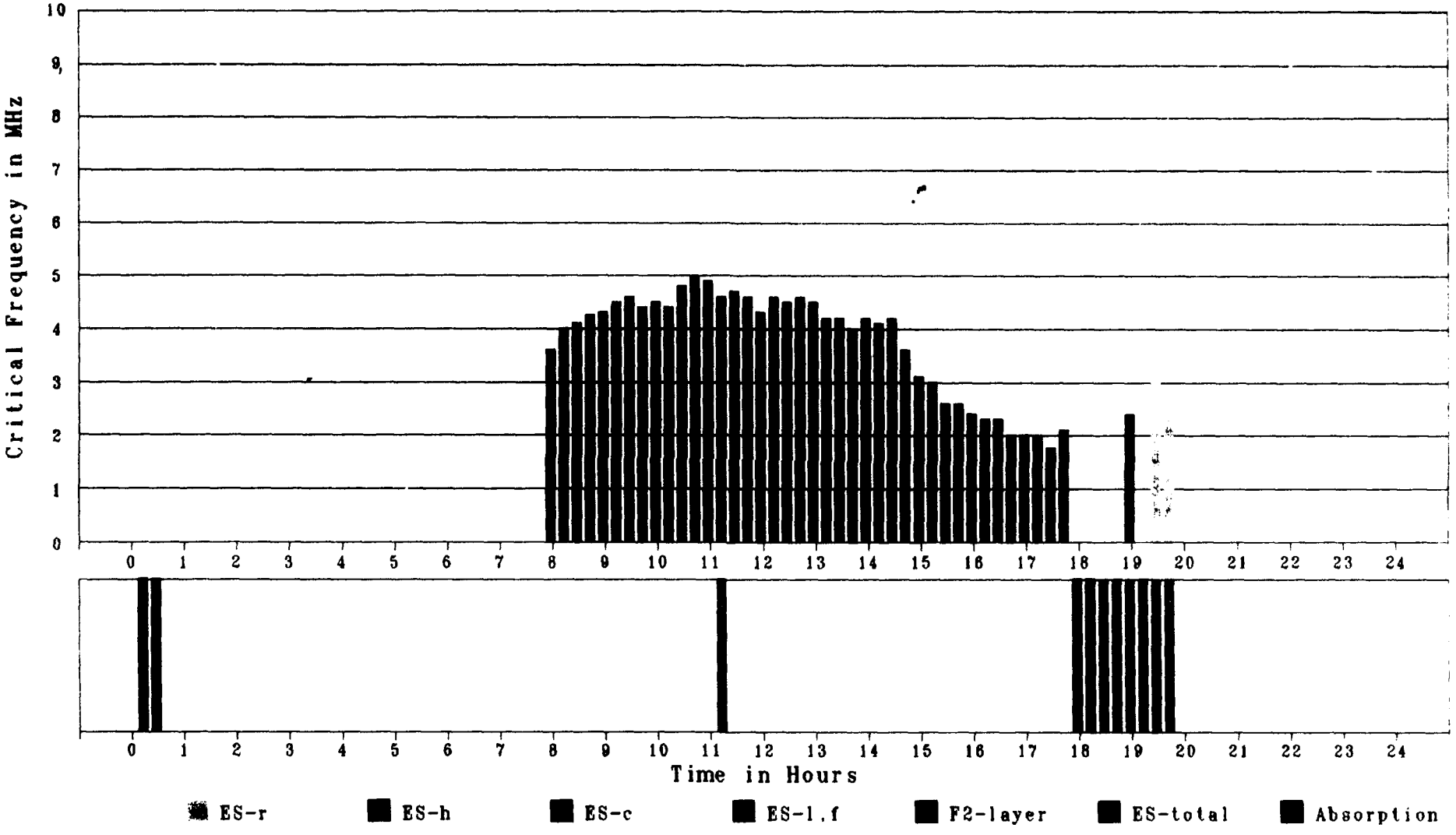


Figure 7A. Critical Frequency vs. Time

Figure 7. Periods of Ionospheric Disturbances, 10 November 1986



Reverse Blank

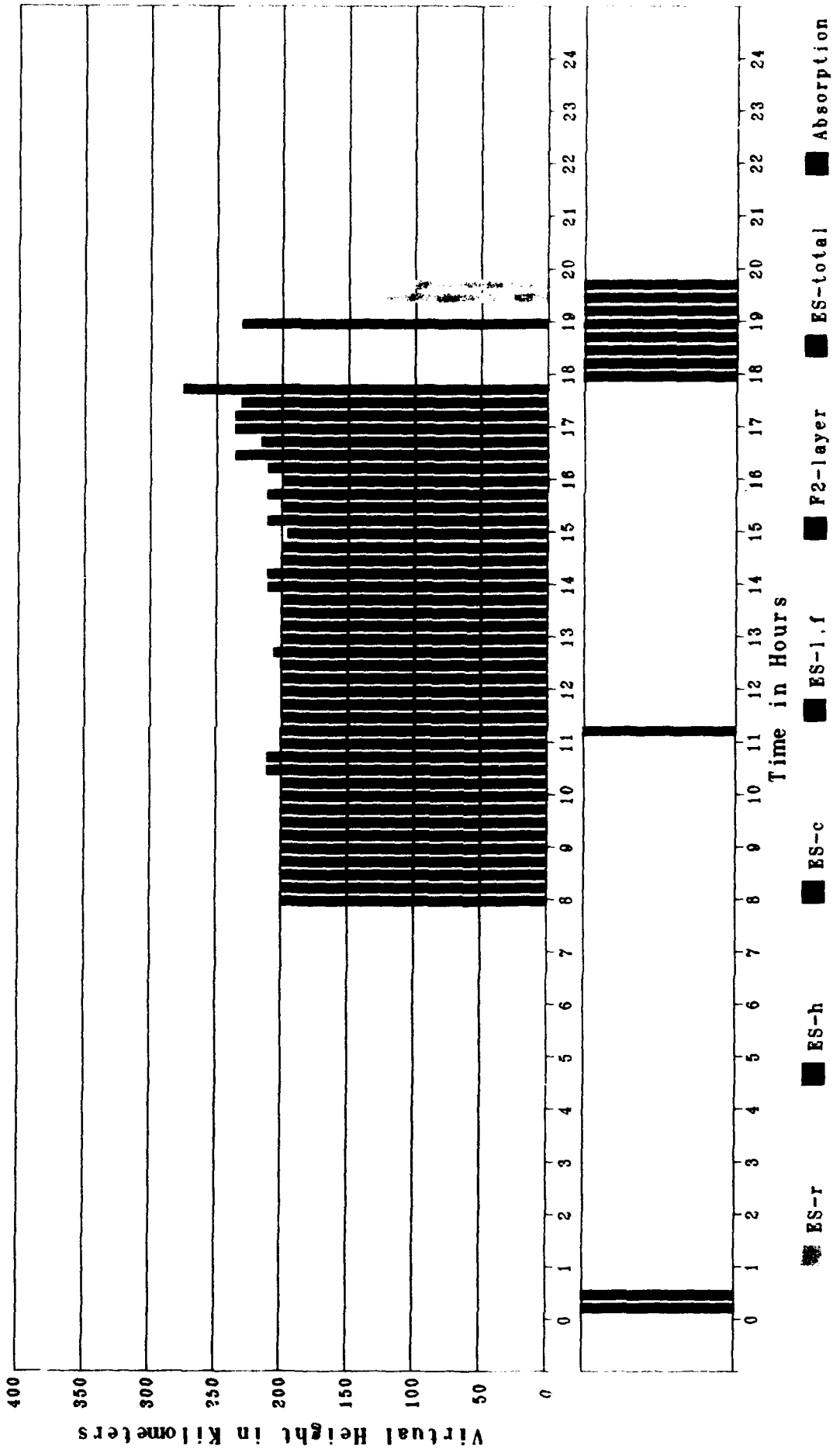


Figure 7B. Virtual Height vs. Time
Figure 7. Periods of Ionospheric Disturbances, 10 November 1986 (Cont'd)

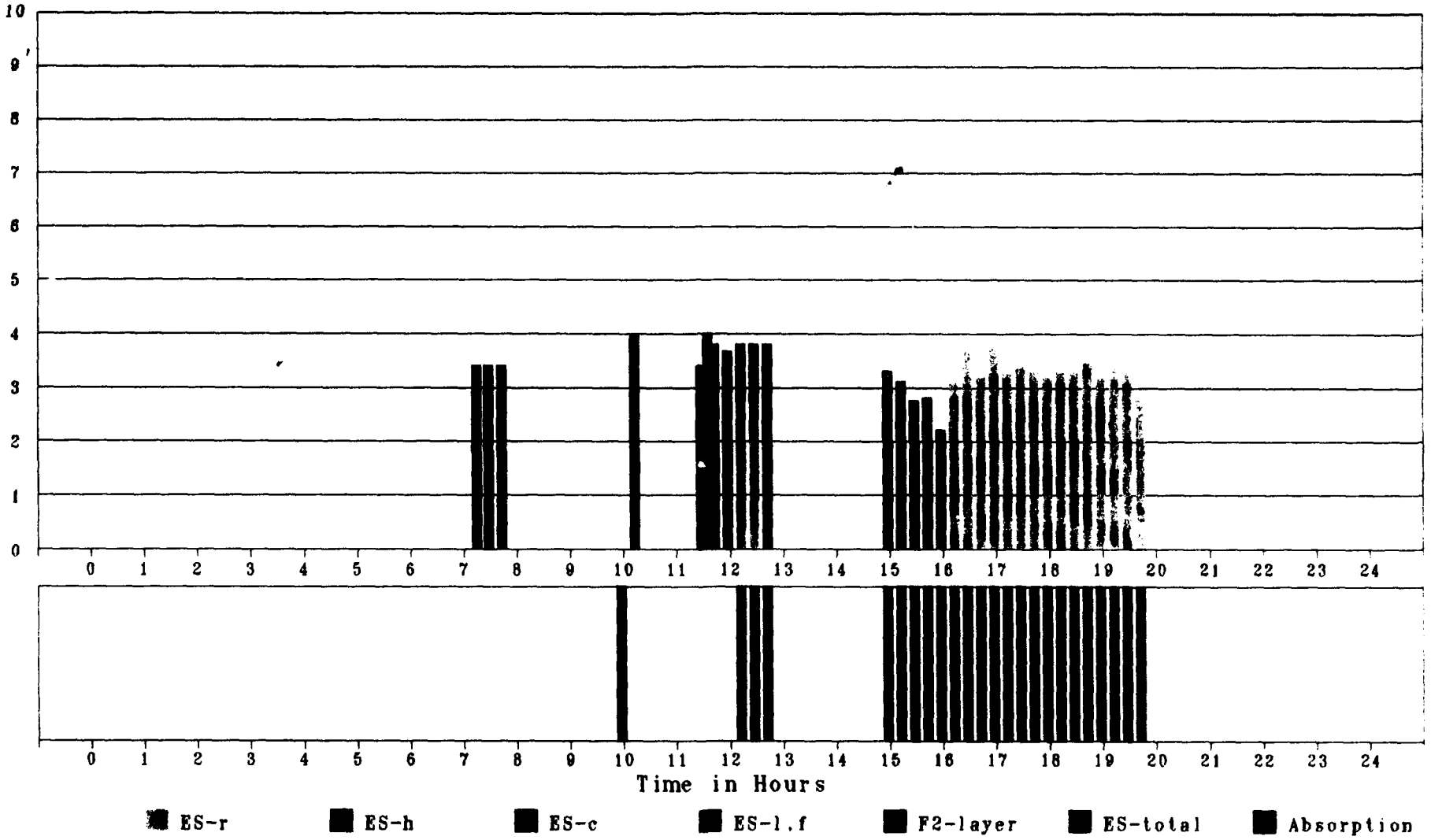


Figure 8A. Critical Frequency vs. Time

Figure 8. Periods of Ionospheric Disturbances, 11 November 1986

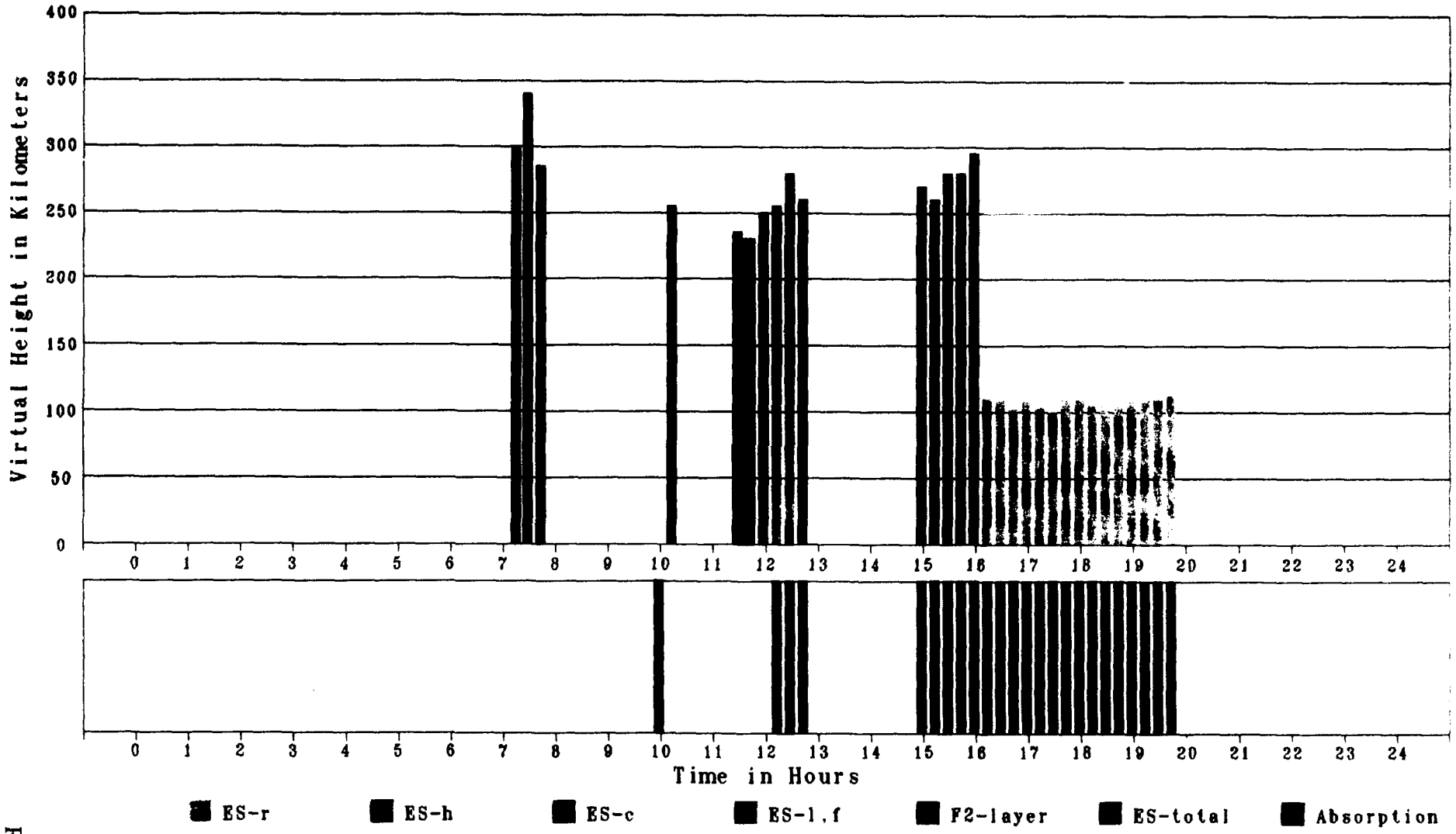


Figure 8B. Virtual Height vs. Time

Figure 8. Periods of Ionospheric Disturbances, 11 November 1986 (Cont'd)



Reverse Blank

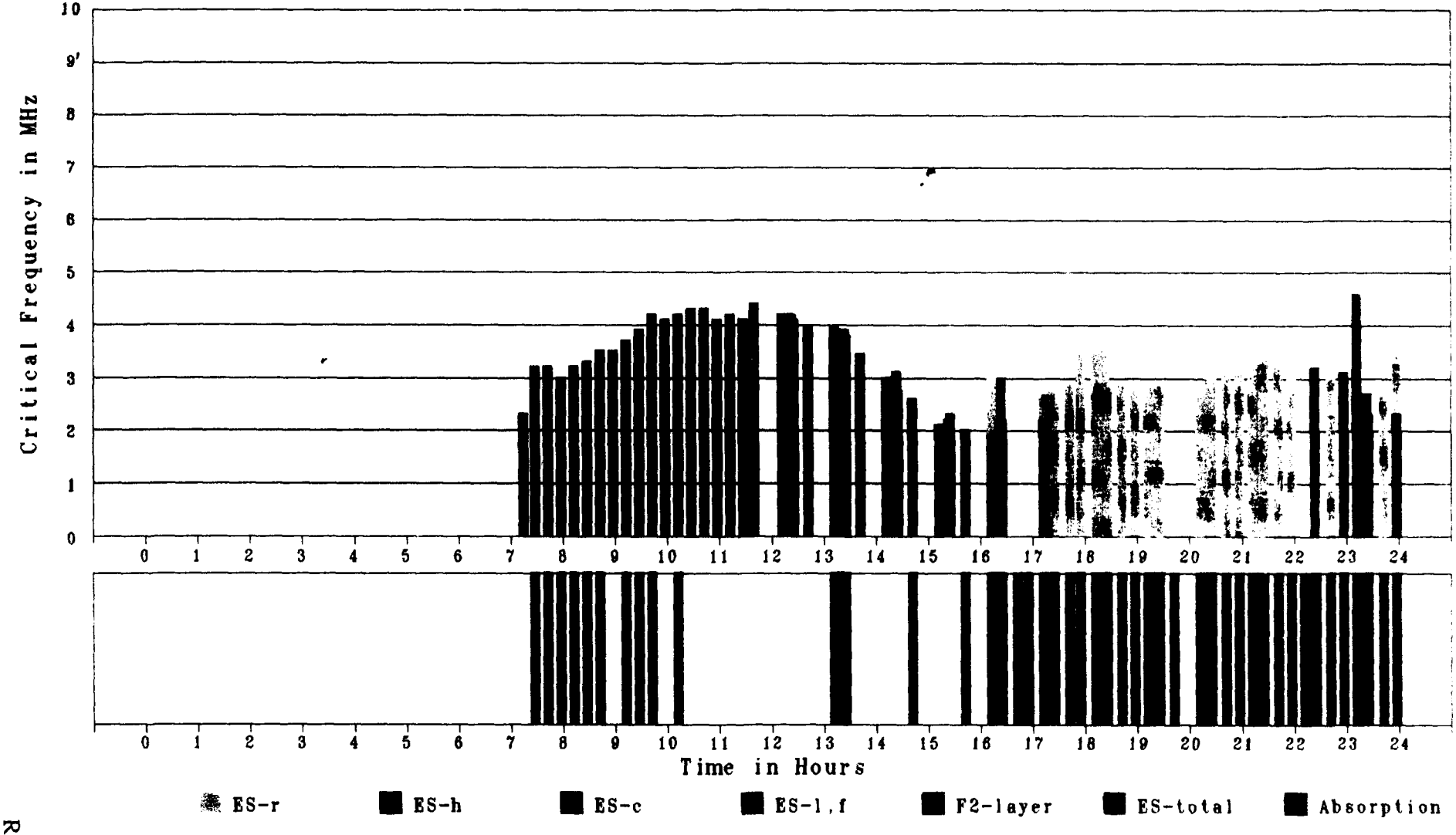


Figure 9A. Critical Frequency vs. Time

Figure 9. Periods of Ionospheric Disturbances, 12 November 1986



Reverse Blank

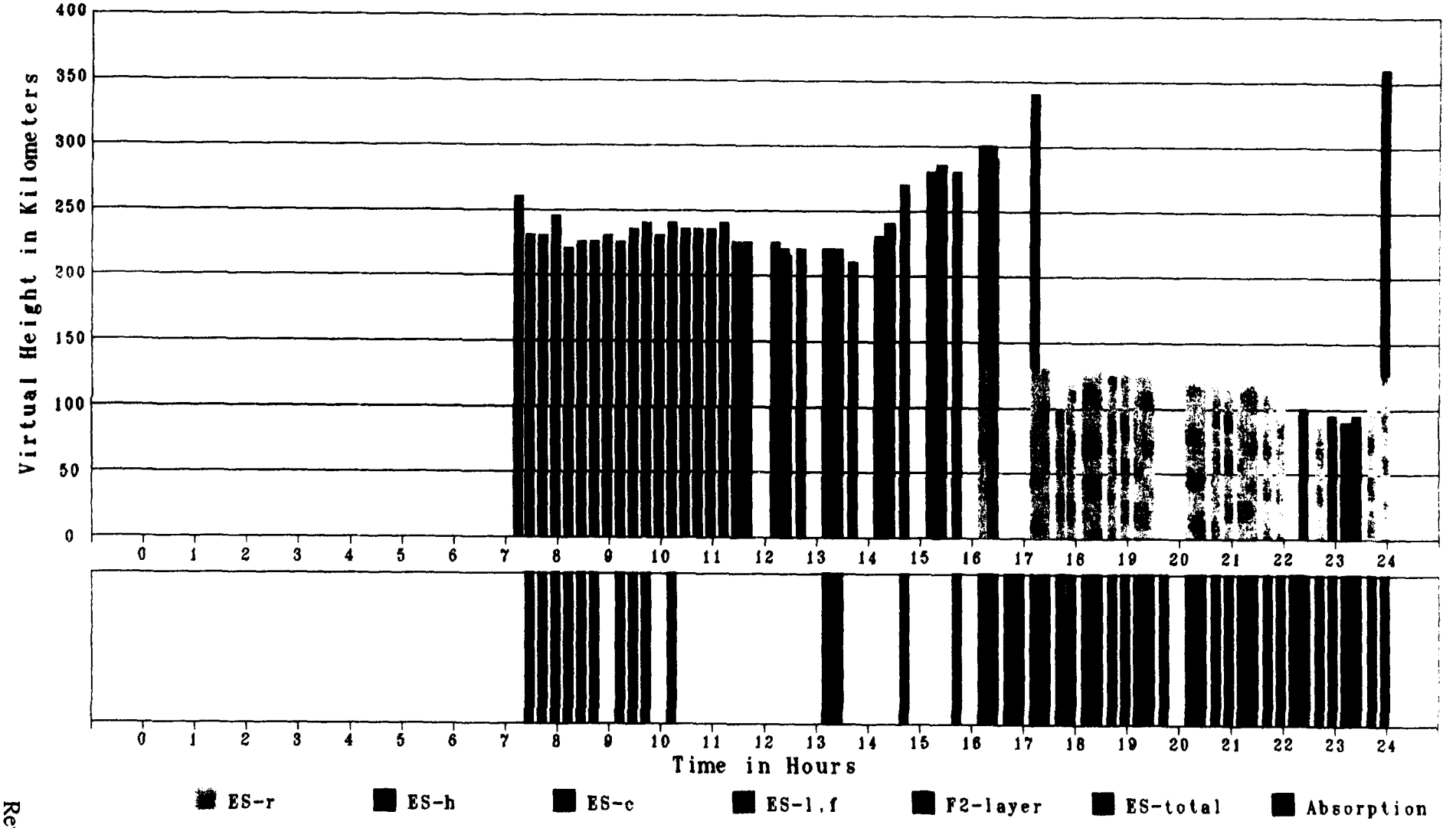


Figure 9B. Virtual Height vs. Time

Figure 9. Periods of Ionospheric Disturbances, 12 November 1986 (Cont'd)

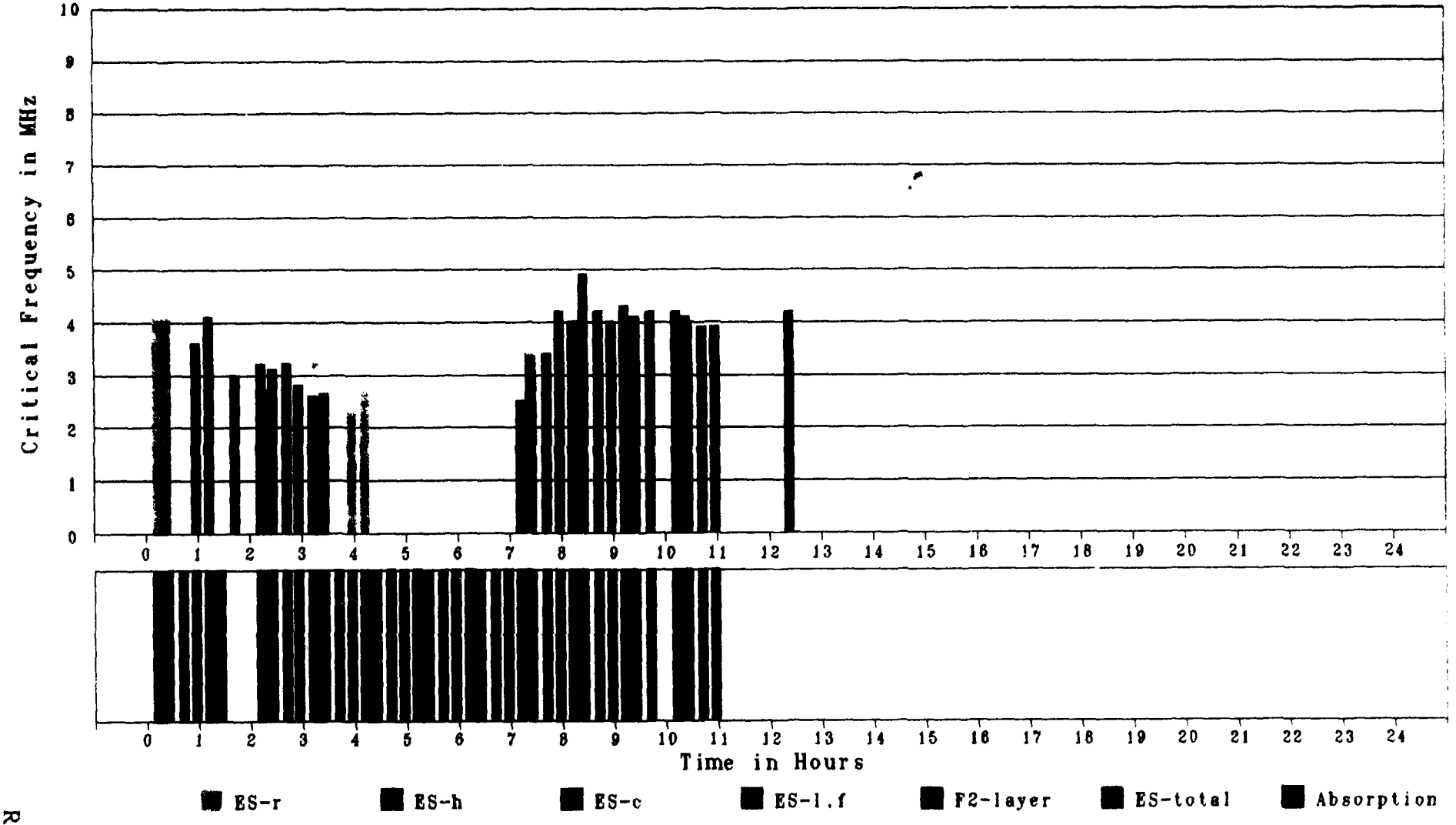


Figure 10A. Critical Frequency vs. Time

Figure 10. Periods of Ionospheric Disturbances, 13 November 1986



Reverse Blank

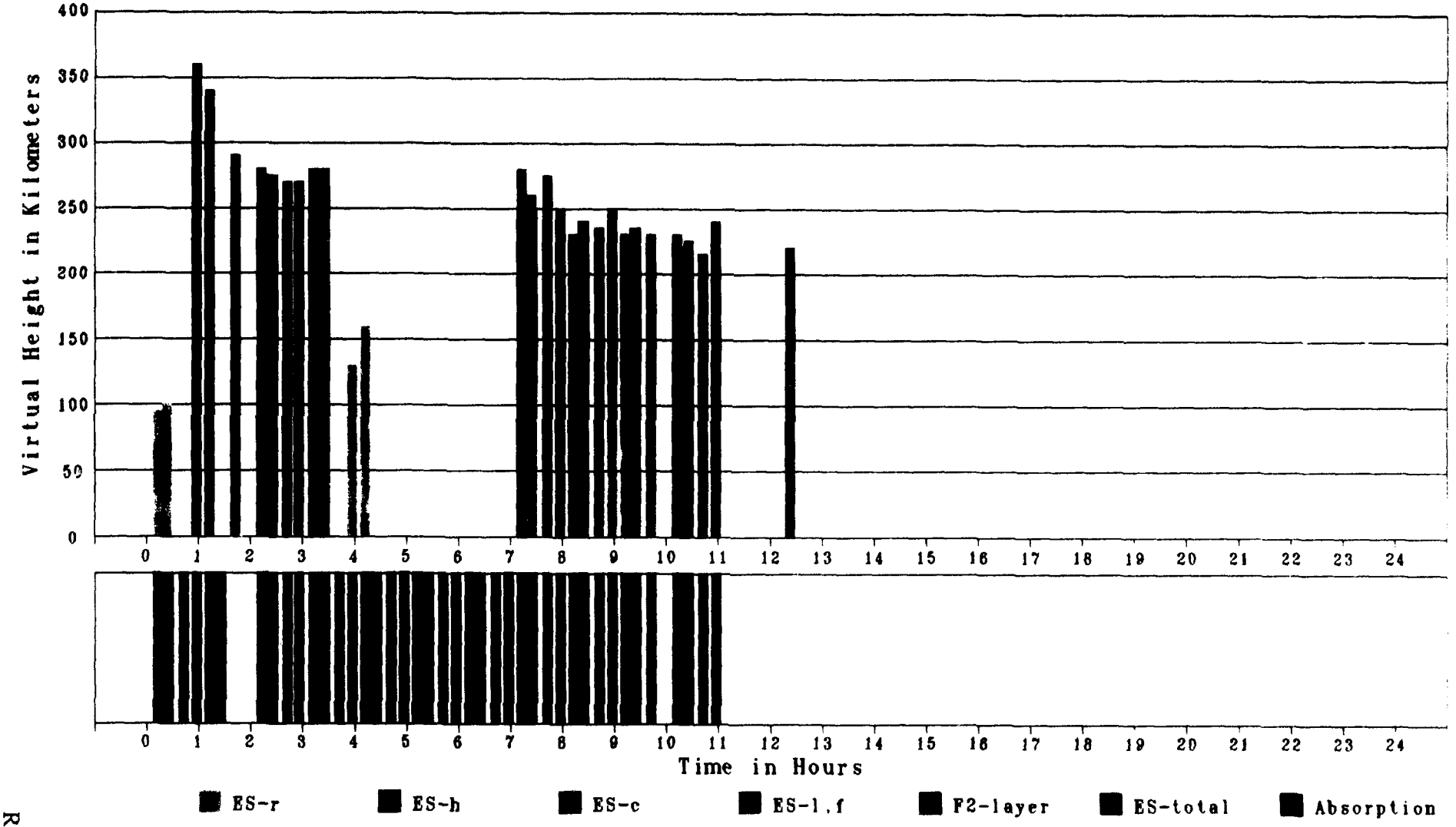


Figure 10B. Virtual Height vs. Time

Figure 10. Periods of Ionospheric Disturbances, 13 November 1986 (Cont'd)



Reverse Blank

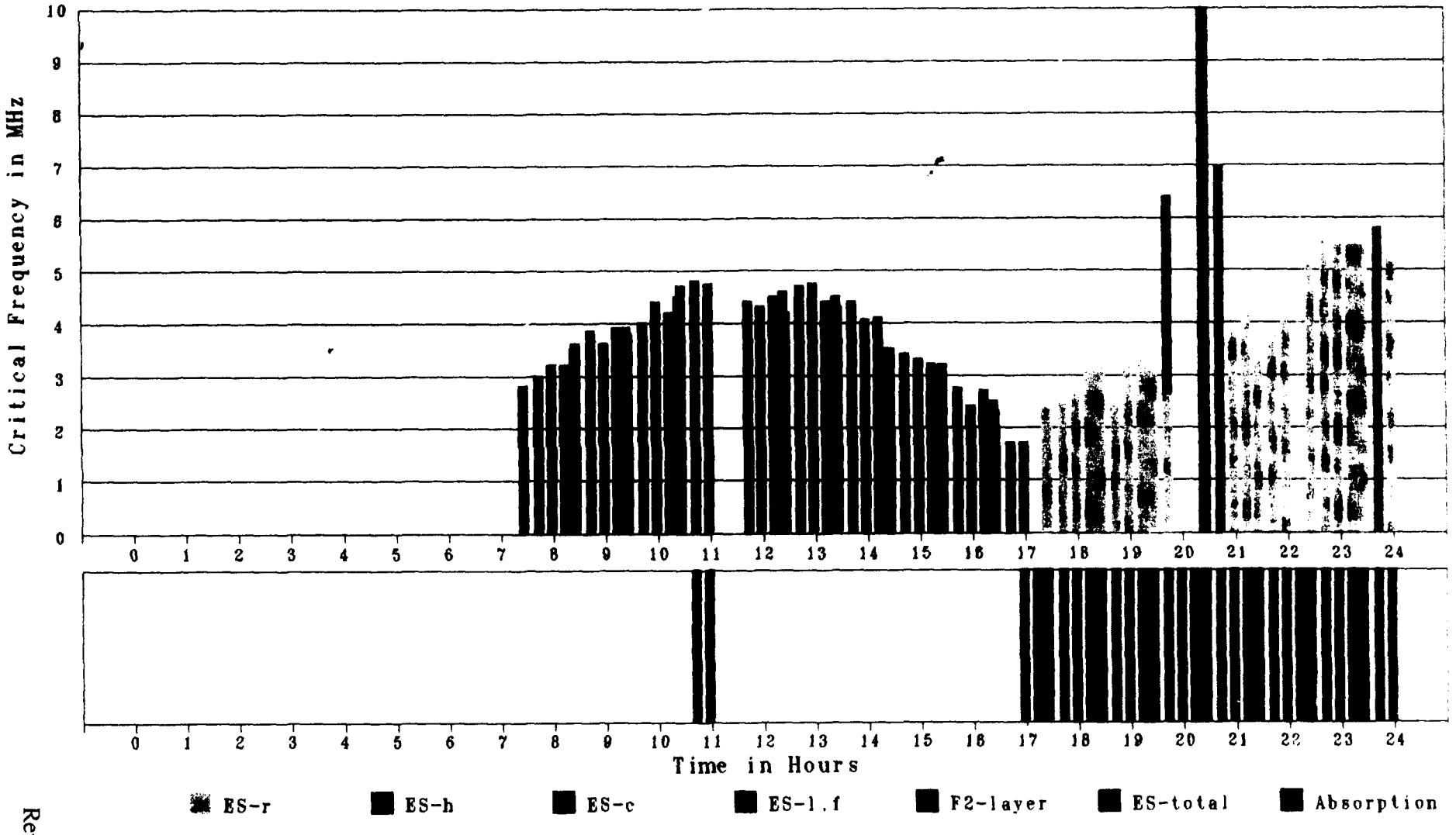


Figure 11A. Critical Frequency vs. Time

Figure 11. Periods of Ionospheric Disturbances, 14 November 1986

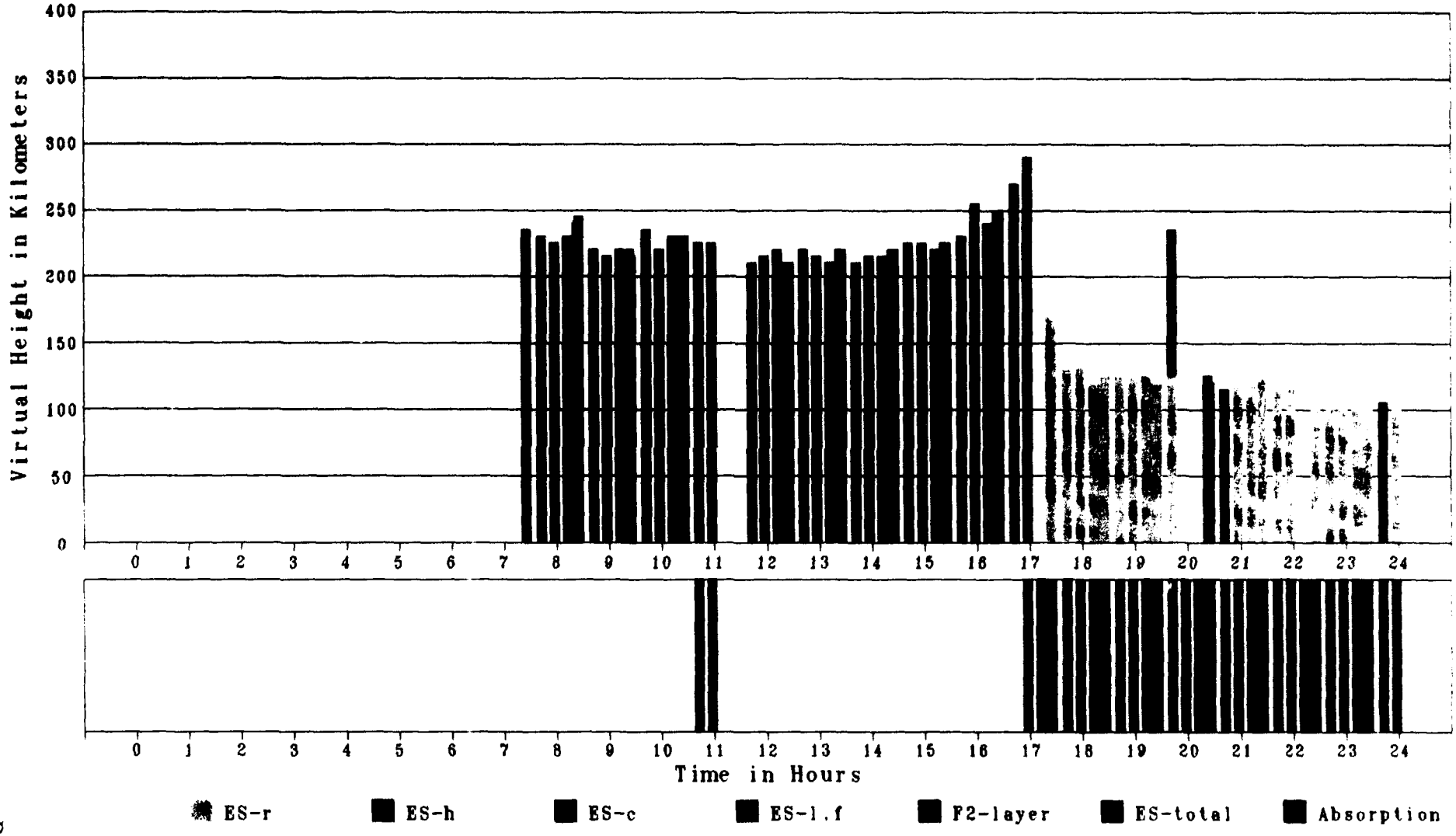


Figure 11B. Virtual Height vs. Time

Figure 11. Periods of Ionospheric Disturbances, 14 November 1986 (Cont'd)

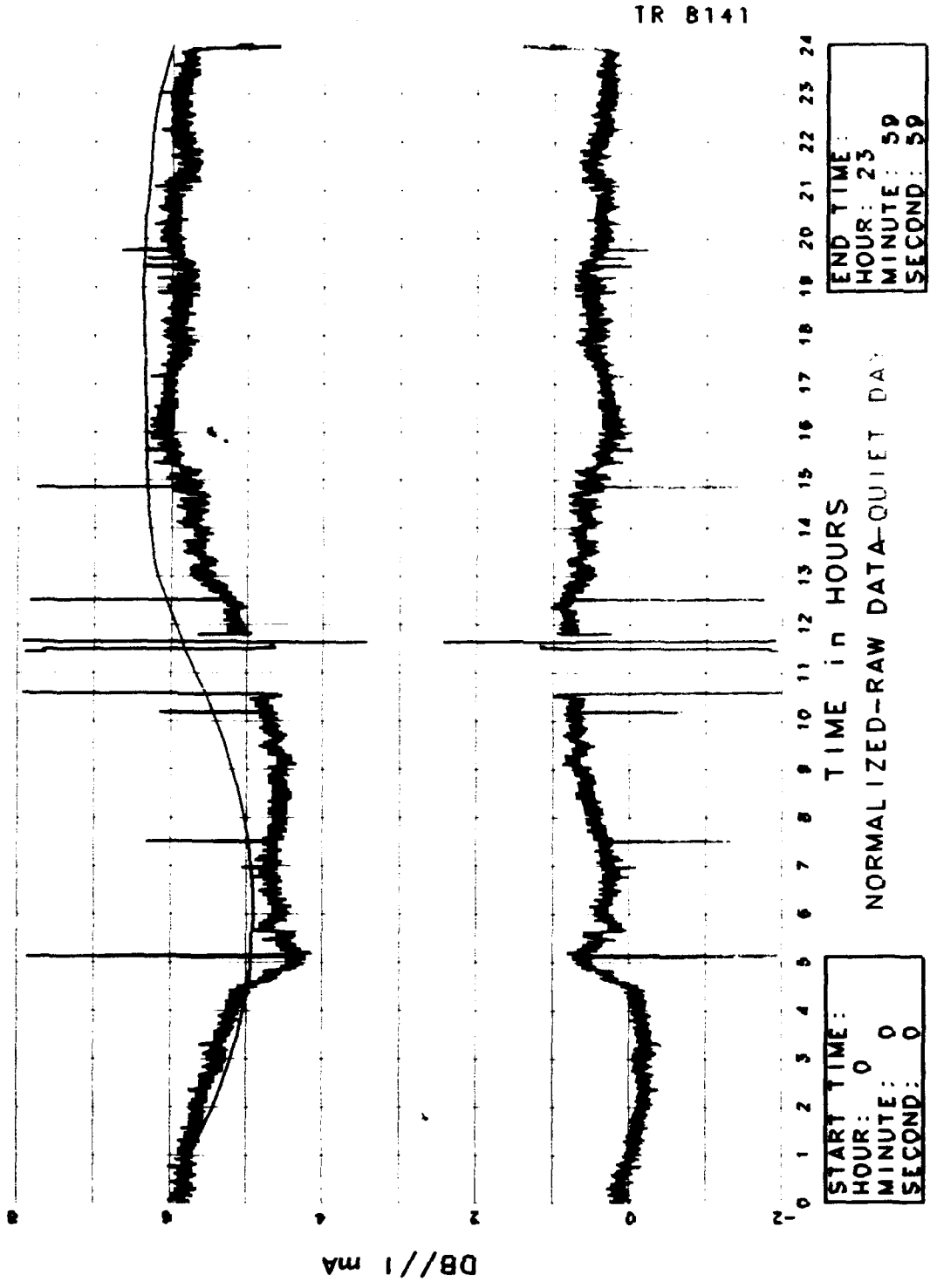


Figure 12. Riometer Data: 3 November 1986

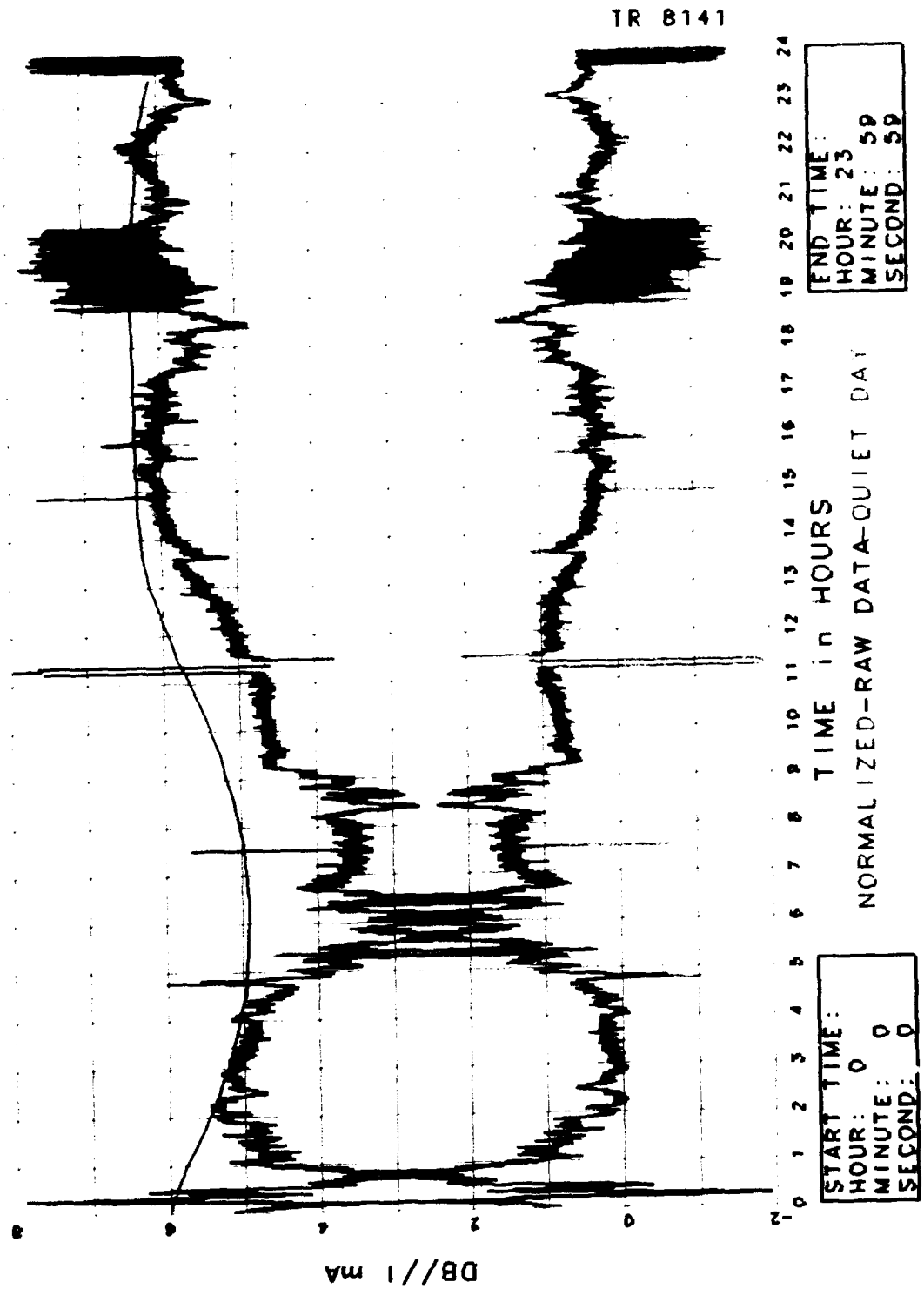


Figure 13. Riometer Data: 4 November 1986

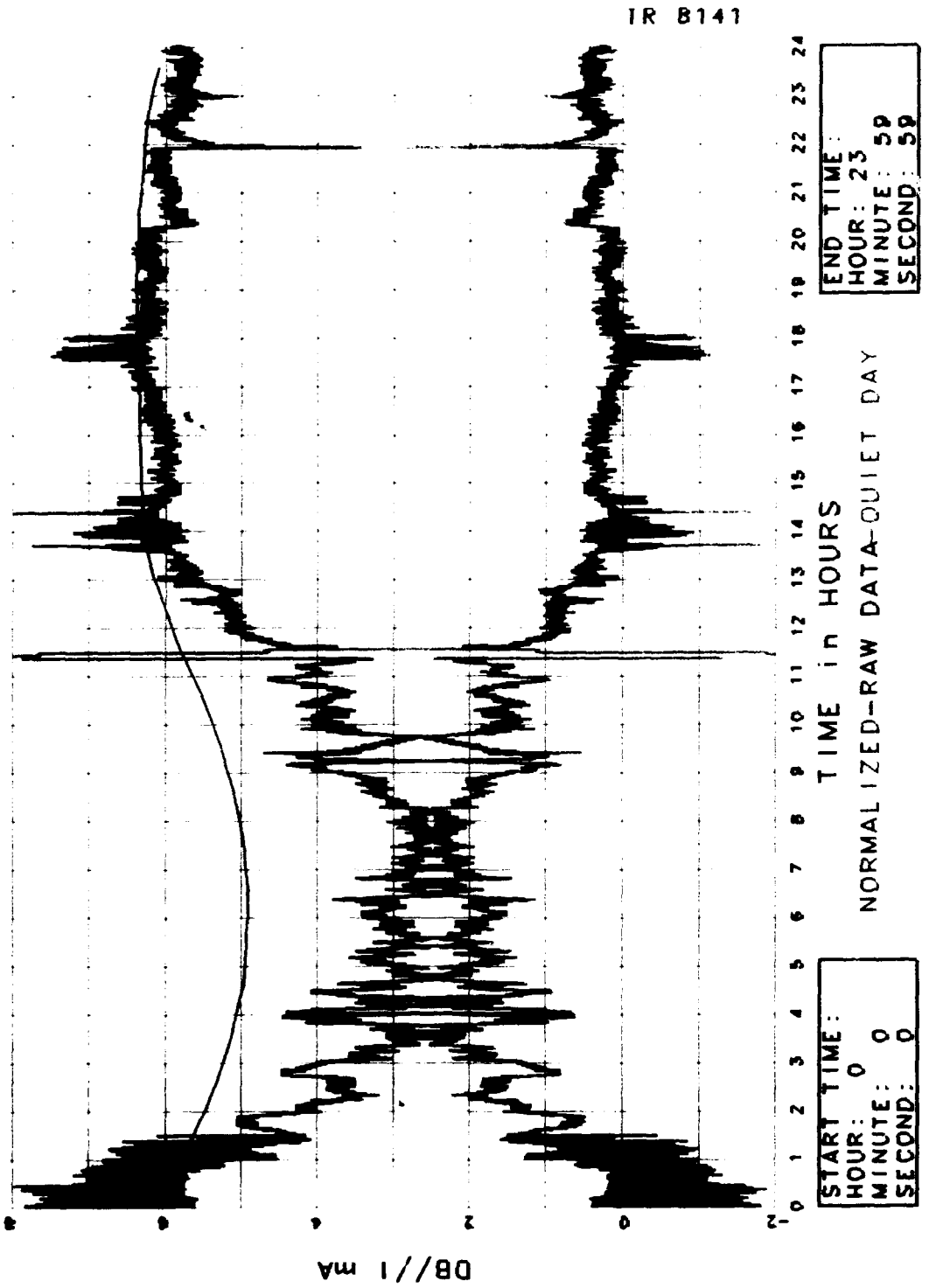


Figure 14. Riometer Data: 5 November 1986

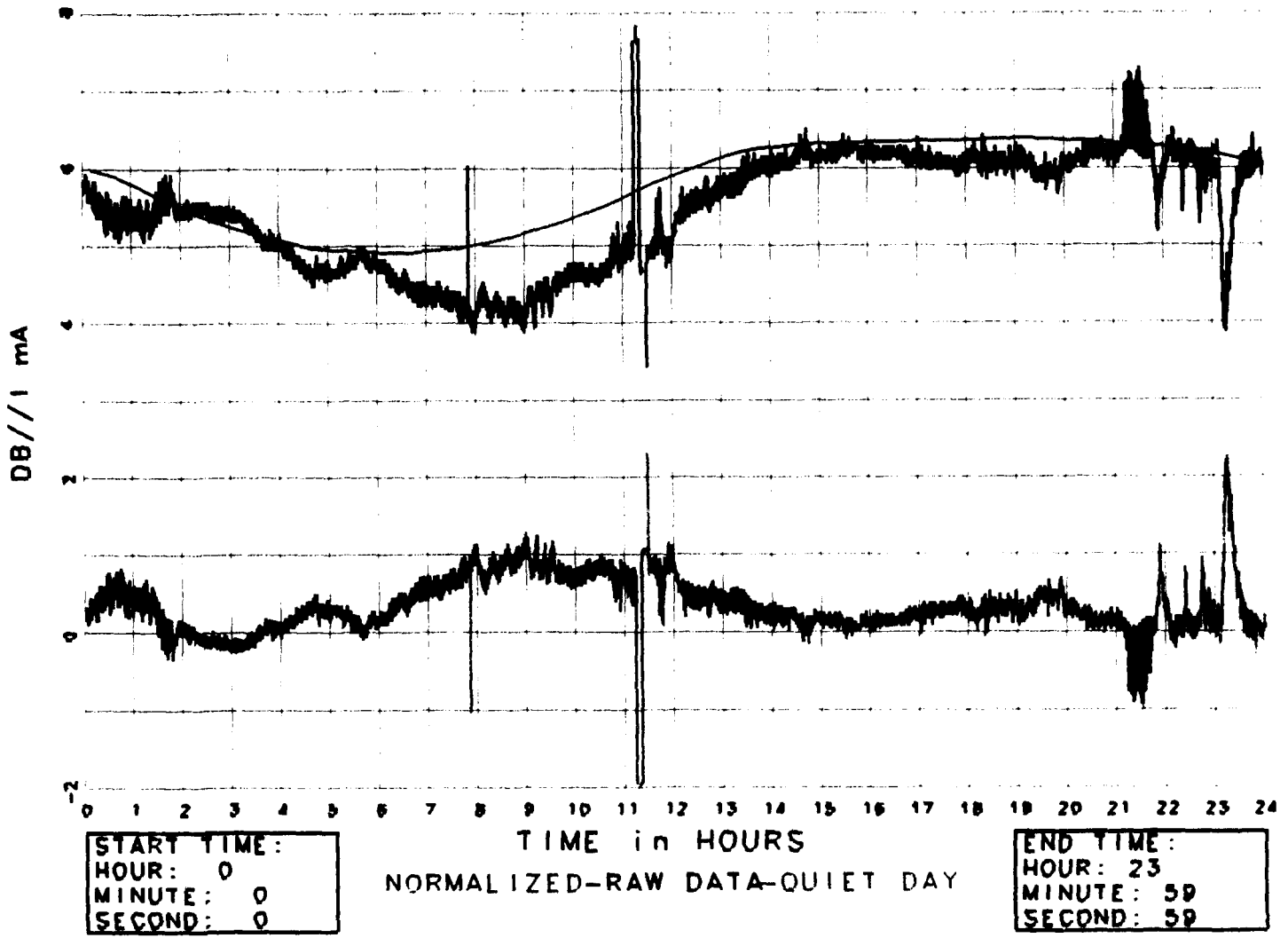


Figure 15. Riometer Data: 6 November 1986

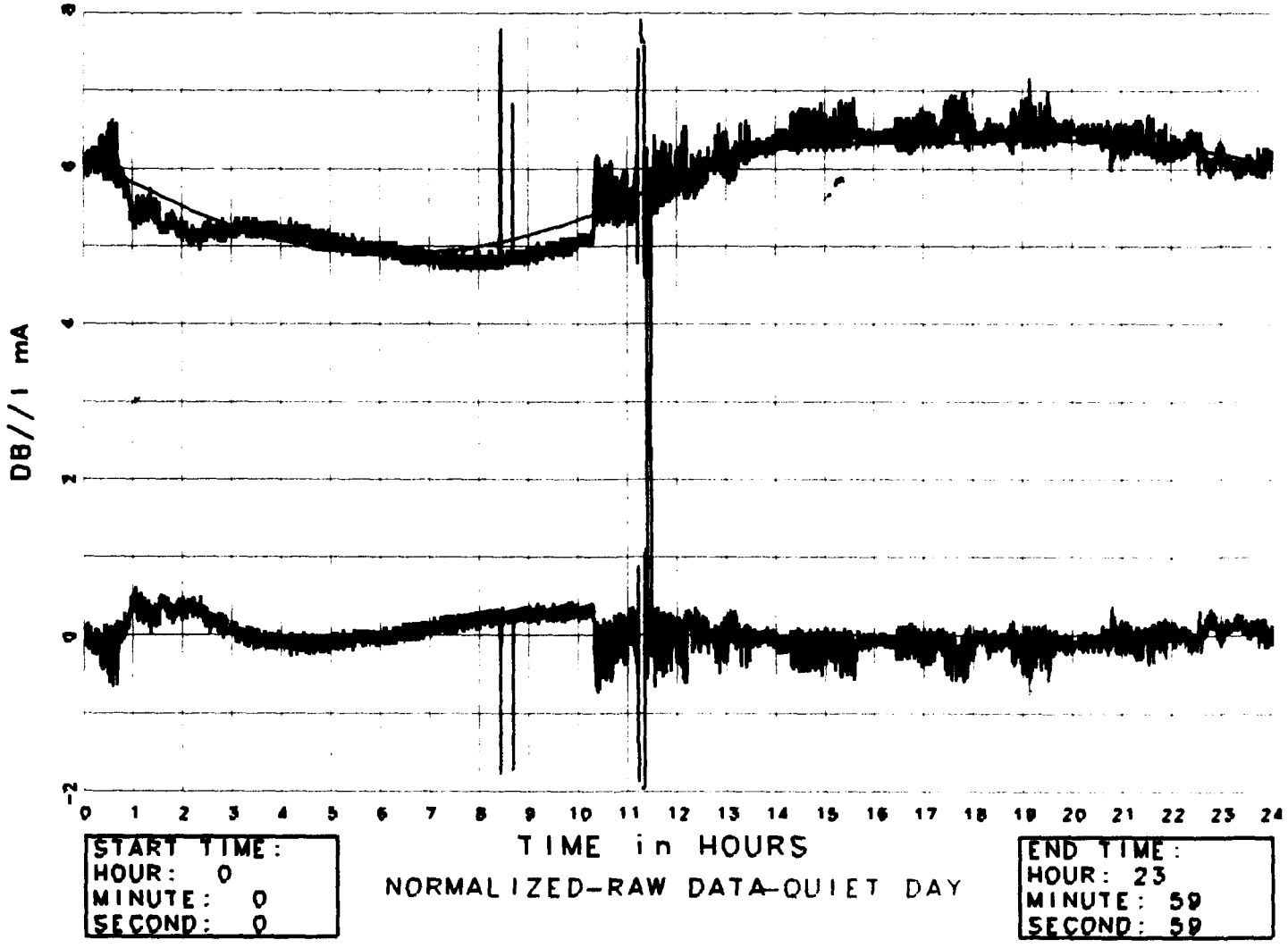


Figure 16. Riometer Data: 7 November 1986

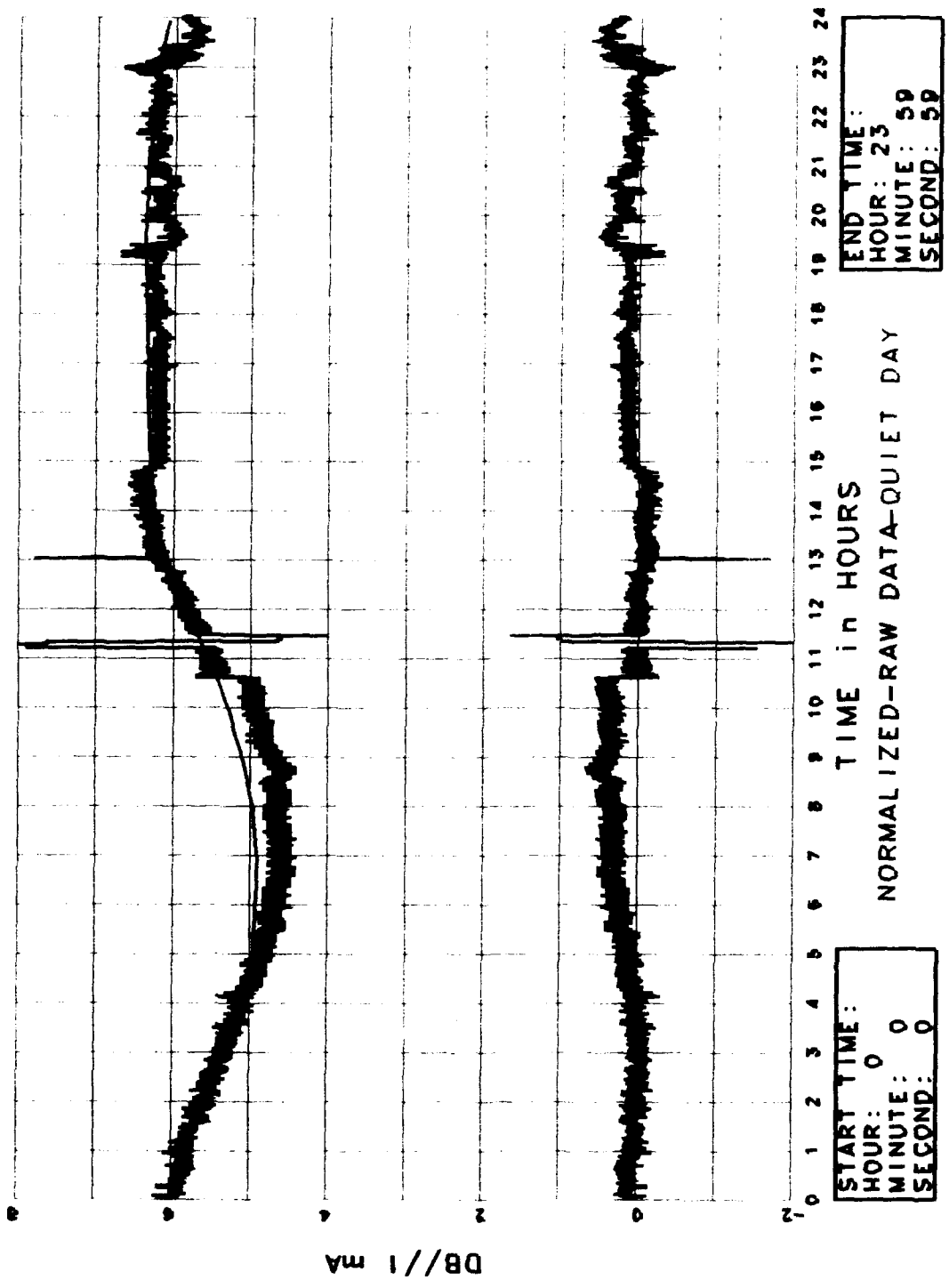


Figure 17. Riometer Data: 10 November 1986

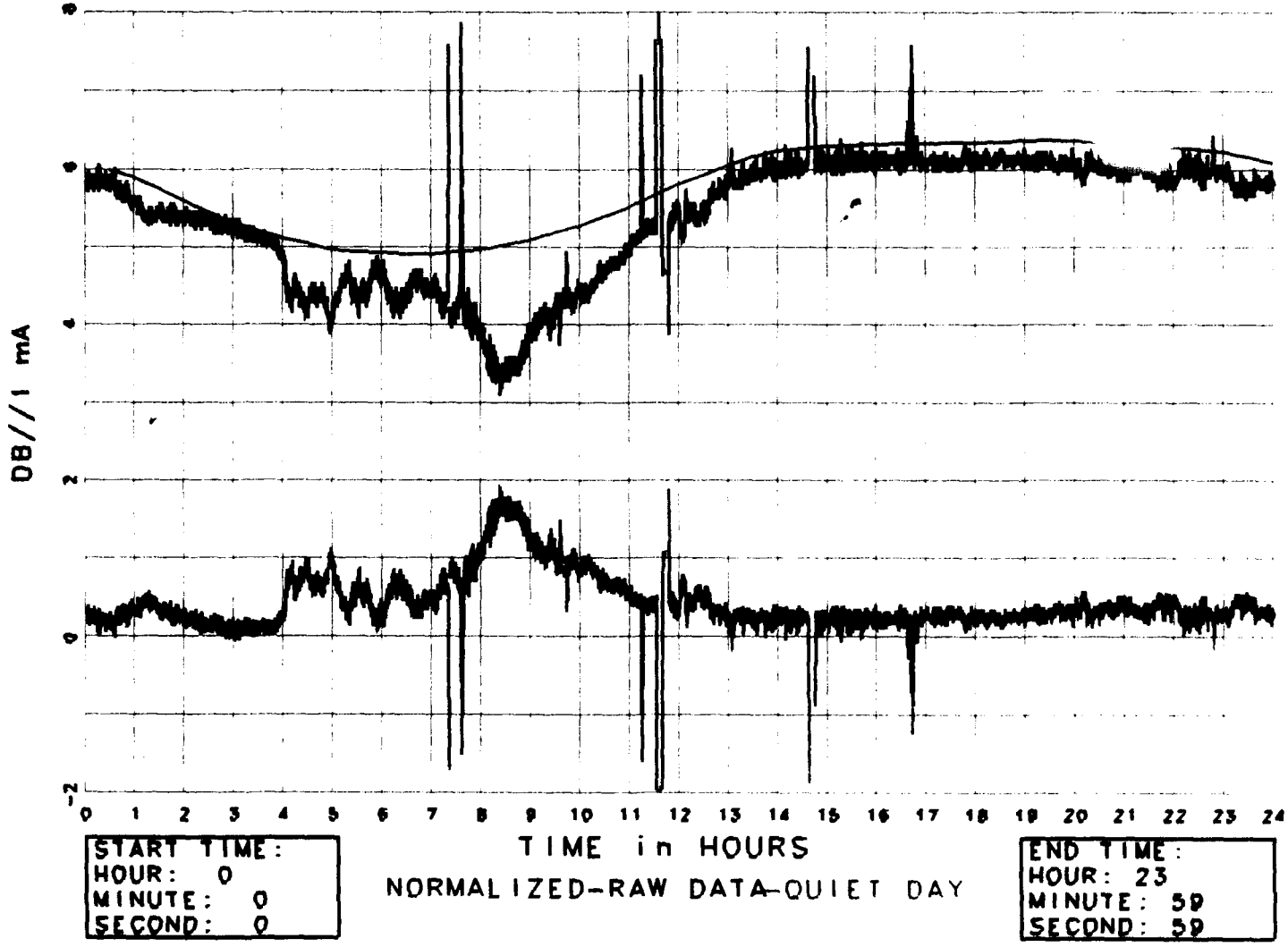


Figure 18. Riometer Data: 11 November 1986

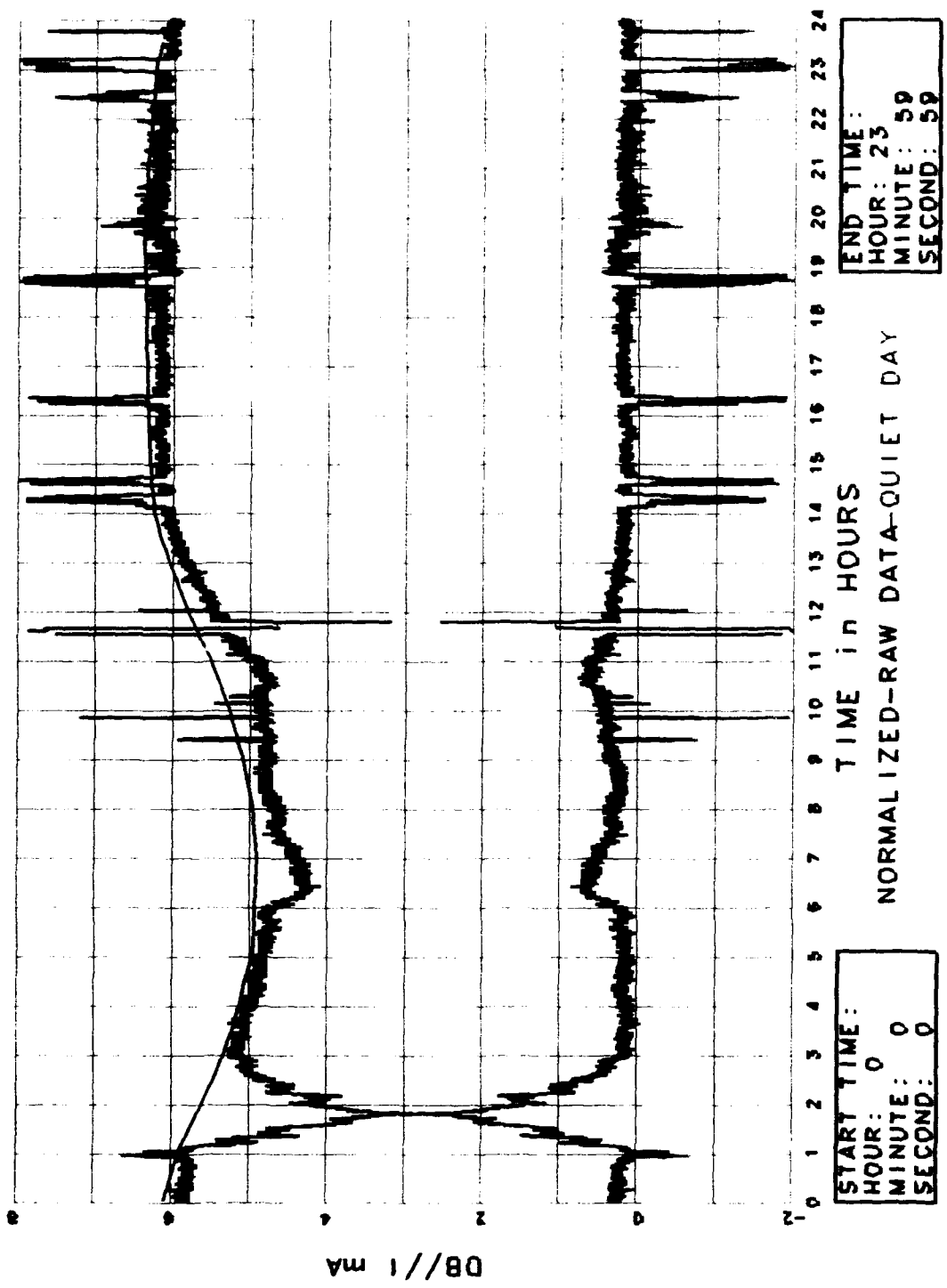


Figure 19. Riometer Data: 12 November 1986

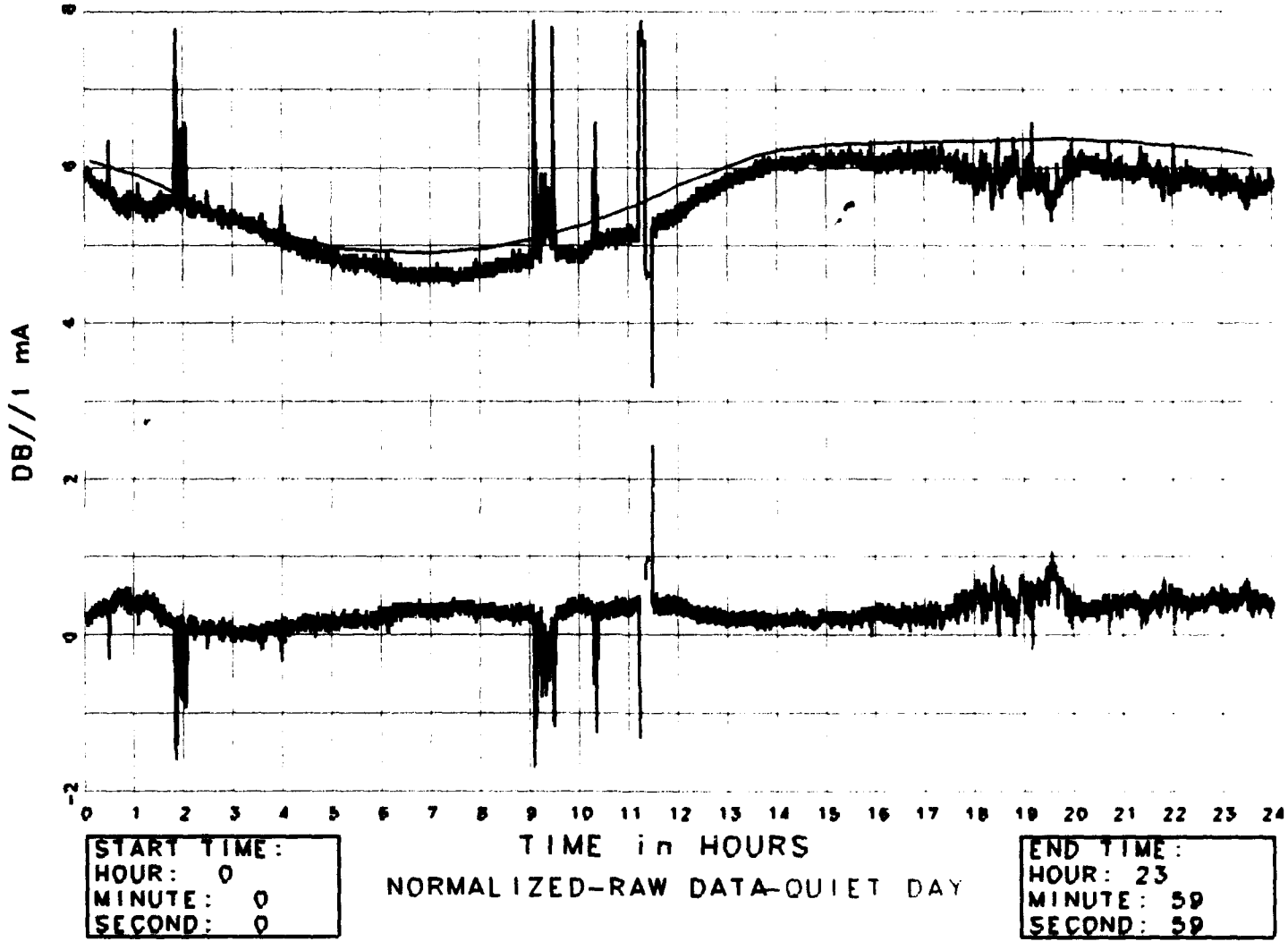


Figure 20. Riometer Data: 13 November 1986

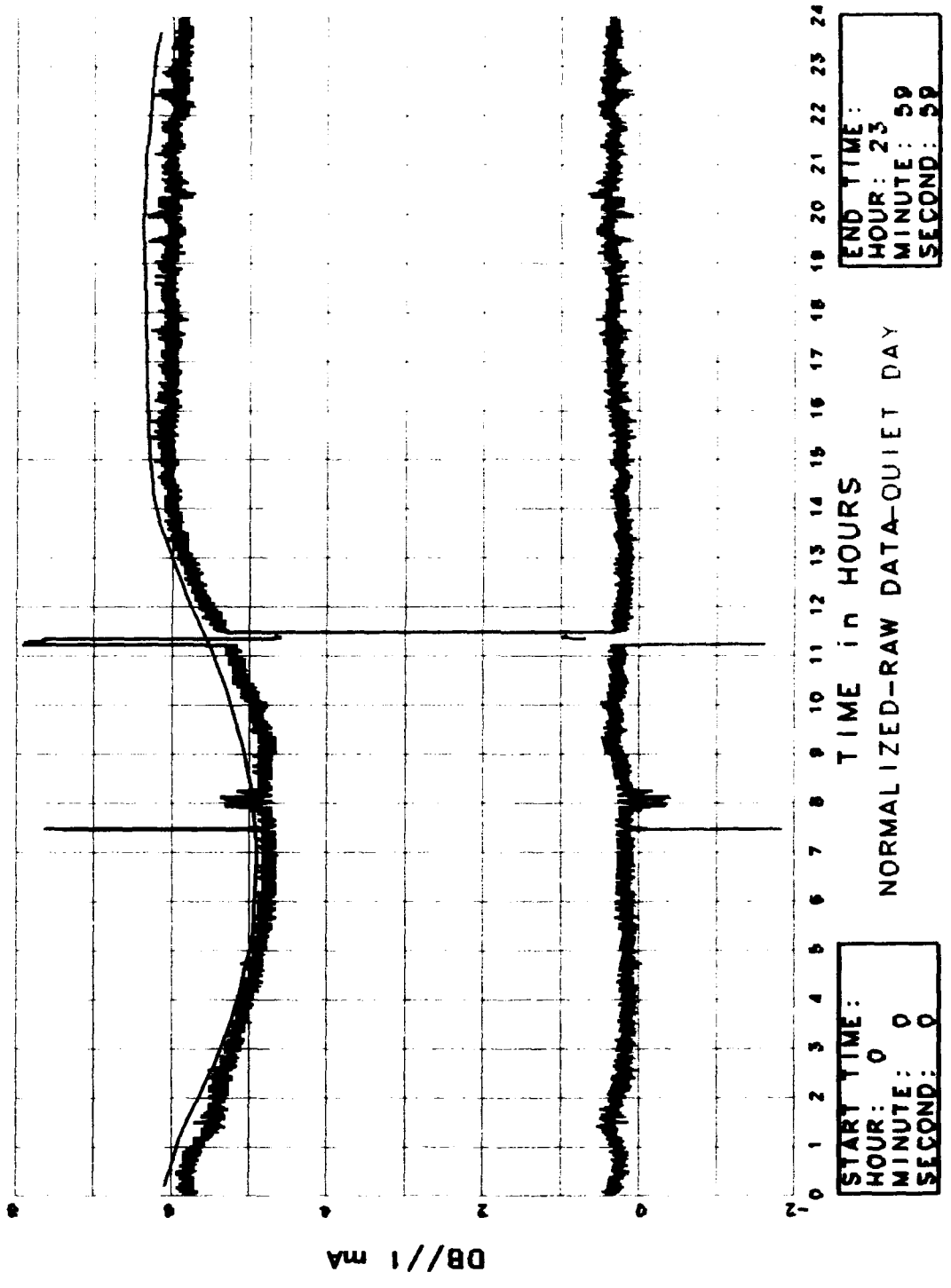


Figure 21. Riometer Data: 14 November 1986

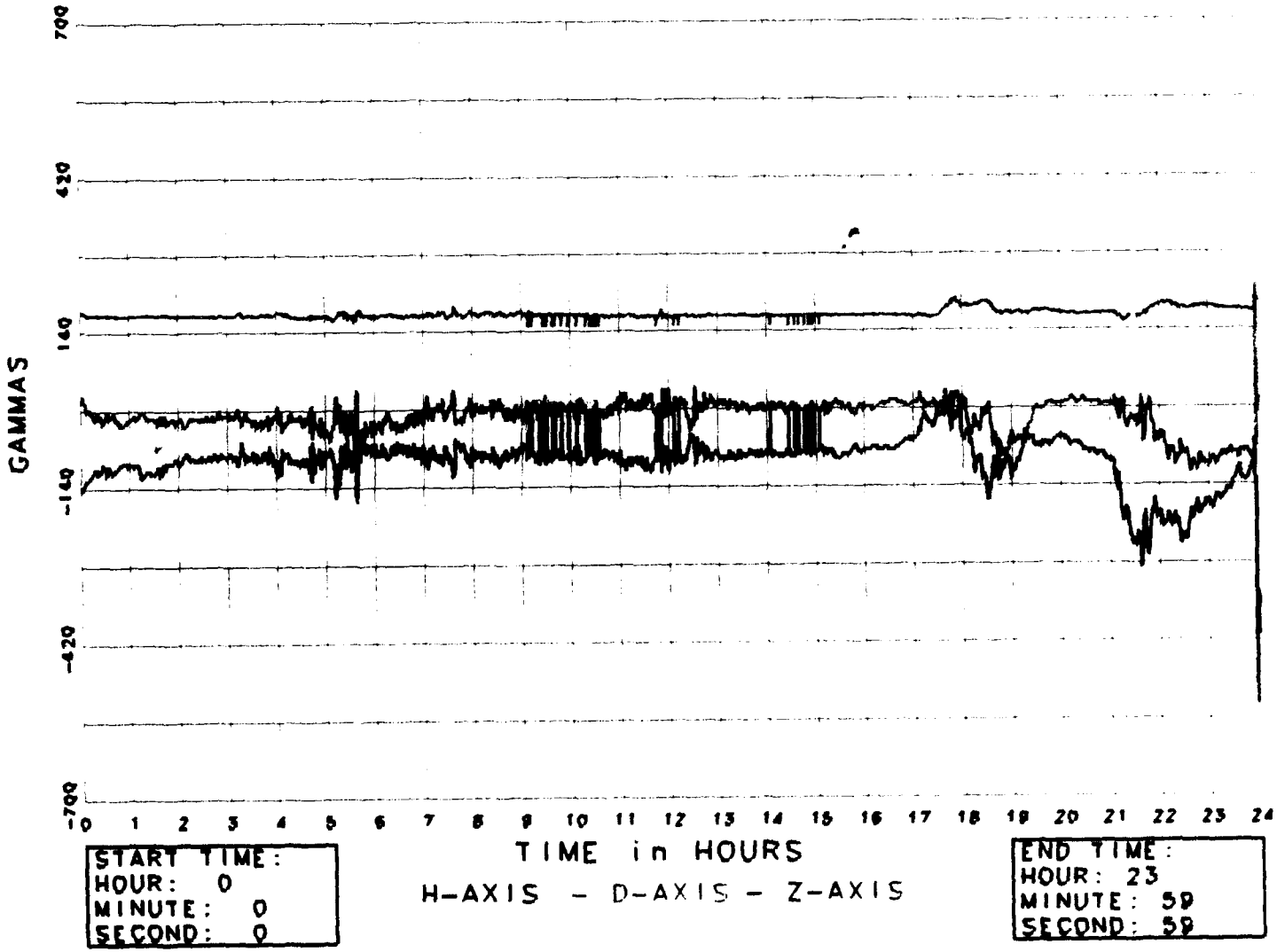


Figure 22. Magnetometer H-D-Z Axis Data: 3 November 1986


Reverse Blank

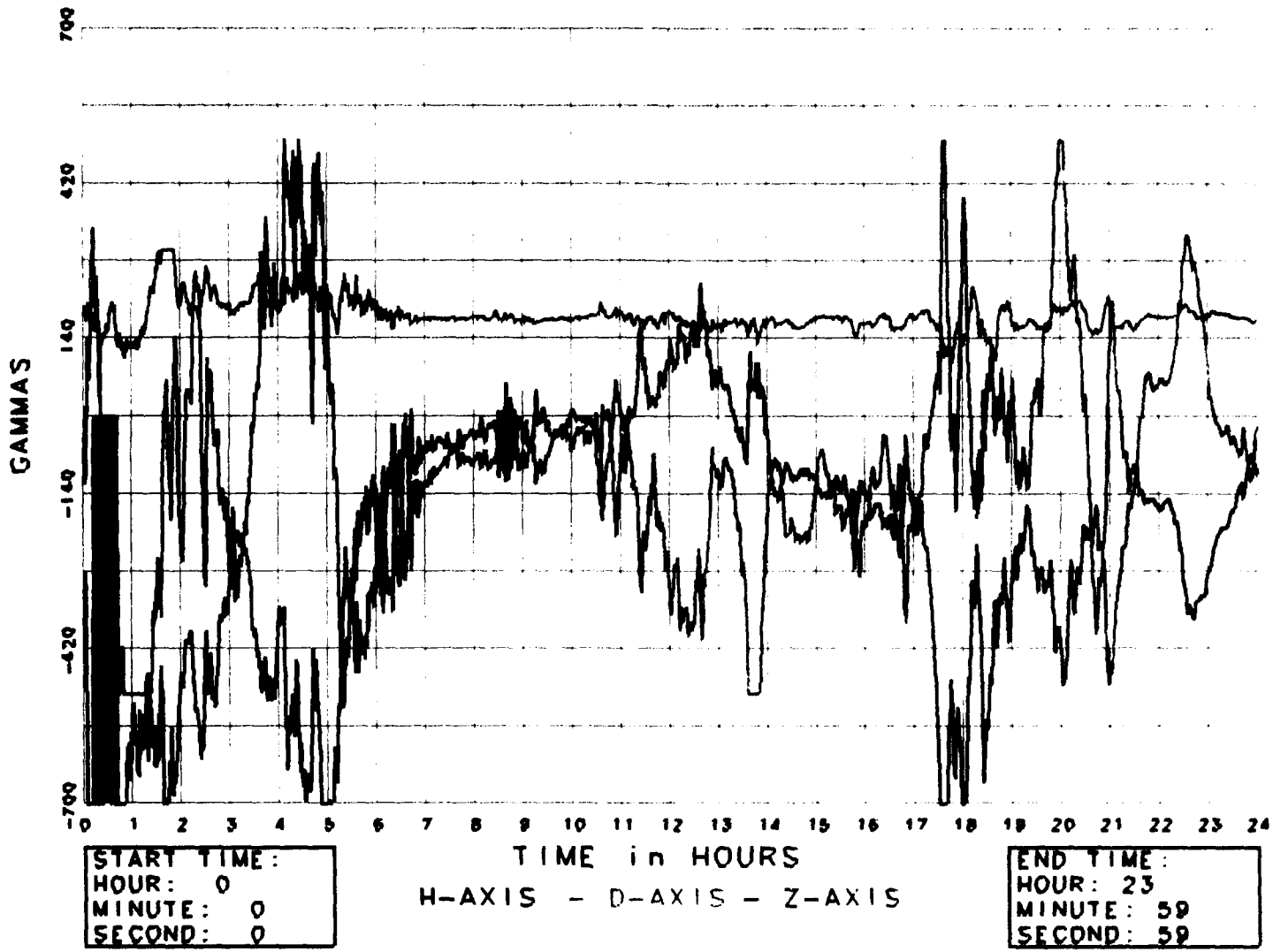


Figure 23. Magnetometer H-D-Z Axis Data: 4 November 1986

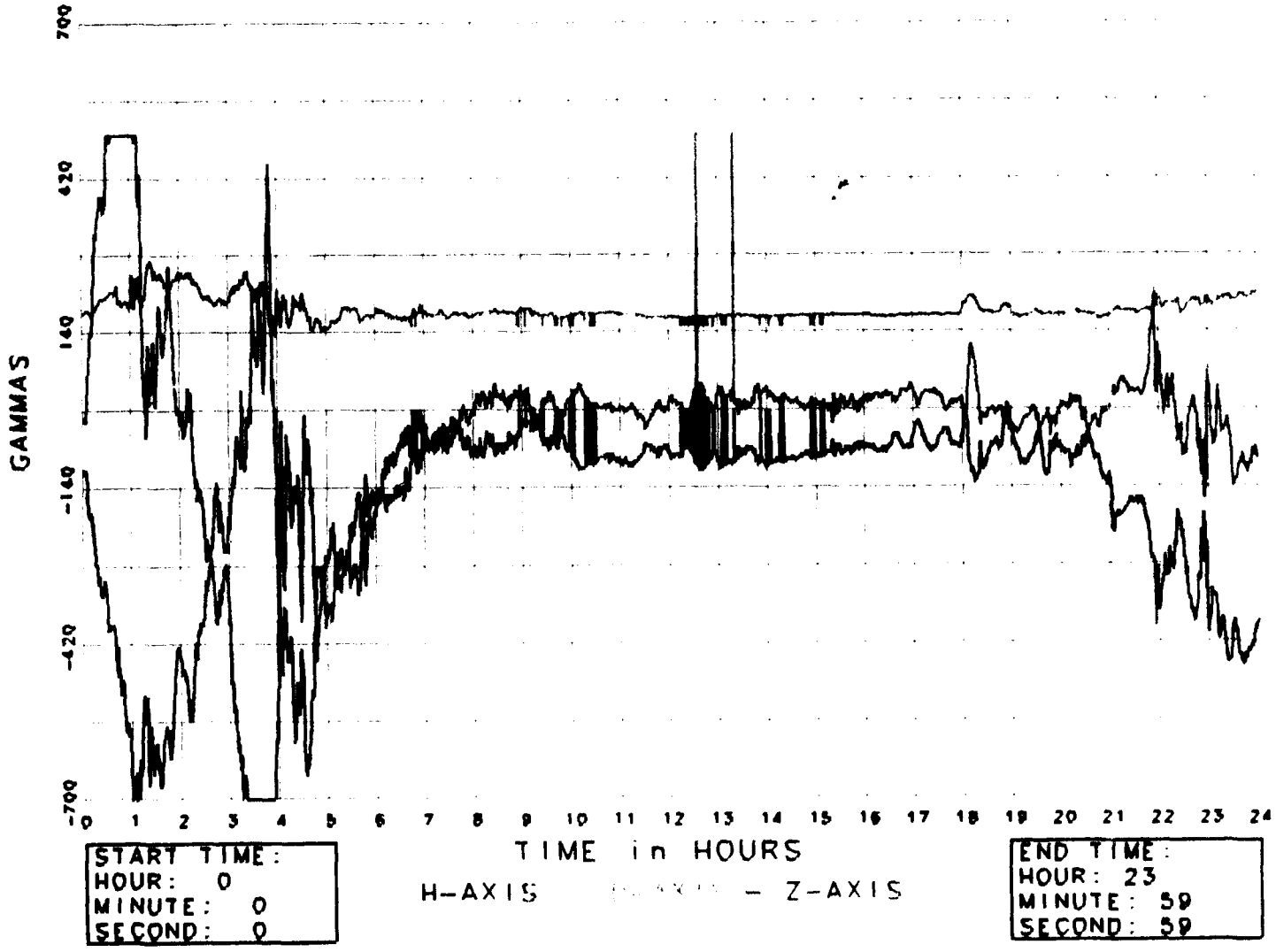


Figure 24. Magnetometer H-D-Z Axis Data: 5 November 1986

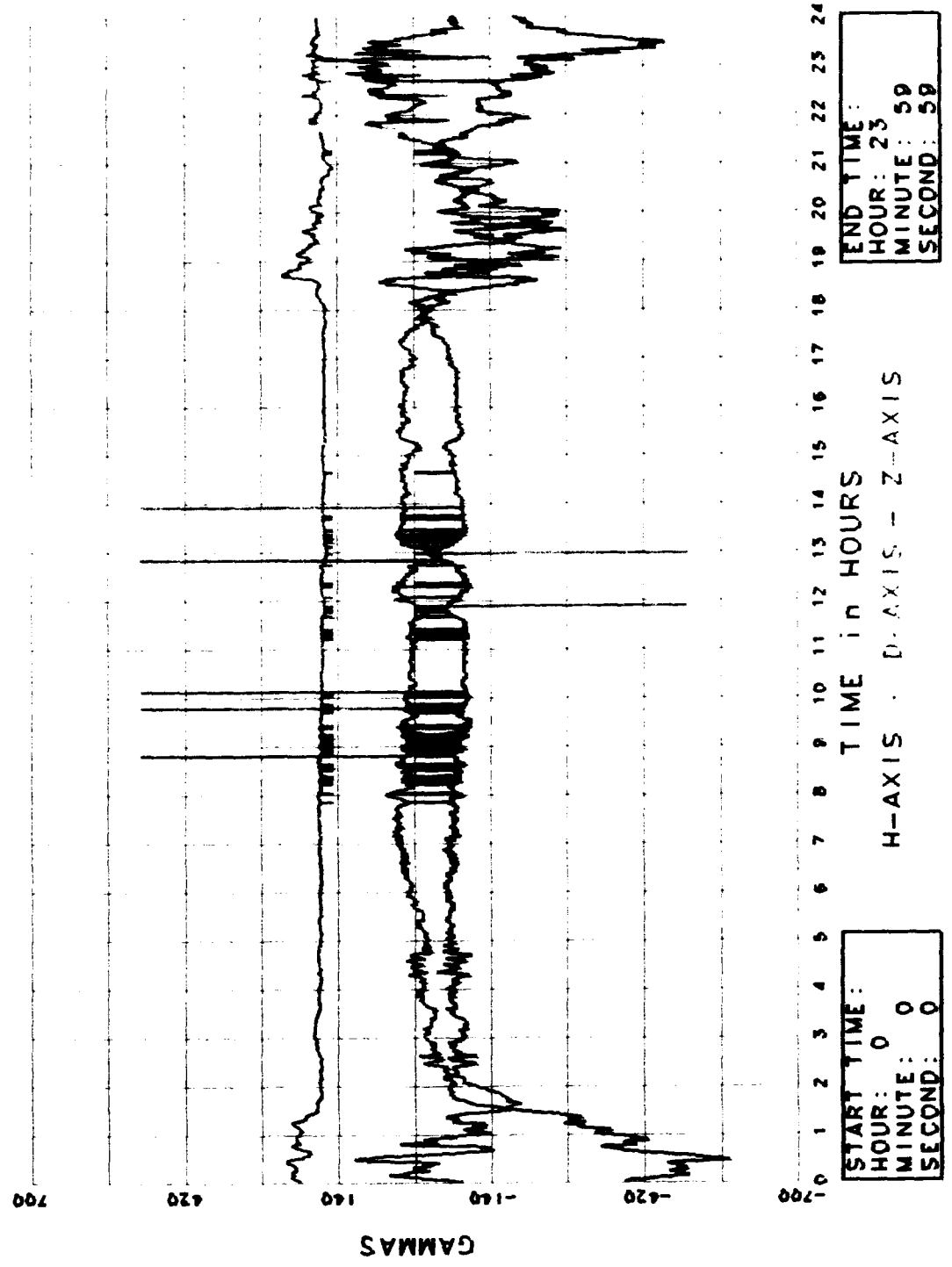


Figure 25. Magnetometer H-D-Z Axis Data: 6 November 1986

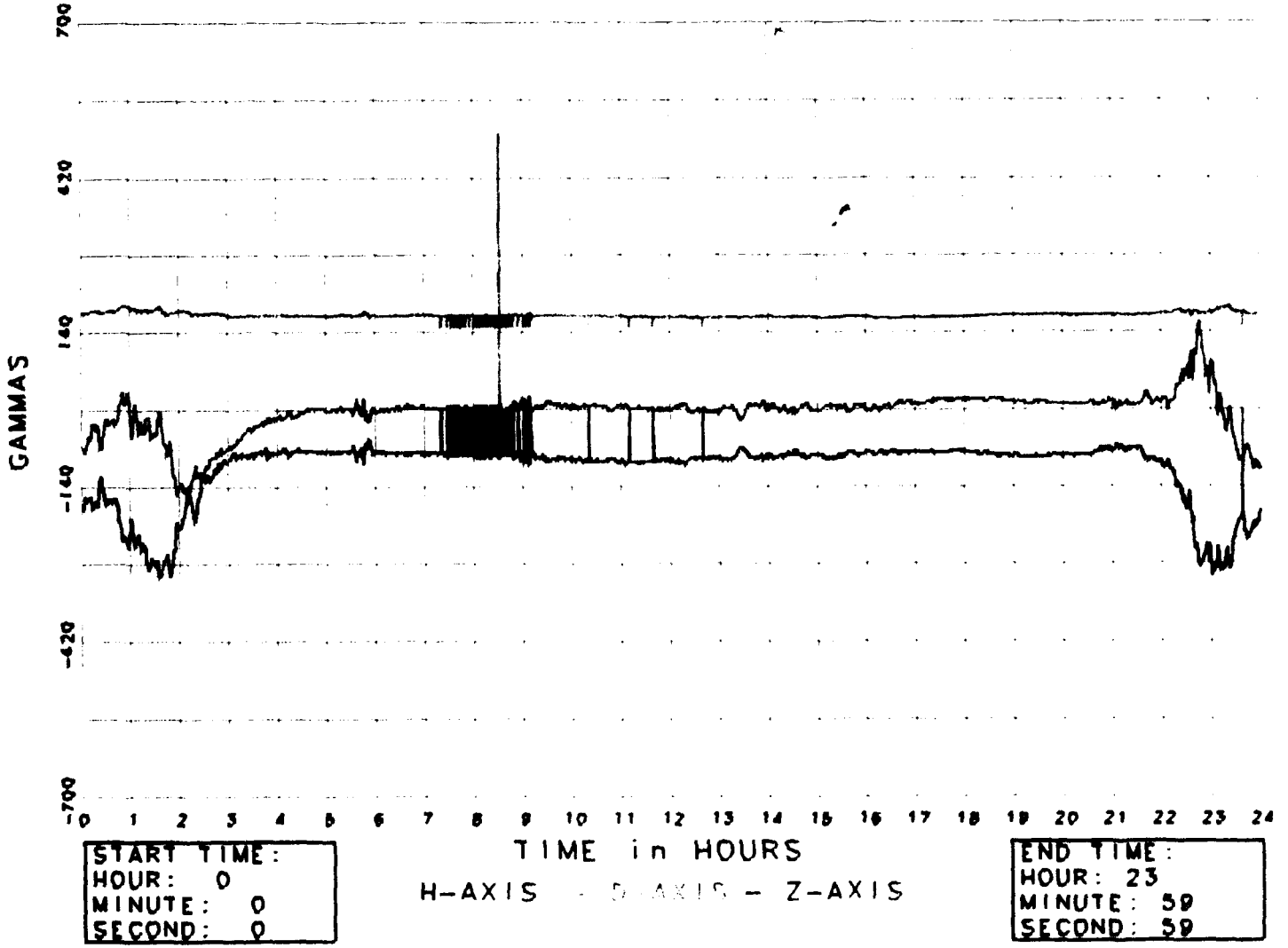


Figure 26. Magnetometer H-D-Z Axis Data: 7 November 1986

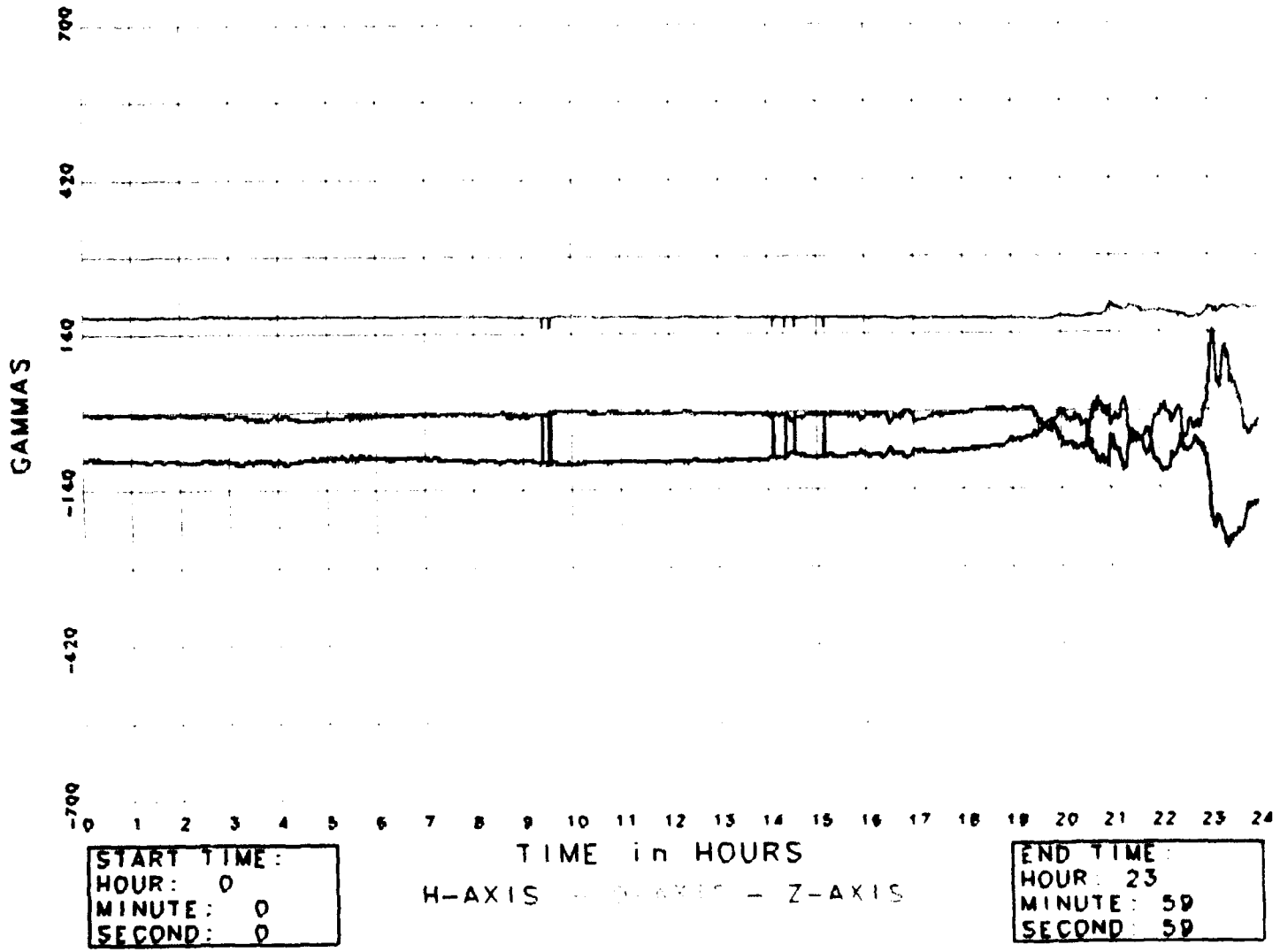


Figure 27. Magnetometer H-D-Z Axis Data, 10 November 1986

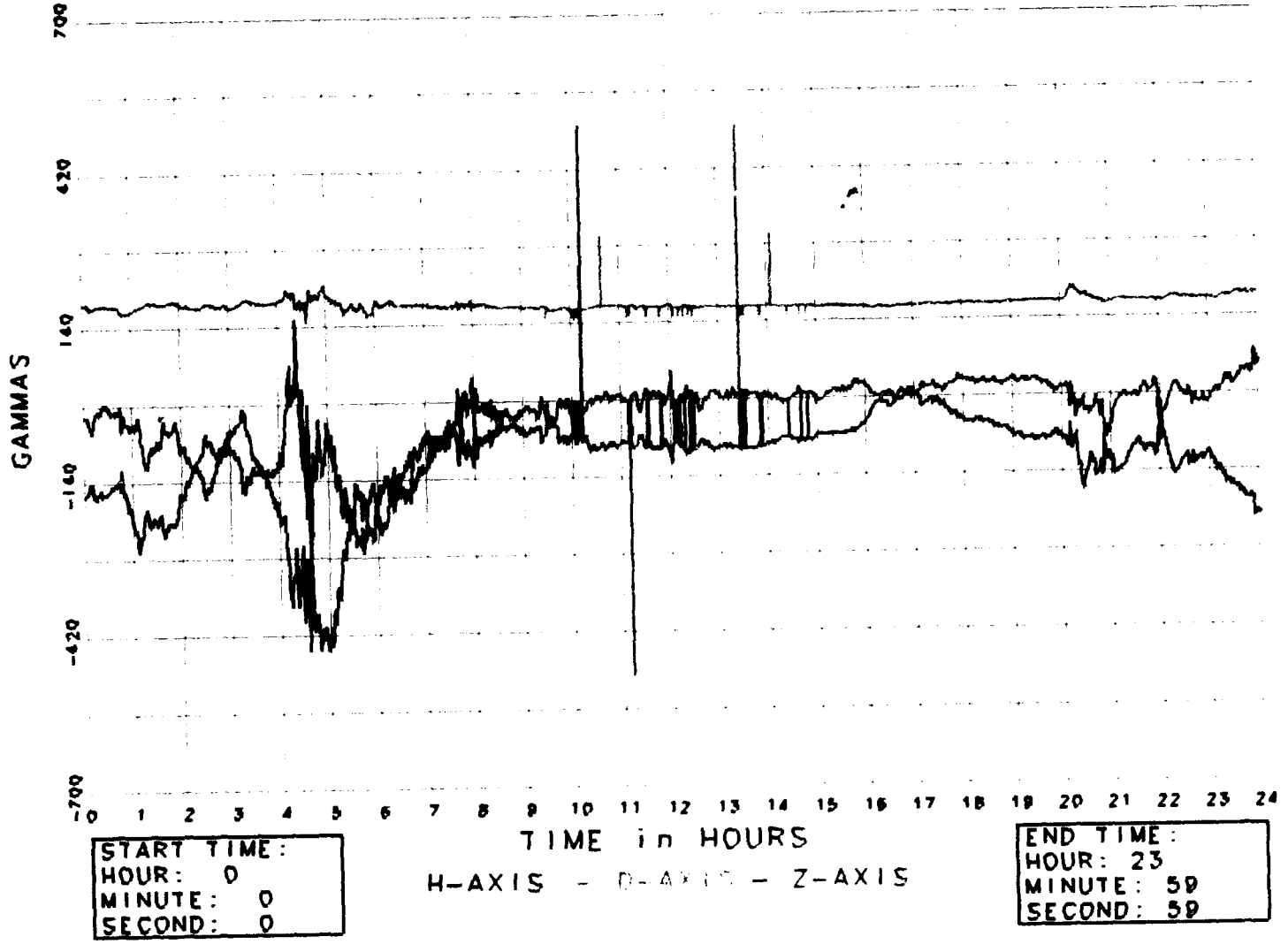


Figure 28. Magnetometer H-D-Z Axis Data: 11 November 1986

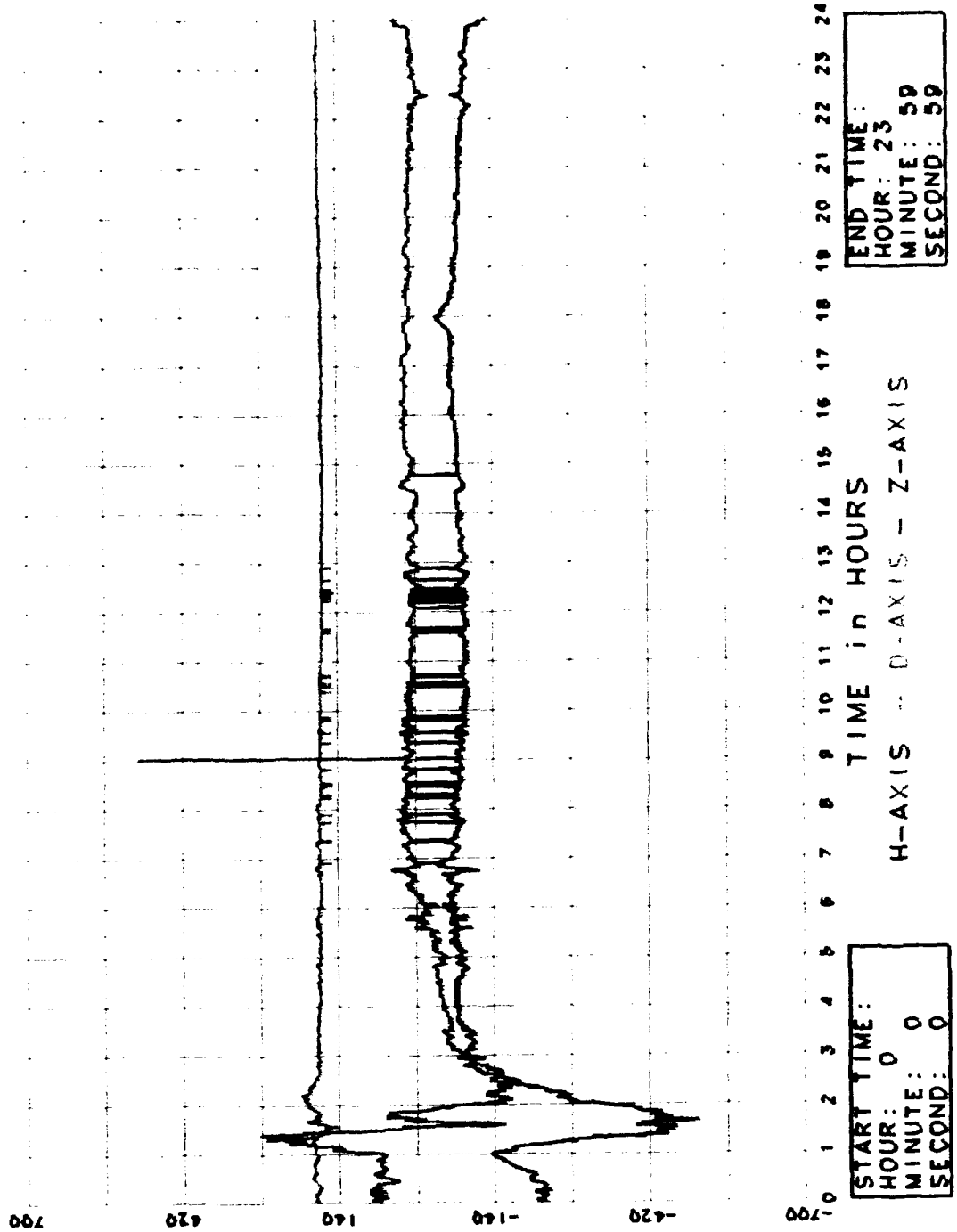


Figure 29. Magnetometer H-D-Z Axis Data: 12 November 1986


Reverse Blank

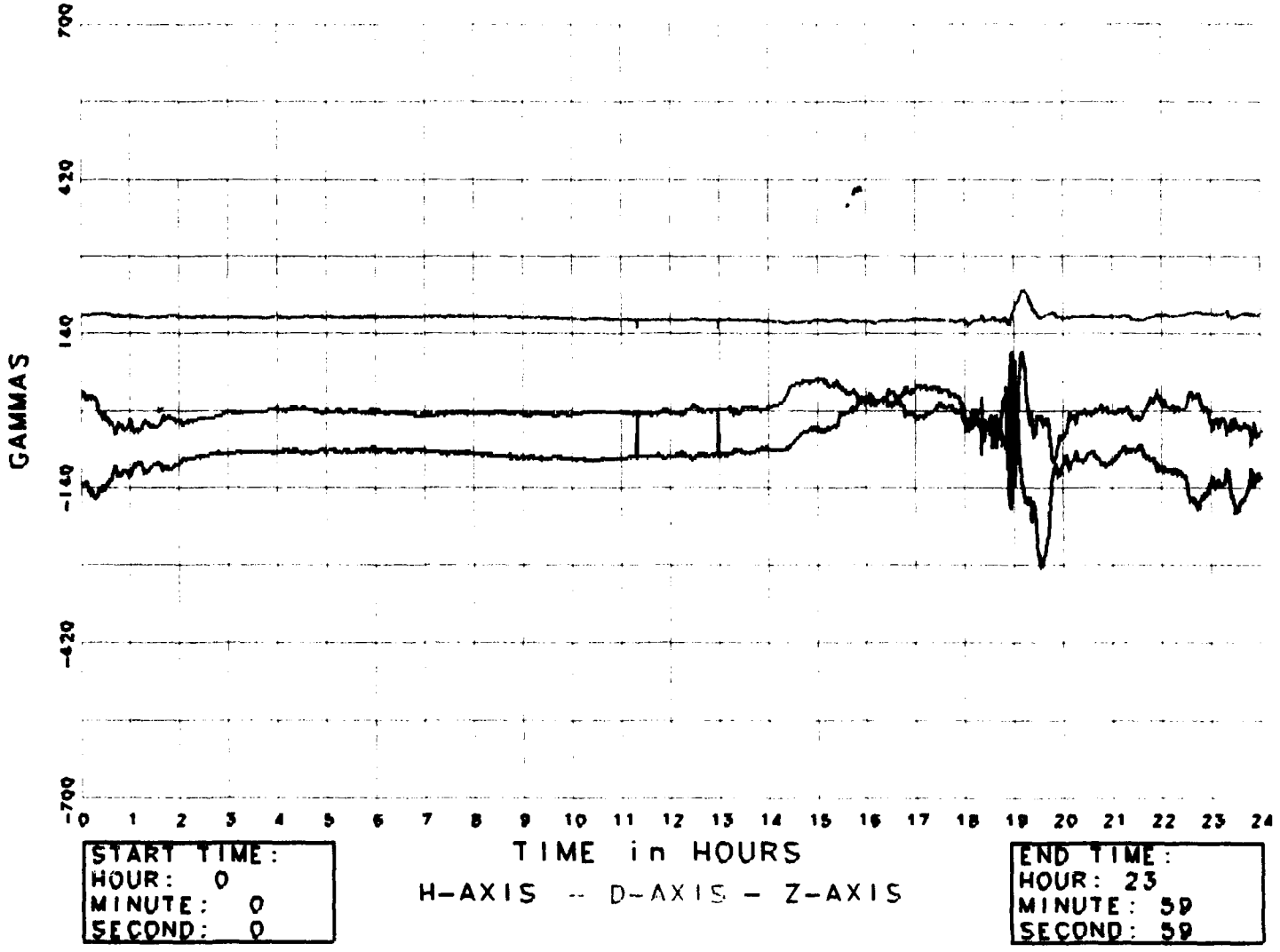


Figure 30. Magnetometer H-D-Z Axis Data: 13 November 1986


Reverse Blank

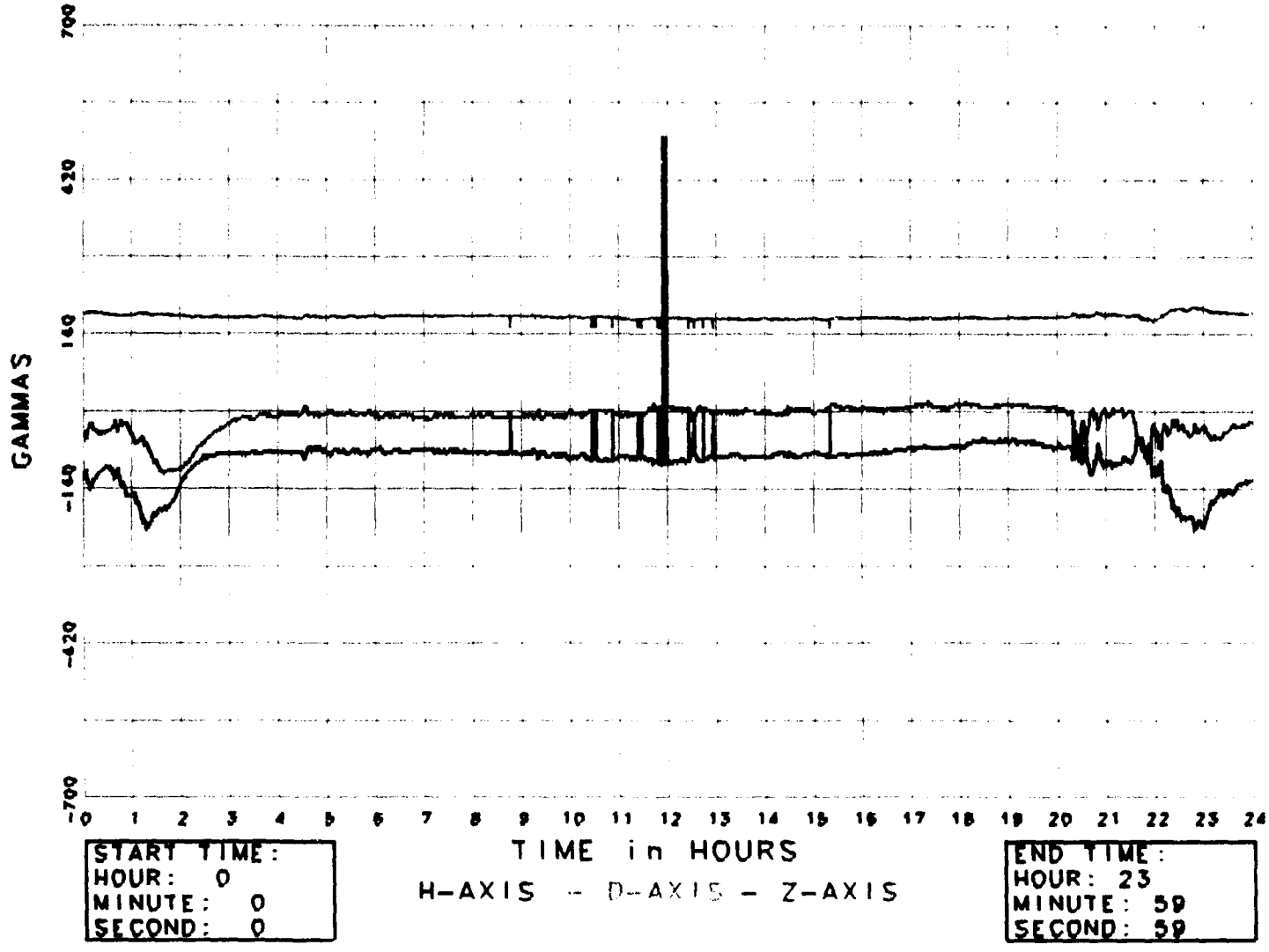


Figure 31. Magnetometer H-D-Z Axis Data: 14 November 1986



Reverse Blank

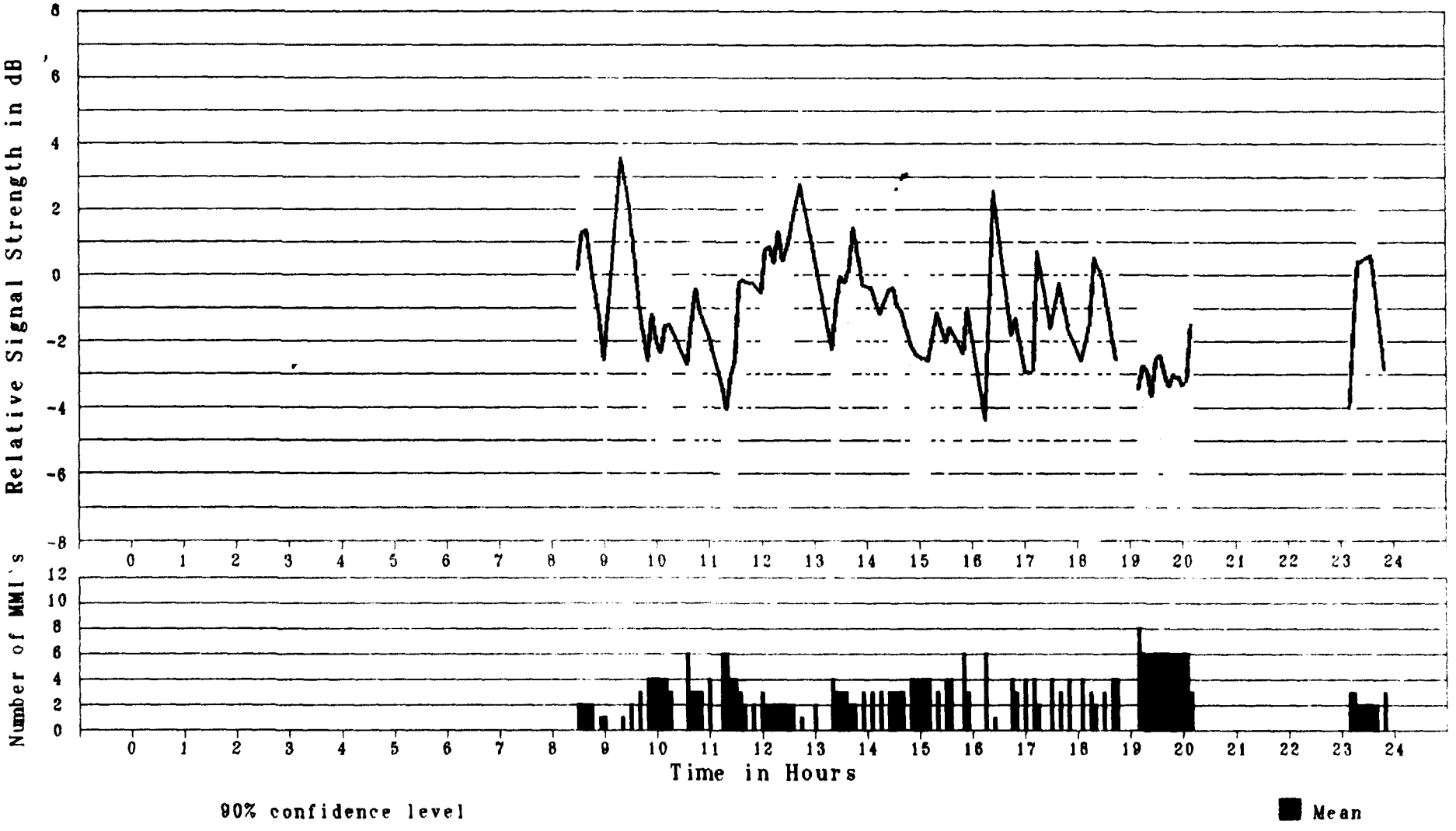


Figure 32. ELF Reception Data, Relative Magnetic Field Strength vs Time, 3 November 1986



Reverse Blank

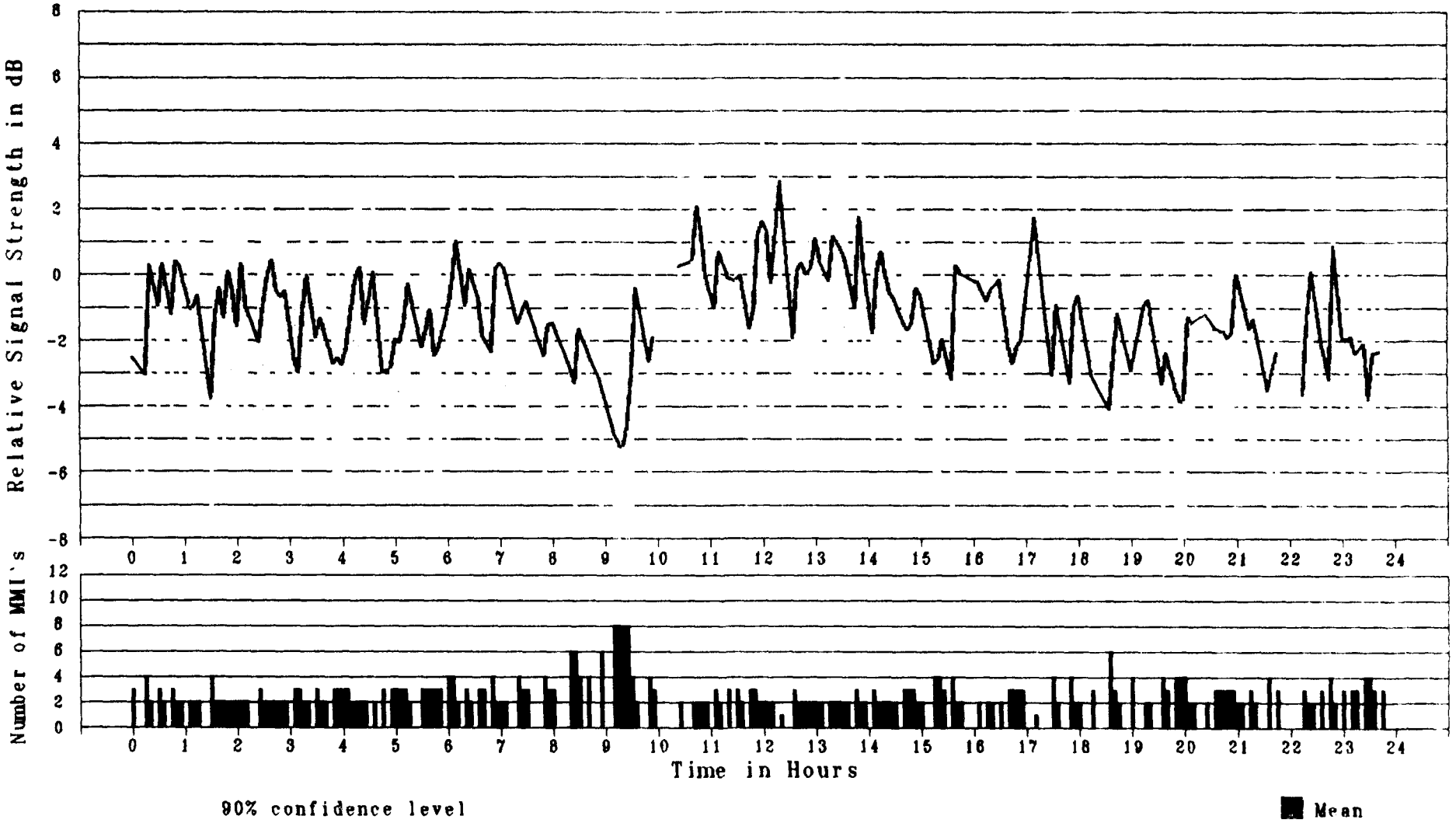


Figure 33. ELF Reception Data, Relative Magnetic Field Strength vs. Time, 4 November 1986

Reverse Blank

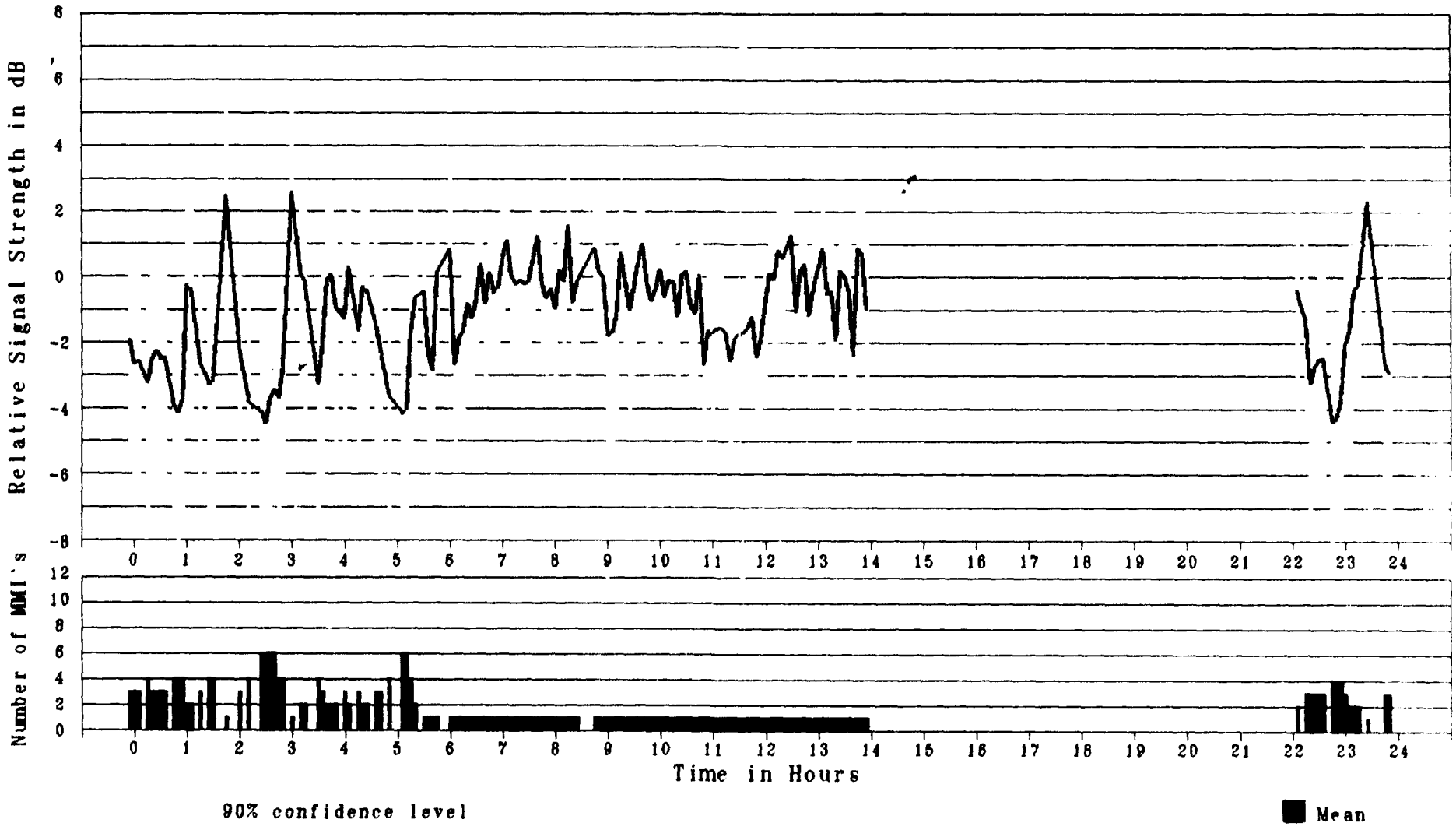


Figure 34. ELF Reception Data, Relative Magnetic Field Strength vs. Time, 5 November 1986

Reverse Blank

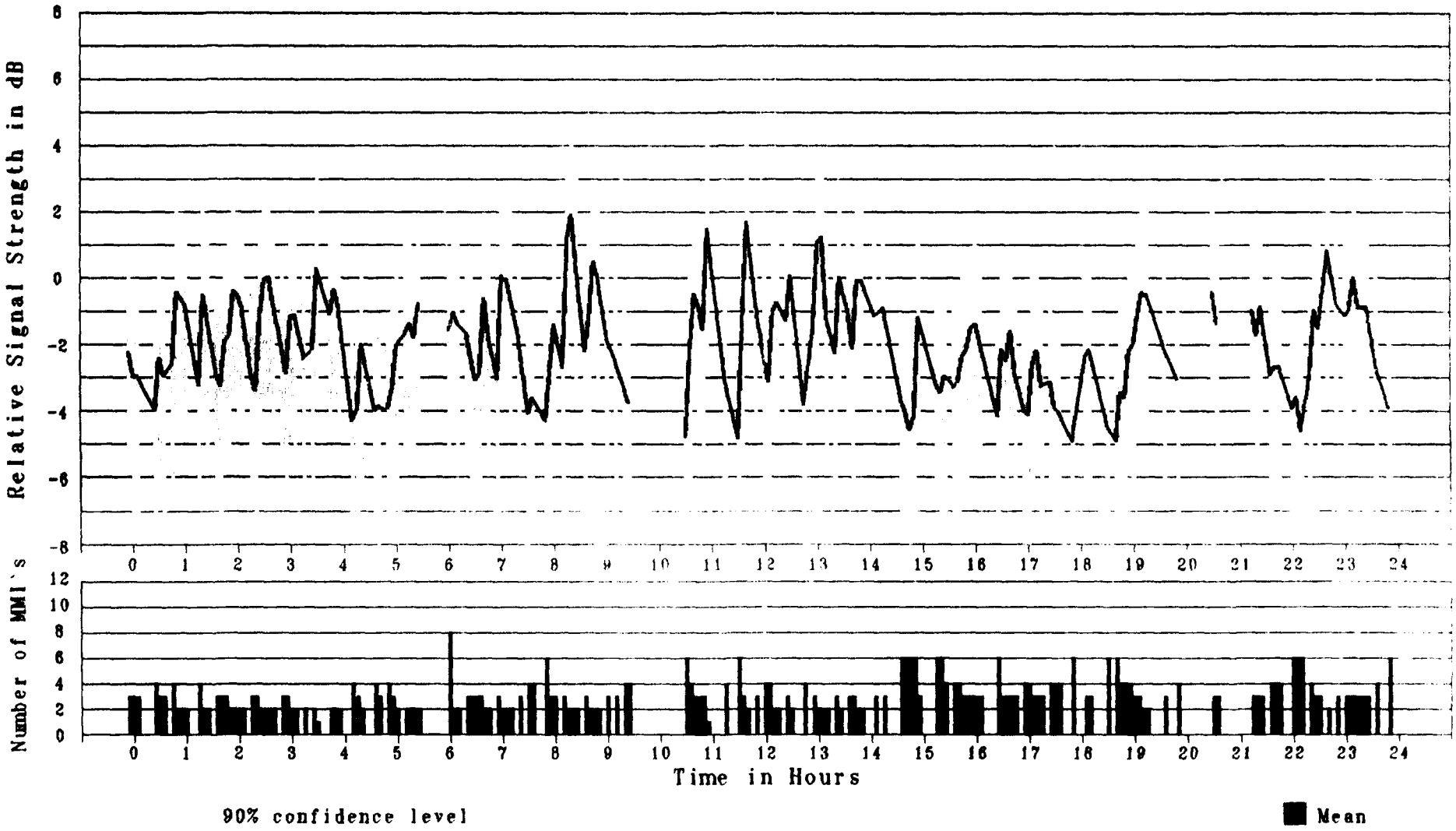


Figure 35. ELF Reception Data, Relative Magnetic Field Strength vs. Time, 6 November 1986



Reverse Blank

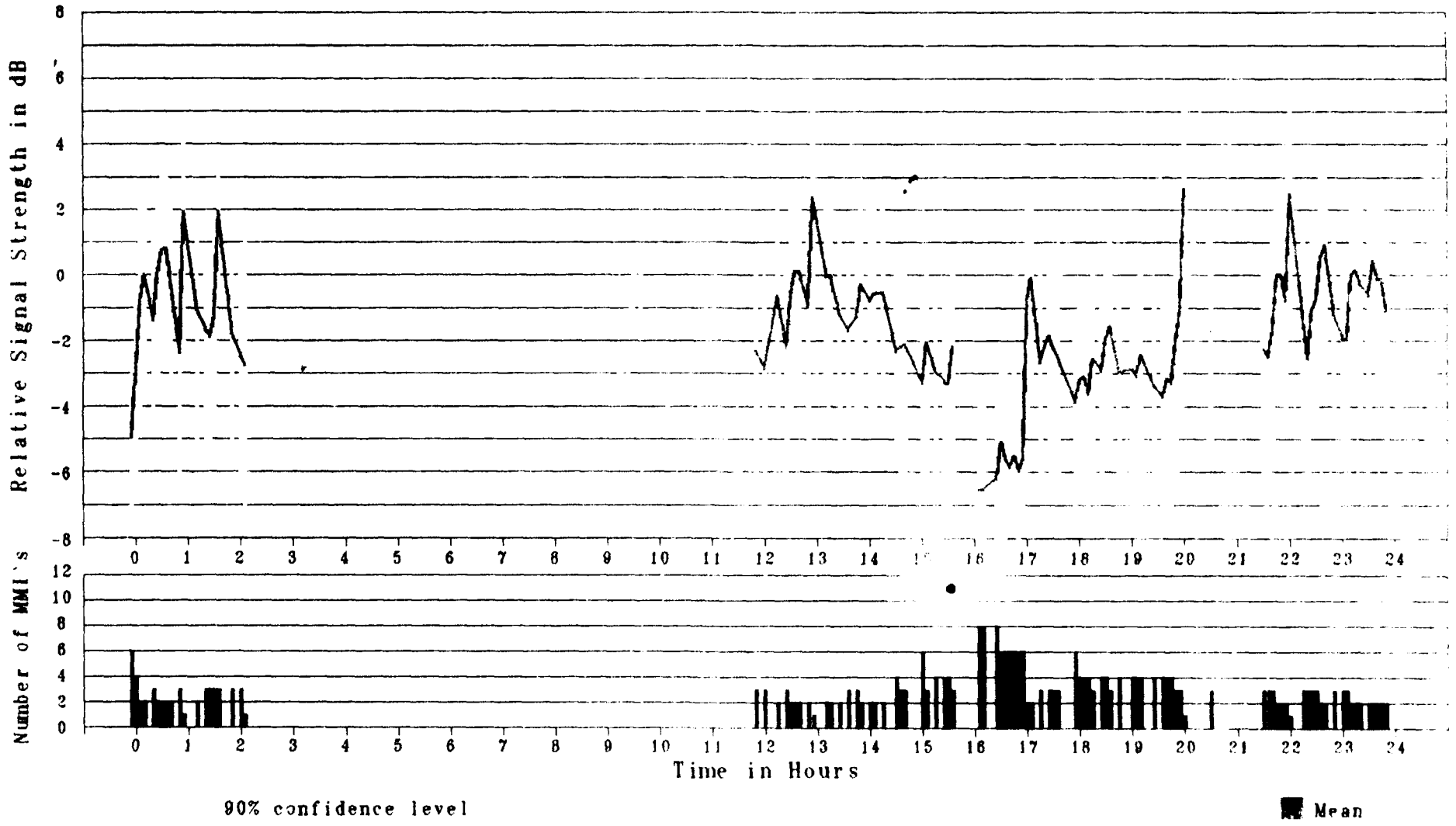


Figure 36. ELF Reception Data, Relative Magnetic Field Strength vs. Time, 7 November 1986

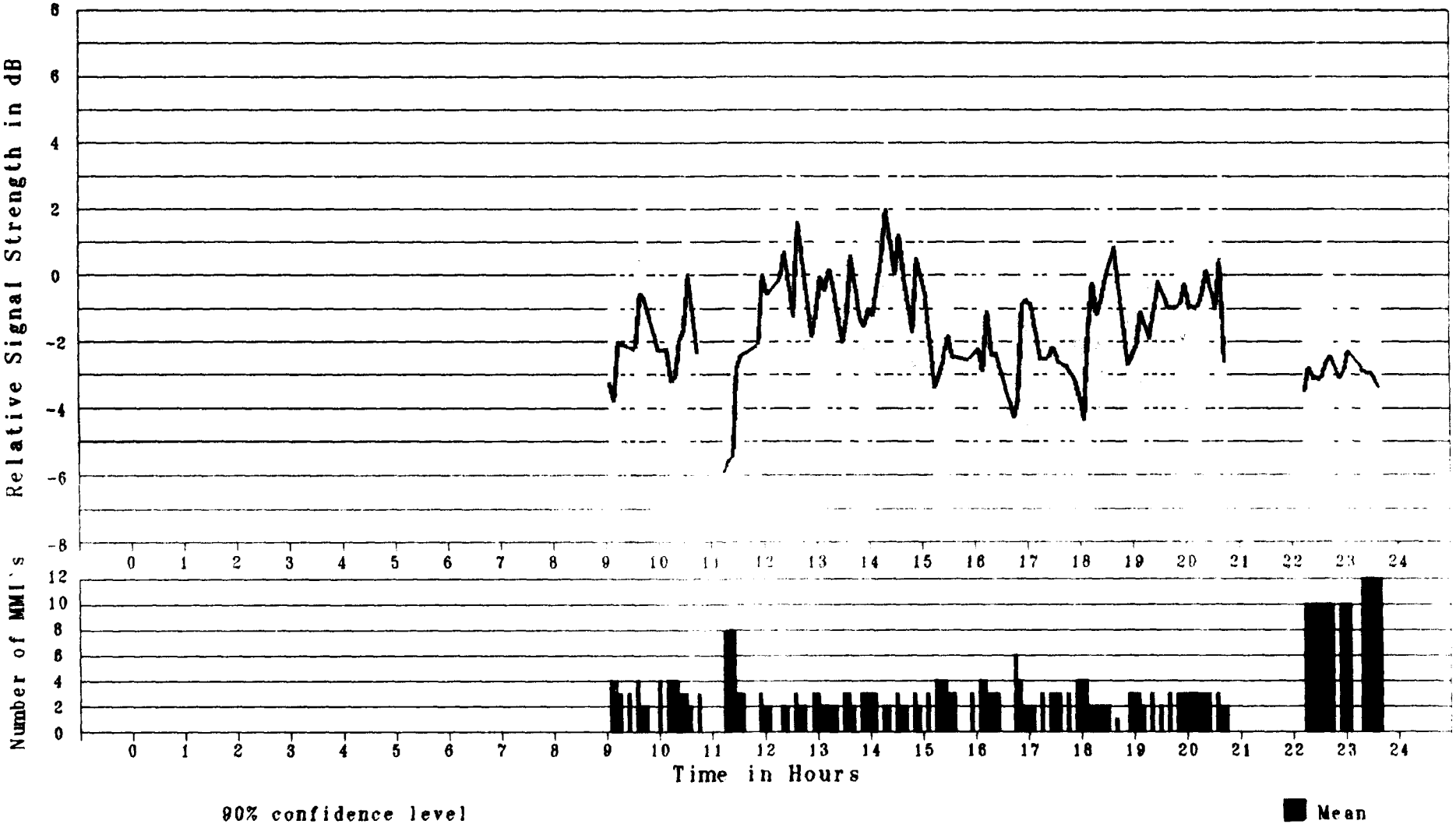


Figure 37. ELF Reception Data, Relative Magnetic Field Strength vs. Time, 10 November 1986

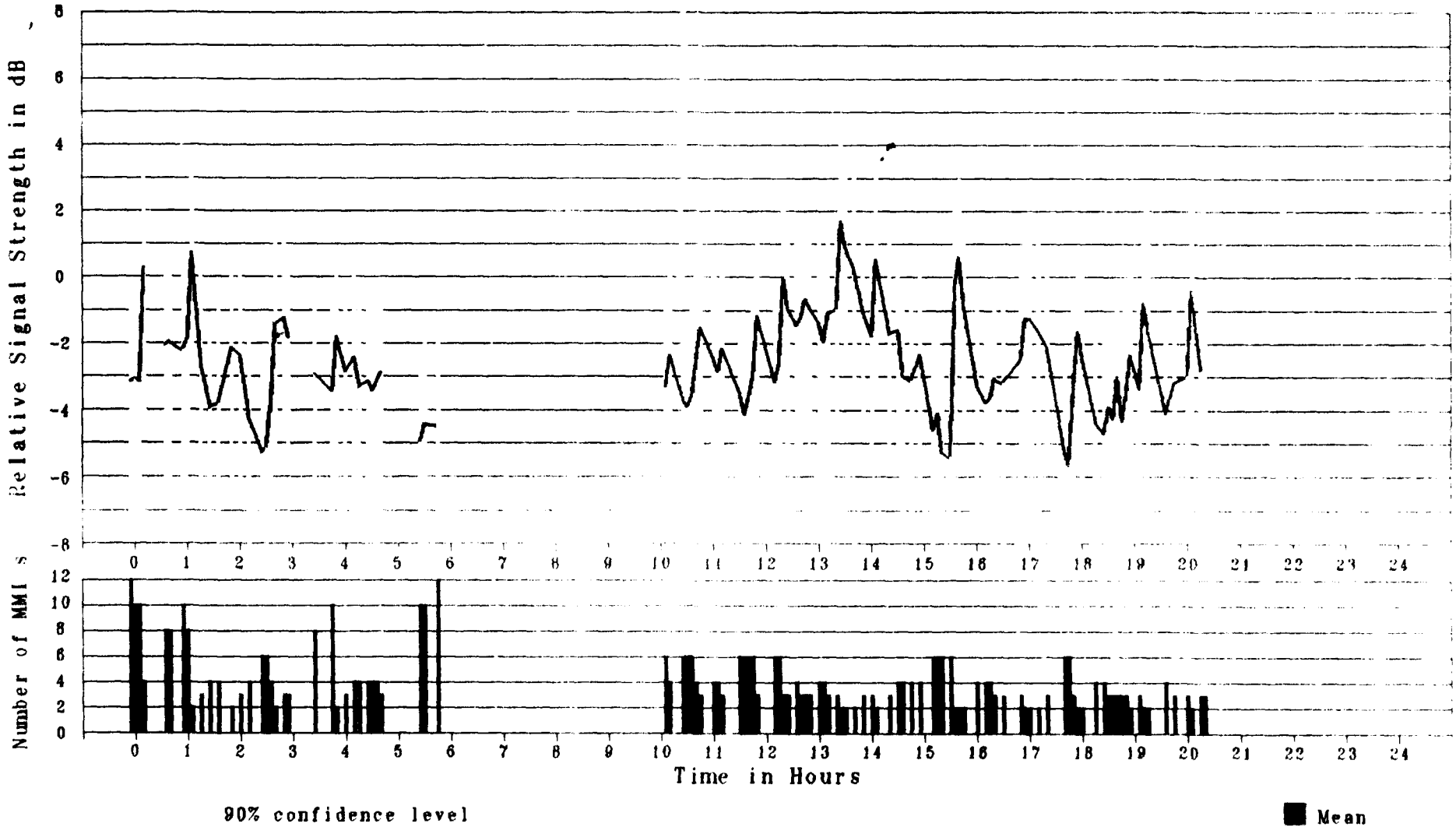


Figure 38. ELF Reception Data, Relative Magnetic Field Strength vs. Time, 11 November 1986



Reverse Blank

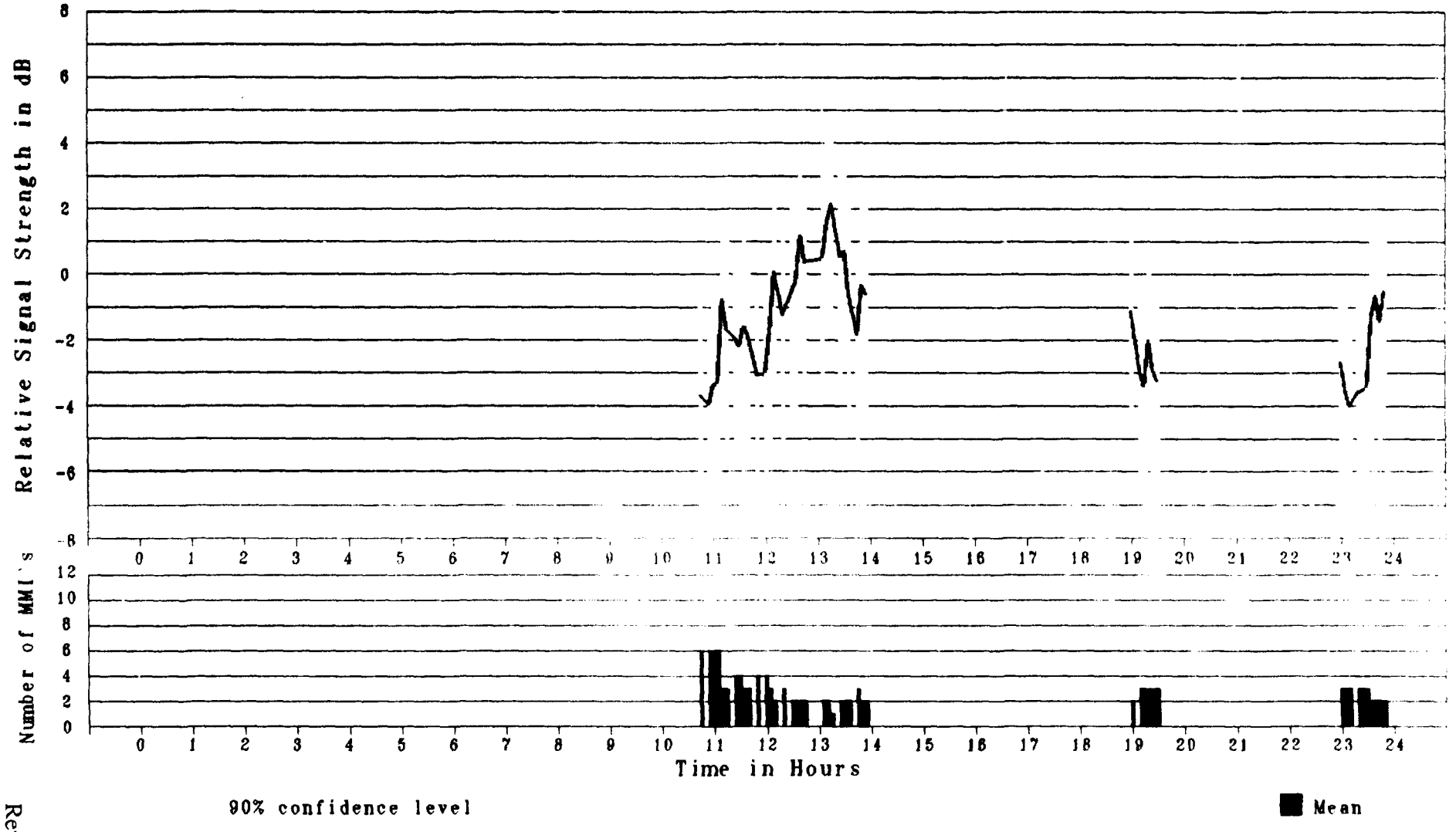


Figure 39. ELF Reception Data, Relative Magnetic Field Strength vs. Time, 12 November 1986



Reverse Blank

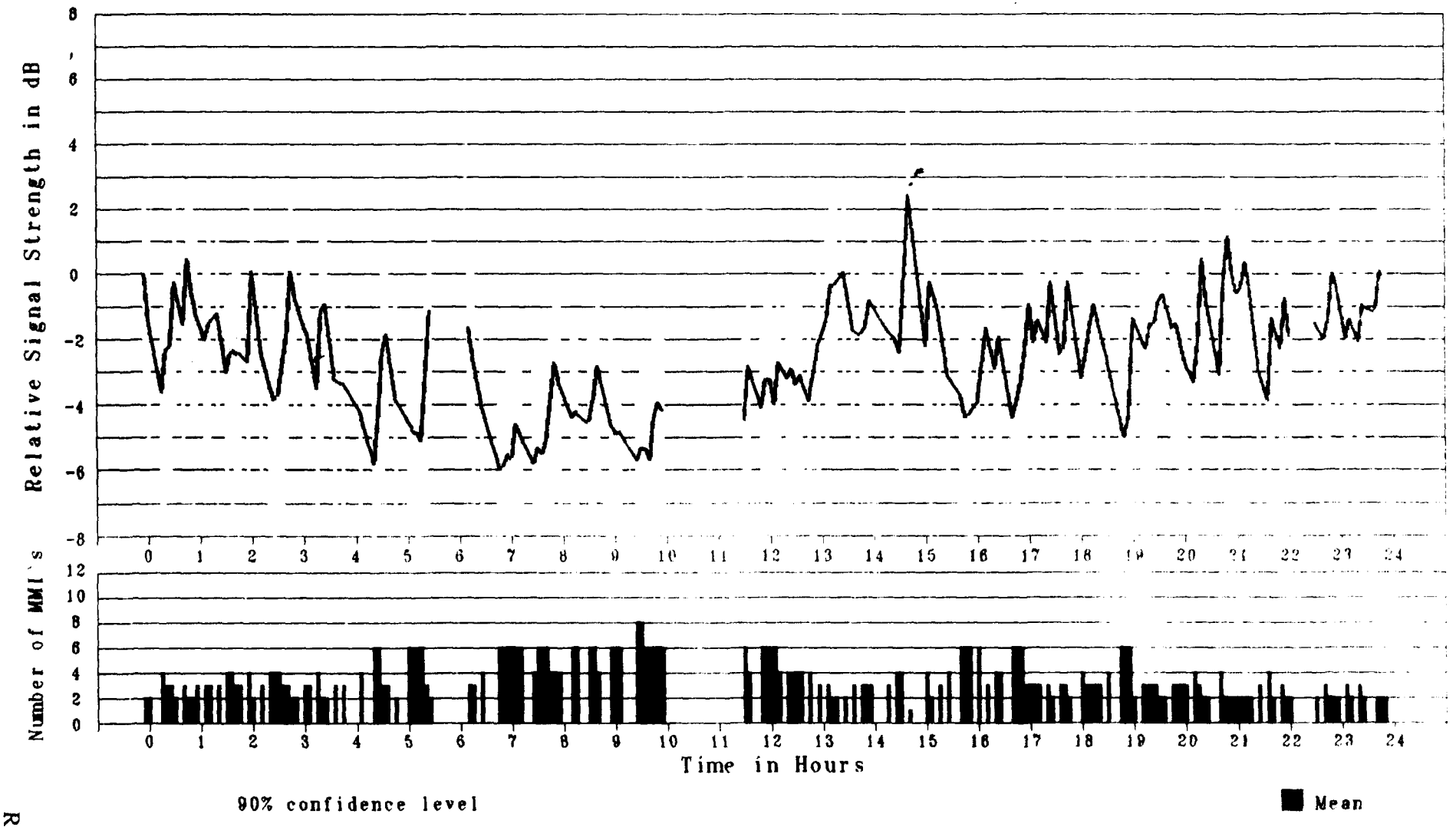


Figure 40. ELF Reception Data, Relative Magnetic Field Strength vs. Time, 13 November 1986



Reverse Blank

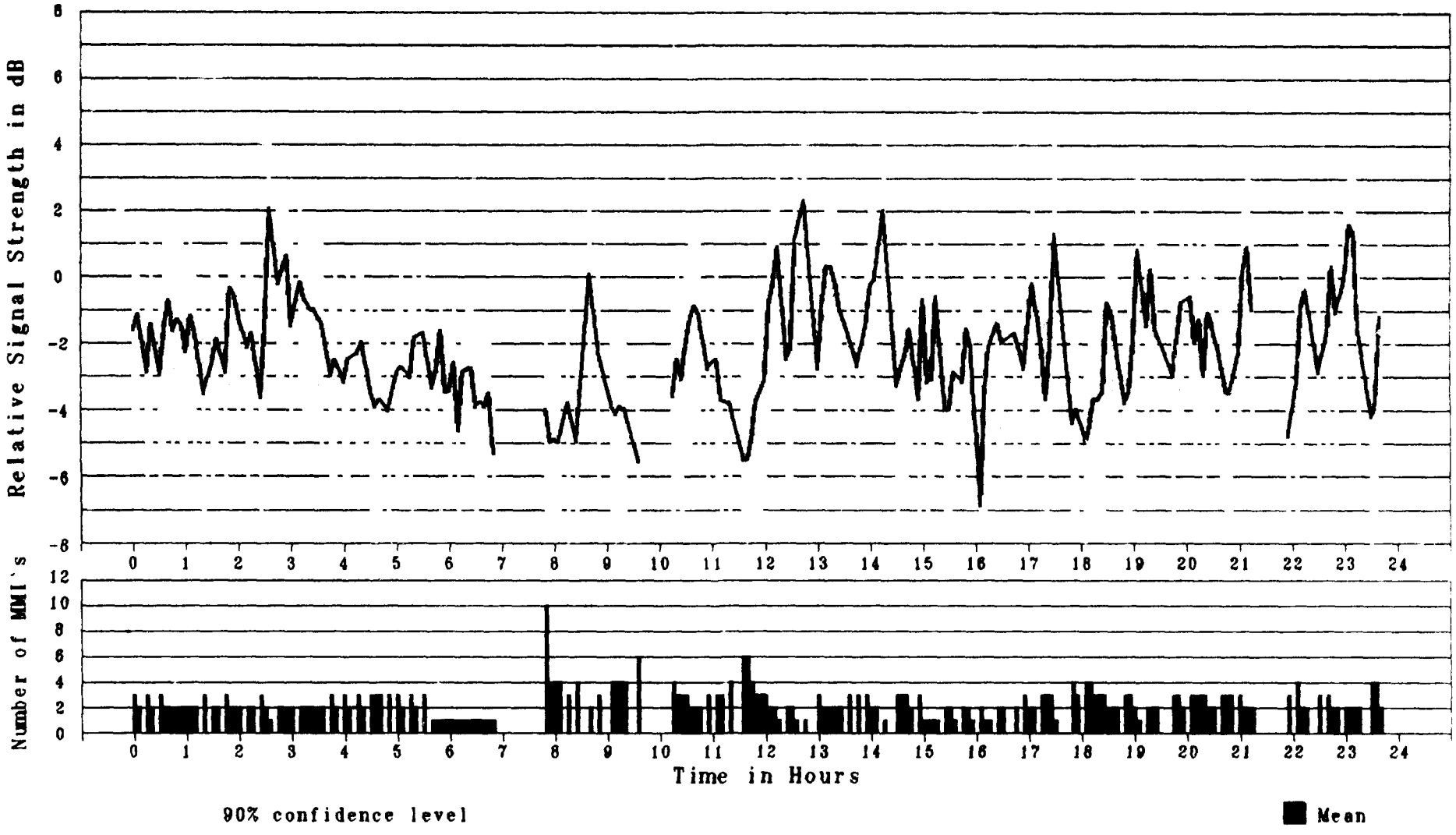


Figure 41. ELF Reception Data, Relative Magnetic Field Strength vs. Time, 14 November 1986



Reverse Blank

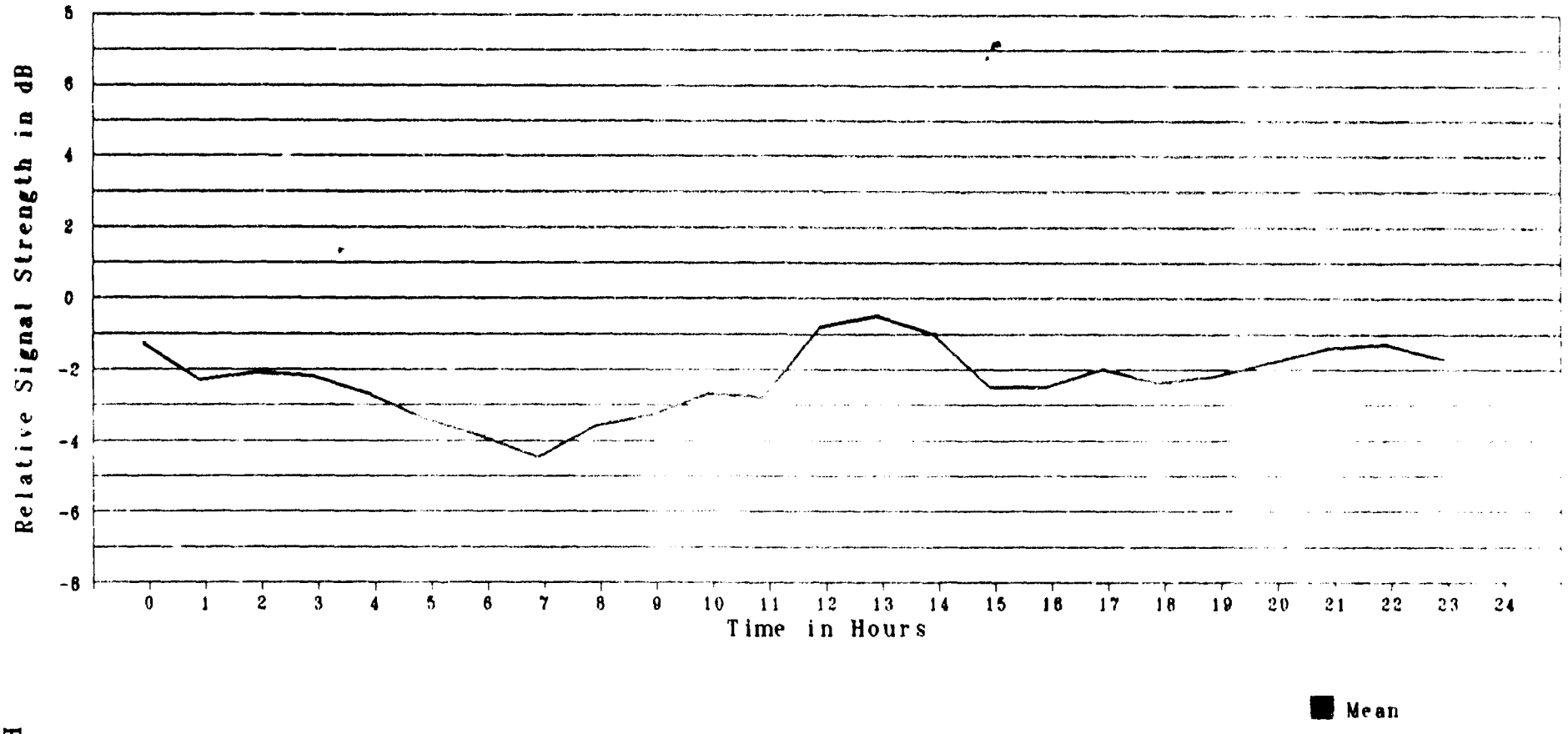


Figure 42. ELF Reception Data, Relative Magnetic Field Strength vs. Time, Hourly Average for 3-14 November 1986

# APPENDIX

# DESCRIPTION OF DIAGNOSTIC IONOSPHERIC INSTRUMENTATION

## DIGITAL IONOSONDE

The ionosonde, which was designed by a staff member* of the Danish firm Elektronik-Centralen, was initially installed to provide data for this experiment at the Andøya Rocket Range during March 1986. Since October 1986, it has come under the administrative control of the Norwegian Defence Research Establishment for day-to-day operations.

The sounder consists of two main subsystems, i.e., the transmitter/receiver subsystem and the data handling subsystem. The transmitter/receiver subsystem contains a pulsed transmitter that transmits 50 microsecond radio frequency (RF) pulses with a selectable repetition frequency of either 50 or 100 pulses per second. The RF for the pulses can be varied between 0.20 MHz and 20 MHz, in steps of 5 kHz. As mentioned earlier, the operational frequency range was chosen to be between 1 MHz and 20 MHz. The resulting transmitter pulses are amplified to a level of approximately 10 W by the power amplifier driver, and further to a level of 2 kW by the power amplifier. The output is then connected to the transmitting antenna, a multiple-wire delta, through an open wire balance transmission line with a characteristic impedance of 470 ohms.

The signals are received on an antenna identical to the transmitting antenna, but orthogonal in direction. The signals are filtered, mixed, up-converted to 30 MHz, amplified, and filtered again through a bandpass with a bandwidth of 100 kHz. The filtered signal is then followed by a second receiver mixer, down-converted to 1.4 MHz, amplified and filtered through another bandpass, with a bandwidth of 25 kHz. The signals are finally detected in a logarithmic detector and are then differentiated and digitized with a one bit resolution. Finally, these digitized pulses are routed through a data sequencer to the data handling subsystem for display and archiving.

The data handling subsystem is based on an Olivetti M-24 personal computer, incorporating a hard disk for temporary storage of the ionograms prior to the twice weekly archiving of the data onto a Cipher cassette tape recorder. All programs were developed in Turbo Pascal. In addition to online screen display and hard disk storage, data output is printed via a Hewlett-Packard ThinkJET printer. Finally, via a software option, 35 mm film images can be scheduled and taken of the sounder's front panel oscilloscope display.

---

* The description of the digital ionosonde described in this report are taken from *Ionosounder Operations Manual and Log* by Jens Østergaard, 24 March 1986.

## RIOMETER

There are several riometers installed and operated at the Andøya Rocket Range. Each riometer operates at a single HF range. There are two master/slave pairs, one operating at 32 MHz and the other at 40 MHz. A final riometer operates at 32.5 MHz. These riometers are part of the polar chain which is owned by and operated for the Danish Meteorological Institute.*

Typical sensors for the riometers are 2 zenith-directed multielement, crossed yagi antennas. The riometer itself is a self-balancing system using a diode for a local noise source. The output of this diode is continuously made equal to the noise power from the antenna. By continuously detecting and compensating for the inequality between the antenna signal and diode noise power, the direct current flowing through the diode is monitored. This permits the antenna noise power to be observed and recorded on a linear scale. This information can be graphically displayed on the paper output of an Esterline-Angus chart recorder or electronically archived on 9-track industry standard digital tapes.

Typically, absorption values of 1 dB at 30 MHz are considered significant. As the absorption intensity varies with frequency in the following manner:

$$\frac{A(f_1)}{A(f_2)} = \frac{f_2^2}{f_1^2},$$

one can readily see that a 1 dB absorption at 30 MHz is even more significant at lower frequencies. For example, at 10 MHz, the absorption is 9 dB!

This relationship is also useful as a diagnostic. If one is operating two riometers, each at a different frequency, e.g., 32 MHz and 40 MHz, one can ensure that an event is not due to local interference. If the two riometer traces simultaneously record the same event in accordance with the above relationship, one can be fairly confident that a true event was observed.

## MAGNETOMETER

Magnetometer observations of the H-axis, D-axis, and Z-axis were also made and archived at the Andøya Rocket Range. The archived digital tapes for the experimental period were forwarded to NUSC for reduction.

In their classic work on geomagnetism, Chapman and Bartels [1940] described some of the storm-time features of 3-axial measurements (H, D, and Z). Typically, the H-axis data show an initial rise and subsequent larger decrease followed by a slow recovery. This characteristic is observable in all latitudes, but the maximum diminution decreases with increasing latitude. In addition, it is somewhat more difficult to determine the average storm-time variations due to the presence of irregular variations that are a regular feature at these higher latitudes. Storm-time variation in the magnitude of Z is opposite to that of H and is much smaller in magnitude. Also, Z exhibits a polarity feature, reversing itself in the southern hemisphere. There are practically no storm-time variations observable in D.

---

* The riometers in the chair stretch from Greenland through Iceland and into northern Norway. Data from all these stations are sent to the Danish Meteorological Institute in Copenhagen for analysis. Dr. Peter Stauning has been in charge of the program for a number of years.

## BIBLIOGRAPHY


Bannister, P. R., "Variations in Extremely Low Frequency Propagation Parameters," *Journal of Atmospheric and Terrestrial Physics*, vol. 37, no. 9, 1975, pp. 1203-1210.

Bannister, P. R., "Localized ELF Nocturnal Propagation Anomalies," *Radio Science*, vol. 17, no. 3, 1982, pp. 627-634.

Bannister, P. R., "The Determination of Representative Ionospheric Conductivity Parameters for ELF Propagation in the Earth-ionosphere Waveguide," *Radio Science,* vol. 20, no. 4, 1985, pp. 977-984.

Barr, R., "The Effect of Sporadic-E on the Nocturnal Propagation of ELF Radio Waves," *Journal of Atmospheric and Terrestrial Physics*, vol. 39, 1977, pp. 1379-1387.

CCIR, *Atlas of Ionospheric Characteristics*, Report 340, Int. Telecommun. Union, Geneva, 1967.

Chapman, S., and J. Bartels, *Geomagnetism*, University Press, Oxford, 1940.

Davis, J. R., "Localized Nighttime D-region Disturbances and ELF Propagation," *Journal of Atmospheric and Terrestrial Physics*, vol. 38, no. 12, 1976, pp. 1309-1317.

Fraser-Smith, A. C., and R. A. Helliwell, "ELF Spheric Occurrences in the Antarctic During a Solar Proton Event; Case Study of Occurrences at Byrd Station During the Event of June 9, 1968," *Journal of Geophysical Research,* vol. 30 no. A5, 1980, pp. 2296-2306.

Greifinger, C., and P. Greifinger, "Approximate Method for Determining ELF Eigenvalues in the Earth-ionosphere Waveguide," *Radio Science*, vol. 13 no.5, 1978, pp. 831-837.

Greifinger, C., and P. Greifinger, "On the Ionospheric Parameters Which Govern High-latitude ELF Propagation in the Earth-ionosphere Waveguide, *Radio Science,* vol 14, no. 5, 1979a, pp. 889-895.

Greifinger, C., and P. Greifinger, "Extended Theory for Approximate ELF Propagation Constants in the Earth-ionosphere Waveguide," DNA Report 5561, T, R and D Assoc., Marina del Ray, CA, 1979b.

Hargreaves, J. K., *The Upper Atmosphere and Solar-Terrestrial Relations*, Van Nostrand Reinhold, NY, 1979.

Katan, J. R., and P. R. Bannister, "Observations of ELF Propagation Variations at Mid and High Latitudes During the November and December 1982 Solar Proton Events," NUSC Technical Report 7341, Naval Underwater Systems Center, New London Laboratory, New London, CT, 5 November 1985.

Katan, J. R., and P. R. Bannister, "Summary of ELF Propagation Variations at Mid and High Latitudes During the November/December 1982 and February 1984 Solar Proton Events," *Radio Science*, vol. 22, no. 1, 1987, pp. 111-124.

Pappert, R. A., "Effects of a Large Patch of Sporadic E on Nighttime Propagation at Lower ELF, *Journal of Atmospheric and Terrestrial Physics*, vol. 42, no. 5, 1980, pp. 417-425.

Pappert, R. A., and L. R. Shockey, "Effects of Strong Local Sporadic E on ELF Propagation," NOSC Report 282, Naval Ocean Systems Center, San Diego, CA, 15 August 1978.

Pappert, R. A., and W. F. Moler, "A Theoretical Study of ELF Normal Mode Reflection and Absorption Produced by Nighttime Ionospheres, " *Journal of Atmospheric and Terrestrial Physics*, vol. 40, no. 9, 1978, pp. 1031-1045.

Space Environment Services Center (SESC), "Preliminary Report and Forecast of Solar Geophysical Data," SESC PRF 584, NOAA, Boulder, CO, 11 November 1986a.

Space Environment Services Center (SESC), "Preliminary Report and Forecast of Solar Geophysical Data," SESC PRF 585, NOAA, Boulder, CO, 18 November 1986b.

Valley, S. L., *Handbook of Geophysics and Space Environments*, McGraw-Hill, New York, 1965.

Wakai, N., H. Ohyama and T. Koisumi, *Manual of Ionospheric Scaling*, Radio Research Laboratory, Tokyo, 1985.

## INITIAL DISTRIBUTION LIST

| Addressee | No. of Copies |
|---|---|
| National Science Foundation (Patrick Smith) | 2 |
| CNO (OPNAV N67, LT T. Green, CDR Ruud) | 2 |
| National Geophysical Data Center (R.Conkright) | 1 |
| Defence Science & Technology Organisation (John Tilbrook, Russell Clarke) | 2 |
| Australian Antarctic Division (Peter McGill) | 1 |
| HQ Australian Defence Force (CAPT David MacCard, LCOL Keith Brewster) | 2 |
| HQ New Zealand Defence Force (Bruce Emirali) | 1 |
| Radio Spectrum Policy, Ministry of Commerce (Wayne Wedderspoon) | 1 |
| DTIC | 2 |